THE GROWTH KINETICS AND INTERFACIAL PROPERTIES OF ELECTROGENERATED BUBBLES

By

NIGEL PETER BRANDON

(PhD Thesis)

Mineral Technology Section

Dept. of Mineral Resources Eng.

Royal School of Mines

Imperial College

London SW7 2BP

To my parents for their encouragement,

and to Jan for her understanding

"I like work: it fascinates me. I can sit and look at it for hours."

Jerome K. Jerome

"Bubble, bubble toil and trouble"

After Shakespeare

ACKNOWLEDGEMENT

I would like to express my gratitude to all those who have contributed to my studies at Imperial College, but particular thanks must go to my supervisor, Dr. G.H.Kelsall, for his continual interest, advice and guidance, and to the students of B421 for their excellent company.

I am grateful to Dr's. A.L.Smith and S.Levine of Unilever Research, Port Sunlight Laboratory, Wirral, Merseyside, and to Dr. J.A.Kitchener of Imperial College, for their advice in some of the theoretical aspects of this work.

Thanks are also due to the Applied Mechanics group of Imperial College for the loan of a signal analyser, to Unilever Research for the loan of a high speed camera, and to Chris Bell for his aid in the printing of this thesis.

Finally, I would like to thank Unilever Research and the Science and Engineering Research Council for their financial support over the past three years.

ABSTRACT

This project studied the factors affecting bubble growth kinetics and departure diameter at microelectrodes, such that single bubble growth could be assured, and under conditions of minimal surfactant contamination. Following detachment, the rise rate of the bubble was measured, this being used as an indicator of electrolyte purity. A lateral electric field was then applied and the resultant migrational velocity of the bubble determined, as a measure of surface charge.

Three modes of bubble growth were identified; at short times inertia control dominated, followed by diffusion control until the bubble diameter exceeded that of the electrode, when gas became 'directly injected' into the bubble.

Bubble departure diameter was dependent on solution pH and applied potential; small hydrogen bubbles were evolved at high pH and large ones at low pH. The converse was observed for oxygen and chlorine evolution. Addition of ionic surfactants reduced bubble departure diameters, masking the influence of pH at high bulk concentrations.

Bubble electrophoretic mobilities showed a pH dependency, indicating preferential OH^- ion adsorption, and exhibited a point of zero charge at pH 2-3 (i.e. bubbles were positively charged

at pH < 2, and negatively charged at pH > 3). In addition, their dependency on bubble diameter and electric field strength implied that both hydrodynamic and field induced polarisation of charge occured at mobile bubble surfaces.

The pH dependence of bubble departure diameter was interpreted in terms of an electrostatic interaction between bubble and electrode double layers; the charge on the latter was characterised as a function of applied potential, electrolyte pH, and concentration of ionic surfactant using a.c. impedance techniques.

Fluctuations in current and potential, arising from bubble growth, were analysed to give their amplitude probability, auto correlation and power spectral density functions. The fundamental frequency of the "noise" correlated with photographic information of the bubble departure frequency.

CONTENTS

		Page
	ABSTRACT	5
	LIST OF CONTENTS	7
	LIST OF FIGURES	12
	LIST OF TABLES	20
1	LITERATURE REVIEW	21
	1 Introduction	23
	2 Electrolytic Bubble Growth	23
	2.1 Mechanism	23
	2.1.1 Electrochemical Kinetics	24
	2.1.2 Bubble Growth Kinetics	26
	2.1.3 Electrode Properties	28
	2.2 Mass Transfer at Electrodes	30
	2.3 Factors Effecting Bubble Growth	32
	2.3.1 Supersaturation and Nucleation	32
	2.3.2 Current Density	34
	2.3.3 Electrode Diameter	37
	2.3.4 Electrode Material	38
	2.3.5 Electrode Morphology/Geometry	39
	2.3.6 Electrolyte/pH	39

2.3.7 Pressure, Temperature and Viscosity 41

2.3.8 Bubble/Electrode Contact Angle 41

2.3.9 Coalescence 43

2.4 Comparison of Electrolytic and Vapour Bubble Growth 44

2.5 Effect of Bubble Growth on Current/Potential Distribution, and Overpotential 47

3 Bubble Properties 50

3.1 Bubble Charge/Electrophoretic Mobility 50

3.1.1 Introduction 50

3.1.2 Bubble Electrophoretic Mobility 51

3.1.3 Bubble Zeta Potential 52

3.1.4 Bubble Charge 57

3.2 Motion of Bubbles in Liquids 59

3.2.1 Mechanics of Motion 59

3.2.2 Surfactant Adsorption on Rising Bubbles 61

3.3 Mass Transfer to a Bubble 63

3.4 Effect of Bubbles on Inter-electrode Properties 64

3.4.1 Solution Conductivity 64

3.4.2 Current Density Distribution 66

3.4.3 Mass Transfer To Electrodes 67

4 Summary 68

2 EXPERIMENTAL DESIGN 69

1 Preparation Of Surfactant Free Electrolytes 70

1.1 Water Purification 70

1.2 Electrolyte Preparation 70

1.3 Detection Of Impurities 73

1.3.1 Surface Tension 73

1.3.2 Cyclic Voltammetry 73

1.3.3 Bubble Rise Rate 74

2 Bubble Electrophoretic Mobility and Growth Measurements 74

2.1 Cell Design 74

2.2 Electrode Preparation 80

3 Current, Potential, Impedance and Electrode Area Measurement 83

3 BUBBLE CHARGE MEASUREMENT 85

1 Electrolyte Purity 86

1.1 Surface Tension 86

1.2 Cyclic Voltammetry 86

1.3 Bubble Rise Rate 88

2 Bubble Electrophoretic Mobility Measurements 93

2.1 Bubble Mobility in Surfactant Free Electrolytes 93

2.2 Bubble Mobility with Added Surfactant 104

3 Summary 110

4 BUBBLE GROWTH KINETICS AND DEPARTURE DIAMETER 113

1 Bubble Growth Kinetics 114

1.1 Bubble Induction Time 114

1.2 The Growth Coefficient 119

1.3 The Time Coefficient 122

2 Electrode Charge 127

3 Bubble Departure Diameter 137

3.1 Influence of pH 137

3.2 Influence of Electrode 153

3.3 Influence of Electrolyte 153

3.4 Influence of Hydrodynamics 160

4 Summary 163

5 POTENTIAL/CURRENT DISTRIBUTION and "NOISE" MEASUREMENT 165

1 Potential/Current Distribution 166

1.1 Potential/Current Transients 166

1.2 Electrode Resistance 172

2 "Noise" Measurement 174

2.1 Microelectrodes 175

2.2 Macroelectrodes 179

3 Summary 182

CONCLUSIONS 185

FUTURE WORK 187

LIST OF REFERENCES 189

NOMENCLATURE 207

A1 THE ELECTROPHORESIS OF A BUBBLE 211

1 Application of the Levich Theory to Bubble Electrophoresis 212

2 Investigation of the Validity of the Lippmann Equation 217

3 The Influence of an Electric Field on the Electrophoretic Mobility of a Bubble 224

4 The Distribution of Charge on the Surface of a Rising Bubble 233

LIST OF FIGURES

Fig.		Page
2.1	Distillation system for the production of surfactant free water.	71
2.2	Electrolyte preparation apparatus.	72
2.3	Bubble rise rate column.	72
2.4	Gas generation device.	72
2.5	Cell used for the measurement of bubble growth kinetics and bubble charge.	76
2.6	The rotating electrode cell.	81
2.7	Microelectrode construction.	81
2.8	Design of the rotating disk electrode.	82
2.9	Design of the rotating cylinder electrode.	82
2.10	Macroelectrode cell design.	84
3.1	Influence of the bulk surfactant concentration (SDS) on the cyclic voltammogram of platinum.	87
3.2	Bubble rise rate in "as distilled" water compared with that predicted in surfactant free water.	89
3.3	Bubble rise rate in sulphuric acid (plus deci-molar sodium sulphate).	90

3.4 Bubble rise rate in sodium hydroxide (plus deci-molar sodium sulphate). 90

3.5 The influence of bubble cleaning on bubble rise rate in molar sodium hydroxide (plus deci-molar sodium sulphate). 91

3.6 Influence of the bulk surfactant concentration (DTAB) on bubble rise rate. 91

3.7 The influence of pH on the electrophoretic mobility of hydrogen bubbles in milli-molar sodium sulphate. 94

3.8 The influence of pH on the electrophoretic mobility of oxygen bubbles in milli-molar sodium sulphate. 94

3.9 The influence of pH on the electrophoretic mobility of chlorine bubbles in milli-molar potassium chloride. 95

3.10 The influence of bubble diameter on the electrophoretic mobility of bubbles in milli-molar sodium sulphate. 95

3.11 The influence of electric field strength on the electrophoretic mobility of bubbles in milli-molar sodium sulphate. 102

3.12 The influence of electrolyte concentration on the electrophoretic mobility of a bubble. 102

3.13 Influence of the bulk DTAB concentration on the electrophoretic mobility of bubbles in milli-molar sodium nitrate. 105

3.14 Influence of the bulk SDS concentration on the electrophoretic mobility of bubbles in milli-molar sodium nitrate. 105

3.15 The adsorption isotherm of SDS and DTAB in water (283). 107

3.16 The pH dependence of the calculated zeta potential and charge density at the gas/liquid interface. 107

4.1 Typical bubble growth curves, observed during hydrogen evolution at a 25 μm diameter platinum electrode. 115

4.2 The influence of applied potential on the reciprocal of the induction time required for bubble nucleation (τ). 115

4.3 The influence of current density on the growth coefficient of a bubble. 120

4.4 The influence of rotation frequency on the growth coefficient during hydrogen evolution at a rotating disk electrode. 120

4.5 The change in time coefficient during the lifetime of a bubble. 123

4.6 The influence of bubble and electrode diameter on the time coefficient. 123

4.7 The relationship between bubble and electrode diameter at differing time coefficients. 126

4.8 The change in current efficiency during bubble growth at microelectrodes. 126

4.9 Complex plane impedance plot for platinum and platinum oxide at a 100 μm diameter electrode. 129

4.10 The equivalent circuit and ideal complex plane impedance plot of a platinum electrode. 129

4.11 The influence of pH on the double layer capacitance of a platinum/platinum oxide electrode. 131

4.12 The influence of pH on the potential of zero charge of platinum and platinum oxide. 131

4.13 Influence of the bulk DTAB concentration on the double layer capacitance of a platinum/platinum oxide electrode. 133

4.14 Influence of the bulk SDS concentration on the double layer capacitance of a platinum/platinum oxide electrode. 133

4.15 Influence of the bulk surfactant concentration on the potential of zero charge of platinum. 134

4.16 Influence of the bulk surfactant concentration on the potential of zero charge of platinum oxide. 134

4.17 The influence of pH on the differential charge of a platinum/platinum oxide electrode. 135

4.18 Influence of the bulk DTAB concentration on the differential charge of a platinum/platinum oxide electrode. 135

4.19 Influence of the bulk SDS concentration on the differential charge of a platinum/platinum oxide electrode. 136

4.20 The influence of pH on the departure diameter of hydrogen and oxygen bubbles at a 10 μm diameter platinum electrode. 136

4.21 The influence of pH on the departure diameter of hydrogen and oxygen bubbles at a 25 μm diameter platinum electrode. 138

4.22 The influence of pH on the departure diameter of hydrogen and oxygen bubbles at a 100 μm diameter platinum electrode. 138

4.23 The influence of pH on the departure diameter of chlorine bubbles at a 10 μm diameter platinum electrode. 139

4.24 Bubble as a segment of a sphere. 139

4.25 The influence of pH on the departure diameter of hydrogen bubbles at a 25 μm diameter silver electrode. 154

4.26 Influence of the bulk DTAB concentration on the departure diameter of oxygen bubbles at a 25 μm diameter platinum electrode. 154

4.27 Influence of the bulk DTAB concentration on the departure diameter of hydrogen bubbles at

a 25 μm diameter platinum electrode. 156

4.28 Influence of the bulk DTAB concentration on the departure diameter of oxygen bubbles at a 25 μm diameter platinum electrode, with varying current density. 156

4.29 Influence of the bulk SDS concentration on the departure diameter of oxygen bubbles at a 25 μm diameter platinum electrode. 157

4.30 Influence of the bulk SDS concentration on the departure diameter of hydrogen bubbles at a 25 μm diameter platinum electrode. 157

4.31 The influence of applied potential and electrolyte symmetry on bubble departure diameter during oxygen evolution at a 10 μm diameter platinum electrode. 159

4.32 The influence of electrolyte concentration (sodium nitrate) on bubble departure diameter at a 25 μm diameter platinum electrode. 159

4.33 The influence of rotation frequency on bubble departure diameter during hydrogen evolution at a rotating disk electrode. 161

4.34 The influence of rotation frequency on the current efficiency of hydrogen evolution at a rotating disk electrode. 161

4.35 Bubble departure diameter during hydrogen evolution at a vertical surface (100 μm diameter platinum electrode). 162

5.1 Typical potential transient observed during bubble growth under galvanostatic control. 167

5.2 Influence of the bulk surfactant concentration (DTAB) on electrode potential during oxygen evolution at a 25 μm diameter platinum electrode. 167

5.3 Schematic illustration of a spherical bubble tangent to a planar disk electrode. 168

5.4 Comparison of measured electrode potential with that predicted by calculation. 168

5.5 Typical complex plane impedance plots at a 100 μm diameter platinum electrode, both with and without a bubble. 173

5.6 The influence of bubble diameter on the resistance of a 100 μm diameter platinum electrode. 173

5.7 Schematic illustration of the potential transients, and corresponding amplitude density function, observed during bubble growth. 176

5.8 Autocorrelation function at a 100 μm diameter electrode during the evolution of 260 μm diameter hydrogen bubbles. 176

5.9 Power spectral density function at a 100 μm diameter electrode during the evolution of 260 μm diameter hydrogen bubbles. 177

5.10 Normalised amplitude probability density function at a 100 μm diameter electrode during the evolution of 260 μm diameter hydrogen bubbles. 177

5.11 Power spectral density function of multiple bubble growth at a 100 μm diameter electrode. 178

5.12 The influence of electrode diameter on the power of the power spectral density function obtained during hydrogen evolution at microelectrodes. 178

5.13 Influence of the lateral displacement of a Luggin probe on the probe/cathode potential drop during gas evolution in a macro cell. 181

5.14 Influence of the vertical displacement of a Luggin probe on the probe/cathode potential drop during gas evolution in a macro cell. 181

A1 Schematic illustration of the "thin shell" model of the double layer. 213

LIST OF TABLES

	Page
1.1 Mechanism of hydrogen evolution in acid solution.	25
3.1 Comparison of electrophoretic mobility measurements made using microelectrophoresis and falling sphere techniques.	104
4.1 The influence of electrolyte concentration on the thickness of the thin film between bubble and electrode during oxygen evolution at a 25 μm diameter platinum electrode	150

CHAPTER 1

LITERATURE REVIEW

1 Introduction

2 Electrolytic Bubble Growth

2.1 Mechanism

2.1.1 Electrochemical Kinetics

2.1.2 Bubble Growth Kinetics

2.1.3 Electrode Properties

2.2 Mass Transfer at Electrodes

2.3 Factors Effecting Bubble Growth

2.3.1 Supersaturation and Nucleation

2.3.2 Current Density

2.3.3 Electrode Diameter

2.3.4 Electrode Material

2.3.5 Electrode Morphology/Geometry

2.3.6 Electrolyte/pH

2.3.7 Pressure, Temperature and Viscosity

2.3.8 Bubble/Electrode Contact Angle

2.3.9 Coalescence

2.4 Comparison of Electrolytic and Vapour Bubble Growth

2.5 Effect of Bubble Growth on Current/Potential Distribution, and Overpotential

3 Bubble Properties

3.1 Bubble Charge/Electrophoretic Mobility

3.1.1 Introduction

3.1.2 Bubble Electrophoretic Mobility

3.1.3 Bubble Zeta Potential

3.1.4 Bubble Charge

3.2 Motion of Bubbles in Liquids

3.2.1 Mechanics of Motion

3.2.2 Surfactant Adsorption on Rising Bubbles

3.3 Mass Transfer to a Bubble

3.4 Effect of Bubbles on Inter-electrode Properties

3.4.1 Solution Conductivity

3.4.2 Current Density Distribution

3.4.3 Mass Transfer To Electrodes

4 Summary

1 Introduction

An adequate description of the chemistry and physics involved in the nucleation, growth and detachment of electrogenerated bubbles is of importance in the design of electroflotation cells, chlor-alkali cells, water electrolysers and electrowinning cells. It is also of interest to those involved in the study of the analogous process of nucleate boiling. Characterisation of bubble properties such as rise rate and interfacial charge is also necessary if processes such as fine particle flotation and bubble coalescence are to be fully understood.

Therefore, a study of the growth kinetics and interfacial properties of electrogenerated bubbles is important if the influence of such bubbles on many physical and chemical processes is to be properly described.

2 Electrolytic Bubble Growth

2.1 Mechanism

Bubble generation by electrolysis is one example of a phase formation reaction, though it has been studied to a lesser extent than other phase transitions such as condensation, evaporation, freezing or electro-crystallisation.

During electrolysis, evolved gas dissolves in the solution adjacent to the electrode, leading to rapid supersaturation of the interfacial solution due to the generally low solubility and

diffusion limited transport of the dissolved gas away from the electrode. When the local solubility value is exceeded, nucleation may occur at cavities which constitute active sites on the electrode surface, shown by Murakawa (1) to be tiny surface scratches for bubbles of oxygen and hydrogen on platinum. Growth of nuclei to form bubbles then occurs by diffusion of dissolved gas from solution. The elementary steps in bubble generation are therefore:

Electrogeneration Of Molecular Species
↓
Diffusion Of Species Away From Electrode
↓
Supersaturation of Electrolyte
↓
Nucleation
↓
Bubble Growth
↓
Departure From Electrode

2.1.1 Electrochemical Kinetics

The initial process in the above sequence involves a number of elementary steps which constitute the mechanism of molecular product formation, as distinct from gas bubble production. Information about these elementary steps can be obtained from Tafel plots, i.e. log(current density) vs. overpotential, for the electronation and de-electronation reactions (2). These enable values of the transfer coefficient for each reaction to be calculated, from which the stoichiometry, and consequently the rate determining step, can be assigned. Hydrogen evolution, for example, has been shown to occur via two principal reaction

paths (3), though both mechanisms initially involve the discharge of protons at the electrode to form adsorbed hydrogen atoms:

In acid $M + H_3O^+ \rightarrow MH + H_2O$

In alkali $M + H_2O \rightarrow MH + OH^-$

Two mechanisms of molecular hydrogen formation are then possible:

(i) Chemical desorption $2MH \rightarrow 2M + H_2(surf)$

(ii) Electrodic desorption $MH + H_3O^+ + M \rightarrow 2M + H_2O + H_2(surf)$

The relative significance of steps (i) and (ii) is dependent upon the electrode material, as is the rate determining step, and is summarised in Table 1.1 below.

Electrode Material	Mechanism
Mercury, lead, cadmium	Proton discharge rate determining followed by electrodic desorption
Nickel, tungsten, gold	Proton discharge followed by electrodic desorption
Platinum, rhodium	Proton discharge followed by chemical desorption

Table 1.1 Mechanism of hydrogen evolution in acid solution

One possible reaction path for oxygen is:

$4M + 4H_2O \rightarrow 4MOH + 4H^+ + 4e$

$4MOH \rightarrow 2MO + 2MH_2O$

$2MO \rightarrow O_2 + 2M$

This applies to oxygen evolution at a platinum electrode in acid solution. Tseung et al (4-6) further discuss oxygen evolving electrodes.

Details of the chlorine evolution reaction can be found in the work of Harrison et al (7-13).

2.1.2 Bubble Growth Kinetics

Westwater and co-workers (14,15) carried out early work on the growth kinetics of electrogenerated bubbles. They observed that, following an initial period of surface tension dominated growth, bubbles grew in the manner described by Scriven (16) for diffusion controlled spherical phase growth in an infinite, incompressible Newtonian fluid:

$$r(t)=2\beta\sqrt{Dt} \qquad (2.1.2\text{-}1)$$

where β, the dimensionless growth coefficient, is a function of the density and composition of each phase:

$$\phi=2\beta^3\exp(\beta^2+\varepsilon\beta^2)\int_{\beta}^{\infty} x^{-2}\exp(-x^2-2\varepsilon\beta^3x^{-1})dx \qquad (2.1.2\text{-}2)$$

where $$\phi=(\rho/\rho').(C_\infty-C_s)/(\rho-C_s) \qquad (2.1.2\text{-}3)$$

and $$\varepsilon=(\rho-\rho')/\rho \qquad (2.1.2\text{-}4)$$

Buehl and Westwater (17) adapted Scriven's work to spherical phase growth tangent to a plane in a uniformly

supersaturated liquid. A relationship similar to equation (2.1.2-1) was derived, the only difference being some divergence in β as $\beta \to 0$.

The initial period of non-asymptotic growth noted above is controlled by physical forces such as surface tension, inertia, pressure, and viscosity, and can be described by the reduced Rayleigh equation (18):

$$r(t)=((2\Delta P)/(3\rho))^{0.5}t \qquad (2.1.2\text{-}5)$$

Transition from this mode of growth to that controlled by mass diffusion occurs in a short time, about 0.01 seconds for the analogous case of nucleate boiling (19).

Sillen et al (20,21) also reported bubble growth to be diffusion controlled, though exact interpretation of their data, and that of Westwater et al (14,15), is often complicated by multiple bubble growth, the consequence of which is to make the analysis of individual bubble growth kinetics extremely difficult.

Verhaart et al (22) studied bubble growth at small electrodes (100 μm diameter), liquid paraffin being used to ensure the growth of large bubbles up to 400 μm in diameter. The authors found $r \propto t^{0.33}$, attributing this to direct gas transfer from electrode to bubble. The mass balance for a single spherical bubble then gives:

$$r(t)=\left[(3\hat{R}TIt)/(4\pi PqF)\right]^{0.33} \qquad (2.1.2\text{-}6)$$

Janssen (23) termed this the "total gas production model" and suggested it applied only when the bubble was large compared to the electrode.

2.1.3 Electrode Properties

Properties of the electrode/electrolyte interface, such as double layer capacitance, potential of zero charge, and adsorbed species (24), may well play a significant role in bubble evolution, though this has been considered little by earlier workers. Here, attention will be confined to the platinum electrode since this has been widely used in bubble growth work.

Bard (25) has reviewed the large body of work concerned with the double layer capacitance of platinum, reporting typical values of 10-40 $\mu F\ cm^{-2}$, the magnitude being dependent on electrode pretreatment, experimental technique and adsorbed gas. The latter is a particular problem with platinum due to the ease with which it can become "hydrogen loaded" (26-29). A further complication is the formation of an oxide at high potentials (25,30-36), the mechanism of which, in acidic solution, can be summarised as follows (37). Starting from an oxide free platinum surface, an increase in anodic potential discharges water to give a PtOH surface species. Above 0.9 V v SHE rearrangement of the deposited PtOH occurs to give OHPt via a place-exchange mechanism:

$$Pt + H_2O \rightarrow PtOH + H^+ + e \rightarrow OHPt$$

with complete surface coverage around 1.1 V v SHE. Above this

potential the OHPt species are oxidised to give the PtO oxide, limiting coverage being attained above 2 V v SHE, where a monolayer of PtO_2 exists on a layer of PtO. However, little work has been done on the effect of these oxides on the double layer capacitance and potential of zero charge (p.z.c.) of platinum.

Gileadi et al (38), using impedance techniques, found a linear relationship between p.z.c. and solution pH:

$$\text{p.z.c.} = 0.56 - 2.3(RT/F)\text{pH} \qquad (2.1.3\text{-}1)$$

and showed the p.z.c. to become more negative with adsorbed hydrogen.

These results have been criticised by Frumkin et al (39-44) on the grounds that theoretically the p.z.c. is too high, and experimentally the pretreatment technique used by Gileadi et al (38) to remove hydrogen from the electrode did not prevent oxidation, hence the results were likely to have been obtained with an oxidised electrode. Frumkin et al (39-44) reported p.z.c. values of around 0.18 V with little pH dependence.

The adsorption of inorganic and electro-active organic compounds on platinum has been reviewed by Bard (25), though no reference has been found to the non-electrochemical adsorption of ionic surfactants. Maximum adsorption occurs at or near the p.z.c. of the electrode since water molecules are then weakly bound and can be most easily displaced by non-ionic molecular species.

2.2 Mass Transfer at Electrodes

In general, gas evolution accelerates mass transfer to an electrode by two effects (45):

(i) The ascending bubbles cause a bulk movement of the fluid.

(ii) When a bubble detaches from the electrode it leaves a void into which fresh solution flows, so enhancing the supply of dissolved species to the electrode.

Here, the latter effect alone will be considered, the former being discussed in section (3.4.3).

Mass transfer at gas evolving electrodes has been studied intensively in the past fifteen years (45-57). Two types of mass transfer model are available (58-64); those which consider microevents dominant (the penetration and micro-convection models) and those which consider the macroflow of a gas-electrolyte dispersion to be decisive.

The penetration model of Ibl and Venczel (47) gives the following expression for the Nernst diffusion layer thickness (δ):

$$\delta=\left[(\pi Dr)/(12V(1-B))\right]^{0.5} \qquad (2.2\text{-}1)$$

based upon two assumptions:

(i) An infinite bubble growth rate.

(ii) Mass transfer enhancement occurs only in the time between bubble detachment and nucleation of a new bubble at the same site.

Therefore the mass transfer coefficient, being inversely related

to δ (65), is proportionalto $\sqrt{V}$. Rousar and Cezner (48) modified this by assuming mass transfer to only occur during bubble growth. The mass transfer coefficient then varied from $V^{0.33}$ to $V^{0.67}$ with low to high bubble coverage, in agreement with experimental data (56).

Stephan and Vogt (57) considered mass transfer arising from the radial flow of electrolyte in contact with a growing, hemispherical bubble. Assuming diffusion controlled growth, a model similar to equation (2.2-1) was derived.

Janssen et al (46,61) and Ngoya (66) adapted the microconvection model of Janssen and Hoogland (67) to allow for bubble coalescence. This has been extended recently to allow for electrolyte flow (58).

From experimental observations, Alkire and Yu (62) suggested that micro and macro-convection occur simultaneously, so that both must be taken into account. Similarly a study by Kuhn and Hamzah (63,64) found neither model to be convincingly superior. However, Elsner and Marchiano (60) recently concluded that macroscopic fluid motion arising from bubble departure was dominant.

Further work is obviously needed before firm conclusions can be drawn.

2.3 Factors Effecting Bubble Growth

2.3.1 Supersaturation and Nucleation

Supersaturation of electrolyte with dissolved gas is a pre-requisite for the nucleation of a bubble and its subsequent growth. However, experimental figures for the degree of supersaturation vary considerably. Kabanov (68) measured a relative hydrogen supersaturation of around 100 whereas the calculated supersaturations of Glas and Westwater (14) lay in the range 1 to 20, depending upon the gas evolved and the current density. Shibata (69-72) showed that the gas concentration in the electrolyte immediately adjacent to the electrode increased with current density, approaching a limiting value around 3 kA m^{-2}, in agreement with the results of Bon and Tobias (73). The values reached were 23-165 times the saturation value, and were strongly dependent on the surface condition of the electrode. This can be attributed to the varying ease of formation of active sites with electrode roughness, so effecting the bubble population density, and hence the supersaturation (74).

Vogt (75-77) explained these contradictory findings by distinguishing between two types of supersaturation; that at the electrolyte/electrode interface (as measured by Shibata) and a lower supersaturation in the vicinity of the adhering bubbles. The former governs bubble nucleation and the latter bubble growth.

At a perfectly smooth electrode, such as mercury, nucleation is governed by the growth of clusters of activated gas molecules (those having energies considerably greater than the average) until a critical size is reached at which they become a nucleus (78,79). Conditions for this heterogeneous nucleation depend on both surface and electrolyte properties and have been reviewed by Cole (80,81). Recent work on hydrogen evolution at a mercury pool electrode (82) has shown bubbles to nucleate at current densities considerably less than that predicted by classical nucleation theory (83-85), though this may be explained by the influence of surface hydrophobicity, induced by surfactant contamination, on the ease of nucleation.

Glas and Westwater (14) found the growth rate of an electrogenerated bubble to depend on the size, shape or some other aspect of the nucleation site, and that the size variability of bubbles from different sites was much greater than that of bubbles from an individual site. They concluded that the size of the nucleation site effected the induction time required before bubble formation; a small site requiring a long induction time, so leading to a large local supersaturation and, in turn, rapid bubble growth for short periods.

Also important is the presence on the electrode surface of micro cavities containing undissolved gas, known as Harvey nuclei (86), diffusion to which takes place at supersaturation. Bubbles form preferentially at these pre-existing nuclei; this following from equation (2.3.1-1) (87) which shows the internal excess pressure of the bubble (ΔP) to be less in a crevice of

mouth radius r than on a planar surface where r=0:

$$\Delta P = 2\gamma/r \qquad (2.3.1\text{-}1)$$

Consequently more gas will diffuse into solution from the bubble when it forms on a plane, due to the bubbles greater internal excess pressure, and the ease of formation is reduced. As $t \to \infty$, the internal excess pressure becomes negligible and growth becomes governed by mass diffusion towards the gas/liquid interface. After bubble detachment, some gas remains in the crevice so the same site becomes available for repeated growth (88). Gas behaviour in a crevice has been studied by a number of authors and a summary is given by Urban (89).

A further influence on preferential nucleation is prepolarization (i.e. initially maintaining the electrode at a high currrent density). Ibl et al (45) noted that this usually resulted in a more reproducible and smaller bubble size, attributing this to the activation of smaller surface irregularities, which act as Harvey nuclei to produce small bubbles.

2.3.2 Current Density

Glas and Westwater (14) found an increase in bubble growth rate with increased current density, as would be expected from Faraday's law. Most authors have reported a corresponding increase in bubble departure diameter (90-93) though Janssen and

Hoogland (94) found this to apply only at current densities in excess of 80 mA cm^{-2}. At current densities below this value the authors concluded that bubble size was current density independent. In contrast, Sillen et al (95) have reported bubble departure diameter to be essentially current independent at all current densities.

Venczel (96) observed bubble departure diameter to increase with current density up to a maximum value, above which the diameter decreased. Under conditions of forced convection Sillen et al (97) reported the departure diameter of hydrogen bubbles to decrease with current density.

No authors offer an explanation for the influence of current density on bubble departure diameter, and conclusions are difficult to draw from available data due to the lack of care taken in eliminating possible variables.

Two models predict the dependence of the growth coefficient (β) on current density. The simplest assumes steady state behaviour such that the rate of gas evolution is proportional to the current (14):

$$r = K_1 i^{0.33} \qquad (2.3.2\text{-}1)$$

$$\beta = K_2 i^{0.33} \qquad (2.3.2\text{-}2)$$

K is a proportionality constant dependent on gas density and solubility. However, this model cannot be exact because bubble production can be intermittant with local storage and depletion of solutes occurring continually.

The second, or non-steady state model, follows that proposed by Hsu (98) for bubble growth on a heated wall. The model incorporates a time lag during which gas is generated, and for the electrogeneration of hydrogen can be expressed approximately by (14):

$$\beta = K_3 i^{0.55} \qquad (2.3.2\text{-}3)$$

Glas and Westwater (14) found the steady state model to best describe hydrogen evolution, while the non-steady state model fitted oxygen and chlorine evolution. Both models were applicable to carbon dioxide.

Rousar and Cezner (48) identified three main regions of bubble formation:

(i) At low current densities (< 10 mA cm^{-2}) the number of active sites is small, and hence so is the coverage of the electrode surface with bubbles. The solution at the electrode is only slightly supersaturated and therefore the majority of dissolved gas diffuses into solution.

(ii) At medium current densities (0.001-1 A cm^{-2}) bubble coverage is greater. Only a small proportion of dissolved gas diffuses into solution and bubble growth is given by the steady, or non-steady, state models.

(iii) At high current densities (1-10 A cm^{-2}) the number of active sites is a maximum and loss of gas into the surrounding medium is negligible.

The above is supported by the observations of Janssen and van

Stralen (46) who found bubble population densities to be current independent above 100 A m^{-2}. However, Wedershoven et al (99) have recently shown bubble population density to increase with current under the same conditions.

Vogt (77) has calculated that only a fraction of evolved gas is transformed into bubbles at the electrode. This fraction, expressed as the efficiency of gas evolution, increased from 10-60 % as current density increased from 10-10 000 A m^{-2} (based upon the supersaturation data of Shibata (70-72)). The author states that 100 % efficiency will only be attained as film electrolysis is approached, i.e. as the electrode becomes completely masked by bubbles.

2.3.3 Electrode Diameter

Glas and Westwater (14) found no variation in bubble size when using electrodes of diameter 0.1 to 0.5 mm. However, Mamakov et al (100) found that on increasing the diameter of a platinum electrode from 0.2 to 1 mm, the bubble size increased from 40-60 to 30-90 µm.

Diffusion to very small electrodes, whether mounted individually (101,102) or in groups (103,104), differs from that at planar electrodes because edge effects become significant. Several workers have attempted to model this as a function of electrode diameter and time (104-106), though the problem can be described by hemispherical diffusion as the electrode diameter tends towards zero.

The "total gas production model" of Janssen (23) is also

more likely to apply at small electrodes.

2.3.4 Electrode Material

Tognoni et al (88) studied hydrogen evolution on various electrodes (graphite, vitreous carbon, platinum, mercury, aluminium, titanium, stainless steel, copper, lead, indium) and found no difference in bubble growth except for mercury, where large quantities of small bubbles developed, and vitreous carbon, where a few large bubbles were produced.

Glas and Westwater (14) studied hydrogen evolution on platinum, copper, nickel and iron cathodes, and found that only the initial growth rate was dependent on the material. They proposed that dependence to be a consequence of a difference in active sites, arising from the differing polishing characteristics of the metals. This would lead to a surface dependent supersaturation (see section 2.3.1) and hence differing initial growth rates.

Bubble evolution on transparent nickel (46,91,99) and gold (97,107) electrodes shows similar trends, though fundamental information about bubble growth cannot be obtained from this work due to the large bubble population densities used.

Fahidy and Abdo (108) looked at the relationship between induction time and applied potential (which included an uncompensated ohmic potential loss) for hydrogen evolution on electrodes of copper, tin and chromium. All gave a linear relationship regardless of the electrode material used.

2.3.5 Electrode Morphology/Geometry

Sillen et al (95) compared nickel gauze and perforated plate electrodes and found essentially no difference in bubble behaviour, but noted that electrodes with small gaps became easily blocked by bubbles.

Kuhn et al (109,110) studied the influence of surface roughness on bubble growth and measured typical coverage factors of 0.6 to 0.8 on going from rough to smooth electrodes, greatly exceeding the values of around 0.25 previously reported by Ibl and Venczel (47). Kuhn et al (109,110) suggested that this was because Ibl and Venczel ignored bubbles which were too small to be viewed by their microscopic technique.

2.3.6 Electrolyte/pH

In alkaline solutions bubbles evolved at the cathode have been found to have smaller departure diameters than those at the anode (95), whilst in acid solutions the converse was observed (111). Coehn (112) stated that the magnitude and sign of bubble and electrode charge control bubble departure diameter, larger bubbles being observed when opposite charges exist. However, Kabanov and Frumkin (113) state that at the moment of departure the equilibrium state of the bubble is fully determined by the forces of surface tension, hydrostatic pressure, and pressure inside the bubble, with electrostatic forces being negligible. More recent workers have also considered electrostatic forces to make a negligible contribution to the force of bubble attachment (20,23,95,114), such that the bubble/electrode contact angle

determines bubble departure diameter (see section 2.3.8). However, the contact angle may be zero in a perfectly clean system, in which case electrostatic interaction would become significant.

Janssen and van Stralen (46) found that the bubble population density increased with electrolyte concentration up to a limiting value at 3 molar potassium hydroxide. However, Wedershoven et al (99) found the population density to increase continuously over the same concentration range, attributing this to the activation of smaller nucleation sites with surface tension changes. The authors also noted a corresponding increase in supersaturation, approximated by comparing experimental bubble growth rates with those predicted by Scriven (16). However, at higher concentrations there was an unexplained decrease in supersaturation.

Janssen et al (115) found that the mean departure diameter of both oxygen and hydrogen bubbles decreased with an increase in the concentration of potassium hydroxide over the range 0.1-7.0 mol dm^{-3}. However, this may have been due to the introduction of impurities with added electrolyte.

Local pH changes, due to the depletion of protons or hydroxyl ions, may also be significant, though little work has been done on this. In a recent review Kuhn and Chan (116) concluded that published results were largely discrepant.

The influence of added organics on bubble size has been studied by Blandamer et al (117) and Venczel (96). They noted that the surface area of hydrogen bubbles decreased with added

alcohol due to a decrease in interfacial tension. Therefore impurities must be avoided when studying bubble growth, though this does not seem to have been appreciated in earlier work.

2.3.7 Pressure, Temperature and Viscosity

Janssen and van Stralen (46) found that the bubble population density increased, and bubble size decreased, with pressure over the range 10^4 to 10^6 Pa. This was confirmed by Wedershoven et al (99), who also reported a corresponding decrease in supersaturation, explaining this as a decrease in the number of active sites with increasing pressure.

Janssen and co-workers (115,118) found the mean population density and departure diameter of bubbles evolved under conditions of forced convection to decrease with temperature over the range tested (297-353 K).

When the electrode temperature reaches the boiling point of the electrolyte, combined gas and vapour evolution occurs (23). With increasing potential the current drops due to a loss of contact at the solid/liquid interface, until eventually film electrolysis is reached when a gas and vapour film completely surrounds the electrode.

Funk and Thorpe's (119) work on glycerol mixtures has shown liquid viscosity to have little effect on bubble growth.

2.3.8 Bubble/Electrode Contact Angle

For very small bubbles the contact angle (θ) can be

approximated as:

$$\cos\theta=(h-r)/r \qquad (2.3.8\text{-}1)$$

Young's equation relates contact angle and surface tension and, in its simplest form, can be expressed as:

$$\gamma_{L/G}\cos\theta=\gamma_{S/G}-\gamma_{S/L} \qquad (2.3.8\text{-}2)$$

Frumkin and Kabanov (113) observed a small bubble contact angle at the rest potential of their mercury electrode, though this may well have been due to impurities as the electrode would otherwise be expected to be hydrophilic. However, the hydrophilic or hydrophobic nature of metal surfaces, particularly the noble metals, has been a matter of some controversy in recent years (120-124). On the basis of recent experiments and theories Schrader (125) concluded that the bubble/electrode contact angle should always be zero, and Gardner and Woods (126) state that those authors who report a significant contact angle have not excluded organic impurities from their system.

The contact angle is important when considering the maximum bubble departure diameter (d_M). Fritz (127), assuming small, nearly spherical bubbles equated surface tension to buoyancy and obtained:

$$d_M=1.184\theta.\left[\gamma/g(\rho-\rho')\right]^{0.5} \qquad (2.3.8\text{-}3)$$

Ibl et al (55,128) have summarised this work and give the following relationship to determine the maximum bubble volume (V_M):

$$V_M=(3/\pi)^3.(\gamma/\rho g)^{1.5}.\theta^3 \qquad (2.3.8\text{-}4)$$

However, the contact angle has been found to have no effect on bubble growth rate (14,16) over the range tested (0-100°).

2.3.9 Coalescence

During multiple bubble growth bubbles may grow by coalescence with others in close proximity. Janssen and Hoogland (67,94) observed that in alkaline solutions nearly all collisions between oxygen bubbles led to coalescence, whereas hydrogen bubbles only coalesced at current densities above 5 kA m^{-2}.

Venczel (96) and Westerheide and Westwater (15) noted that, following the coalescence of nearly identical bubbles, the resulting bubble jumped off the surface only to return to the electrode (e.g. bubble jump following the coalescence of 56 and 64 μm diameter bubbles is reported by Westerheide and Westwater (15)). Neither author offered an explanation of this phenomena, though one may lie in the electrostatic interaction between bubble and electrode proposed by Coehn (112), i.e. fluid flow resulting from coalescence causes bubbles to depart from the electrode, the bubbles then being brought back by electrostatic

attraction. When bubbles of differing size coalesce the larger "swallows" the smaller without significant disturbance (15,114).

Thonstad and Tobias (129) studied the coalescence of bubbles growing slowly at adjacent 127 μm diameter electrodes, concluding coalescence to be determined by the balance of two opposing forces, i.e. excess pressure inside the bubble versus electrostatic repulsion between the like charged bubble double layers.

Yang and Maa (130) also studied the coalescence of bubble pairs, observing dilute surfactant solutions (0.1-20 mg dm^{-3}) to increase the coalescence time. The authors attributed this to local surfactant depletion, and consequent surface tension increase, at the growing gas/liquid interface.

2.4 Comparison of Electrolytic and Vapour Bubble Growth

A similarity exists between electrolytic bubble growth and vapour bubble growth arising from superheating. The growth of bubbles on electrodes is mass transfer controlled and driven by supersaturation, whereas the growth of vapour bubbles (nucleate boiling) is controlled by heat transfer, with superheat as the driving force. Both forms of bubble generation are dominated by inertial forces during the initial growth period, though van Stralen (131) concluded that this was more significant during nucleate boiling.

A number of workers have attempted to correlate the two processes (132-134), Bhattacharya and Lienhard (132) concluding

that both are characterised by the same functional equation:

$$R=\Pi(r,Ja,\omega) \qquad (2.4\text{-}1)$$

Should nucleate boiling and electrolytic bubble growth be analogous, use can be made of the large quantity of literature concerning vapour bubble growth (135-147). Darby and Haque (148) stated that the combination of atomic to molecular hydrogen was rate determining for hydrogen evolution on a platinum electrode and, as there is no analogous mechanism in nucleate boiling, caution should be exercised in postulating an analogy between the two. However, these authors appear to have confused molecular hydrogen formation with bubble formation, throwing doubt upon their conclusion.

For water electrolysis in acid media, Janssen (23) defined two regions analogous to those observed in nucleate boiling:

(i) Convection Region. At low current densities, or temperatures, gas dissolves into the bulk solution by diffusion or convection only.

(ii) Isolated and Coalescing Bubble Region. At higher current densities bubbles grow in a non-uniform concentration or temperature field, though the origin of the field differs. In nucleate boiling, heat is transferred from a wall, whereas during electrolysis the gas flux originates in the electrolyte adjacent to the electrode.

When discrete bubbles were formed in nucleate boiling, Abdelmessih et al (137) observed a flow around the

vapour/solution interface during both bubble growth and collapse, and it has been proposed (114) that a large number of small bubbles are formed at high current densities due to this effect. Han and Griffith (138) suggest that the momentum imparted to the liquid ahead of the bubble tends to lift it off the surface if the bubble growth decelerates rapidly enough, and for such bubbles the inertial force alone overcomes surface forces. Siegel (139) states that if a site emits rapidly growing bubbles then these are more likely to exhibit a significant inertial effect.

Trivedi and Funk (114) observed similar phenomena to those described above during electrolytic bubble evolution, possibly for similar reasons. They concluded that inertial forces play an important role in the detachment of small bubbles (12-120 μm), whereas buoyancy determined the departure diameter of larger bubbles.

In contrast to other workers Chesters (149) stated that when a bubble grows rapidly, its growth is impeded by the inertia of the surrounding liquid, concluding that bubbles grow to a greater size before detachment.

Applying van Stralen's relaxation microlayer hypothesis of nucleate boiling (146,131) to electrolysis, Janssen (23) derived an expression for bubble departure diameter at large Jakob numbers ($Ja > \pi/6$):

$$Ja=\Delta C_o/\rho' \qquad (2.4\text{-}2)$$

$$r(t)=(12/\pi)^{0.5}.\Delta C_o/\rho' e.(Dt)^{0.5} \qquad e=2.718 \qquad (2.4\text{-}3)$$

For low Jakob numbers, at which electrolytic bubble growth more typically occurs, Janssen obtained:

$$r(t)=(2\Delta C_0 Dt/\rho')^{0.5} \qquad (2.4\text{-}4)$$

2.5 Effect of Bubble Growth on Potential/Current Distribution and Overpotential

The presence of a bubble on an electrode increases overpotential for two reasons. Firstly bubbles, being non-conducting, distort the potential and current distribution, so increasing the effective current density over regions of the electrode. Secondly, and according to Kuhn and Stevenson (151) more importantly, adhering bubbles create a two dimensional resistive layer on the electrode (152,153).

Sides and Tobias (154) presented an analytical solution for the primary current and potential distribution around a spherical bubble making tangential contact with an infinite planar electrode. Zero at the contact point, the calculated current reached 1 % of its undisturbed value at 30 % of the bubble radius from that point, going through a shallow maximum two radii away. Dukovic and Tobias (155) produced a numerical solution to a similar problem which allowed for gas diffusion and migration, diffusion of the active ion, and concentration and activation overpotentials. The attached bubble was assumed to be of constant size and contained within a stagnant mass transfer boundary layer. The authors found the current density

just beneath the bubble to be several orders of magnitude greater than that at large distances, in contrast to the primary current distribution calculated by Sides and Tobias (154). This was attributed to a reduction in the concentration overpotential of dissolved gas in the vicinity of the bubble.

Sides and Tobias (154) found the incremental ohmic resistance of a sparse array of bubbles to be given by:

$$\Delta R = 2A_0 n\pi r^3/KS \qquad A_0 = 0.9015 \qquad (2.5\text{-}1)$$

Equation (2.5-1) predicts a resistance increase of only 1 % when the bubble diameter is a tenth of the inter-electrode gap. However, when closer than three diameters the bubbles interact significantly, introducing a pinching factor and resulting in a larger than predicted potential disturbance. The pinching factor was estimated to be two or three for a close packed bubble array, though Sides and Tobias (156) later stated that the conductivity of such an array was reduced by a factor of nearly 5.

Wilson and Hulme (157) re-examined the primary current/potential distribution problem and confirmed the result of Sides and Tobias by a more rigorous route. The authors extended the model to apply at all contact angles, concluding the contact angle to be important in so far as it fixed the bubble shape.

Vogt (158) criticised the work of Sides and Tobias (154) as being too complex when the pinching factor was not known.

Assigning an effective conductivity (K') to the bubble layer, Vogt derived:

$$\Delta R = b/AK.((K/K')-1) \qquad (2.5\text{-}2)$$

where b is the thickness of a resistive layer at the electrode (for spherical bubbles b=2r).

Sides (159) modelled a densely populated bubble layer as a hexagonal array of dielectric spheres. Resistance sharply increased as close packing was approached, leading the author to conclude that resistance arising from constriction of the potential outweighed any resistive contribution made by masking of the electrode surface.

Experimental data does not distinguish between the contributions made to the overpotential by local current density enhancement or resistive shielding (160-171), though recent workers (151-153) have concluded that a thin high resistance gas film at the electrode largely determines measured overpotential. Resistance is reported as being independent of current density but dependent upon the gas evolved, the latter arising through the differing bubble diameter at anode and cathode (see section 2.3.6). Fortin et al (172) have modelled the behaviour of a gas film, studying the influence of current density, inter-electrode gap and electrolyte velocity on the geometry of the gas layer.

3 Bubble Properties

3.1 Bubble Charge/Electrophoretic Mobility

3.1.1 Introduction

The formation of double layers, and the separation of electrical charge at solid/liquid, gas/liquid or solid/gas interfaces, is a general phenomenon which has been widely discussed, a recent review being given by Hunter (173). Here only the gas/liquid interface and its interfacial charge will be considered. Such an interface is in general expected to adsorb, or negatively adsorb, ions and so gain an effective electrical charge. When the solution contains ionic surfactants the presence of this effect is not doubted but, in solutions containing non ionic surfactants or only simple electrolytes, the existence of a significant charge is less definite (174). However, a simple electrolyte which increases the surface tension of water must be negatively adsorbed at the gas/solution interface, and unequal negative adsorption of oppositely charged ions (H^+ and OH^- in aqueous solution) will then constitute a charge separation. The resulting interfacial charge influences free ions in the bulk, attracting ions of opposite charge (counter ions) and repelling like (co-ions). Electric double layer theory is concerned with the distribution of these ions and the resulting interfacial electric potentials. The potential difference between the slippage plane, i.e. the plane where

electrolyte can move relative to the charged interface, and the bulk solution is known as the zeta potential (ζ) and is generally assumed to approximate to the potential at the outer Helmhotz plane.

3.1.2 Bubble Electrophoretic Mobility

The electrophoretic mobility of a bubble is defined as the velocity at which it is deflected under a given potential gradient, and has been studied for over a century with little success. McTaggart (175,176) and Alty (177,178) captured bubbles on the axis of a horizontal cylindrical tube, closed at both ends with disc electrodes. By rotating the tube bubbles were held on the axis and the velocity under an applied potential gradient measured. The technique was corrected by Bach and Gilman (179) to allow for electro-osmotic flow of electrolyte.

Dibbs et al (180) and Samygin et al (181) attempted to determine the Dorn potential (which arises from distortion of the diffuse layer when a bubble moves in a liquid) of a swarm of bubbles and a single bubble respectively, but had little success. The work was continued by Usui et al (182,183) and Sotskova et al (184) who measured the Dorn potential of a swarm of argon bubbles, calculating bubble zeta potentials from this (see section 3.1.3).

Microelectrophoresis has also been used to determine bubble electrophoretic mobility (185-189). A microelectrophoresis cell usually consists of a horizontal tube, of either rectangular or cylindrical cross section, provided at each end with a porous

plug leading to reversible electrodes, e.g. Ag/AgCl. The bubbles are viewed through a microscope, a potential gradient applied and the mobility measured. However, in addition to the electrokinetic potential at the gas/solution interface, the field parallel to the cell wall produces electro-osmotic motion of solution at the glass/solution interface. In the closed cell this leads to a return flow along the horizontal axis and means that measurements can be carried out only at "stationary" levels where the net flow is zero (173).

Collins et al (185-187) generated oxygen bubbles at the tip of a platinum wire by applying a 12 V pulse to an oxygen saturated solution of sodium sulphate, cetyltrimethyl ammonium bromide, and ethanol. The authors found that the bubbles, about 35 μm in diameter, had mobilities of $3\text{-}5\times10^{-8}$ m^2 s^{-1} V^{-1} in 0.01 to 0.00005 mol dm^{-3} sodium sulphate, the mobility decreasing with ionic strength due to double layer collapse. However, the authors seemed to ignore hydrogen evolution at the counter electrode, and the solution purity was unspecified, which throws doubt on the validity of the results. Fukui and Yuu (188) used the same experimental design and conditions but extended the bubble size to 75 μm using a TV camera and video-recorder, though the same experimental drawbacks apply. Mobilities of $0\text{-}6.5\times10^{-8}$ m^2 V^{-1} s^{-1} were observed in 0.2 to 0.0001 mol dm^{-3} sodium sulphate.

3.1.3 Bubble Zeta Potential

The double layer theory of solid particles is well defined (173), and the same theories can be applied to bubbles which

have adsorbed sufficient surfactant to render their surface immobile (see section 3.2.2).

The theory was first treated by Helmholtz (190) and Smoluchowski (191) who derived:

$$u=(E\varepsilon\zeta)/(4\pi\eta) \qquad (3.1.3\text{-}1)$$

which is only applicable when the particle or bubble (of diameter a) is large compared to its double layer thickness (κ^{-1}), i.e. at large κa (> 100). For small κa (< 0.1) Huckel (192) applied the theory of conductance in strong electrolytes and derived:

$$u=(E\varepsilon\zeta)/(6\pi\eta) \qquad (3.1.3\text{-}2)$$

Henry (193) showed that both Smoluchowski's and Huckel's equations were limiting forms of:

$$u=(E\varepsilon\zeta/6\pi\eta).1+\lambda f(\kappa a) \qquad (3.1.3\text{-}3)$$

where $\lambda=(K-K')/(2K-K')$, K and K' representing the conductivity of electrolyte and particle respectively.

Henry's treatment accounted for the electrophoretic retardation resulting from the opposing movement of counter ions and associated solvent. However, it did not allow for the so-called relaxation effect arising from the accompanying distortion of the ionic atmosphere, which is significant for

intermediate κa. Booth (194,195) and Overbeek (196,197) studied this region and showed electrophoretic mobility (u/E) to vary as a power series of zeta potential. More recently numerical solutions have come from Wiersma et al (198) and O'Brien and White (199).

Therefore, bubble electrophoretic mobility measurements in concentrated surfactant solutions can be analysed using these theories. However, in a clean system bubbles have mobile interfaces at which the tangential component of fluid velocity is continuous. This invalidates interpretation of bubble mobility data by theories developed for solid particles, though most authors have ignored this.

No theoretical work has been carried out on the mobility of gas bubbles, but an analogy can be drawn to work on fluid (200-202) or mercury (203,204) drops, both of which have mobile interfaces.

Booth (200) adapted the theory of Henry (193) to fluid drops. For $\kappa a \gg 1$, and assuming the double layer charge to reside at the interface, the electrophoretic velocity is given by:

$$u=(E\varepsilon\zeta)/(6\pi\eta).[(3\eta'(1+\lambda)+2\eta(1-2\lambda))/(3\eta'+2\eta)] \quad (3.1.3\text{-}4)$$

For a gas bubble the internal viscosity (η') can be taken as zero. In this case, Booth's equation predicts zero electrophoretic velocity regardless of zeta potential, contrary to experimental evidence (174-178), though the possibility of a

contamination-induced mobility must be considered. Booth suggested that the assumption of constant viscosity and charge throughout the double layer may be invalid for gas bubbles.

Sengupta (202) modified Booth's theory by introducing the surface conductivity correction first proposed by Henry (205) and Booth (206) for solid particles. This allowed for an excess conductivity (K_s) in an infinitesimally thin surface layer, though no mechanism by which such a layer could exist was given. Using otherwise identical assumptions to Booth (200), and assuming zero internal viscosity, Sengupta derived the following equation for a bubble :

$$u=(E\varepsilon\zeta)/(2\pi\eta).K_s/(K_s+Ka) \qquad (3.1.3\text{-}5)$$

This predicts a decrease in velocity with bubble size, and overcomes Booth's anomaly of zero mobility. However, Sengupta's treatment is not necessarily correct because no attempt was made to model the redistribution of charge around rising bubbles in the presence of an electric field.

Levine and O'Brien (204), adapting the theory of Levich (203), derived the equation:

$$u=(E\sigma a)/(3\eta'+2\eta).\left[1-(\sigma^2/K(3\eta'+2\eta))\right] \qquad (3.1.3\text{-}6)$$

for mercury drops at large κa and small charge densities. While equation (3.1.3-6) cannot be applied directly to gas bubbles, since mercury drops are assumed ideally polarisable, it is

interesting to see that equation (3.1.3-6) predicts electrophoretic velocity to increase linearly with drop size.

Collins et al (185-187) reported zeta potentials of 50-60 mV for oxygen bubbles in the presence of a cationic collector. Fukui and Yuu (207), in their work on electroflotation, used a similar technique to Collins et al except that the bubbles were removed from the flotation cell and then introduced into the microelectrophoresis cell. They determined the zeta potential of oxygen bubbles in 0.0001 to 0.01 mol dm^{-3} $AlCl_3$ to lie in the range 50-10 mV. The same authors (188) reported zeta potentials of 0 to 85 mV for oxygen bubbles in CTAB (cetyltrimethyl ammonium bromide) using a microelectrophoresis technique.

Usui et al (182,183) considered the influence of the ionic surfactants sodium hexadecyl sulphate, and hexadecyltrimethyl ammonium bromide. If their data is extrapolated to very low surfactant concentrations, a bubble zeta potential of -10 to -20 mV is indicated.

Lopatenko (208) reported a technique for determining bubble zeta potential from the pH change induced by gas dissolution in an electrolyte, though this cannot be correct since pH is not indicative of surface charge.

Kubota et al (189) produced small air bubbles by pressure release, added surfactant, and poured the resulting suspension into a conventional microelectrophoresis cell. On adding a cationic surfactant, 0.01 to 1.0 mol dm^{-3} cetylpyridinium chloride, zeta potentials of 14-32 mV were calculated. An anionic surfactant, sodium dodecyl sulphate, gave potentials of

-30 to -160 mV over the range 0.02 to 3.0 mol dm^{-3}. Kubota et al (189) compared their results with those obtained by Dorn potential measurements on 1-2 mm diameter bubbles (209). The latter gave zeta potentials 10-80 % greater than those obtained using microelectrophoresis, the authors attributing this to differing flow dynamics past bubbles of differing diameters.

Cichos (210,211) used spinning cylinder electrophoresis, pioneered by McTaggart (175,176) and Alty (177,178), to determine the zeta potential of air bubbles. A value of -34 mV was obtained which remained constant over the concentration range 0.1 to 0.00001 mol dm^{-3} potassium chloride.

All the above workers used the theory of Smoluchowski (191) to obtain zeta potential values from their electrophoretic mobility data.

3.1.4 Bubble Charge

Huddleston and Smith (174) carried out two experiments in an attempt to determine the charge at the gas/solution interface. They first used spinning cylinder electrophoresis to study nitrogen bubbles and, by extrapolation of their data, found the isoelectric point to lie in the pH range 1-2. However, the authors found three main disadvantages to the technique:

(i) The single bubble used was likely to adsorb any surfactant impurity from solution.

(ii) The electrophoretic force was proportional to the square of the bubble radius due to the action of Coriolis forces.

(iii) The force on the bubble due to spin prevented the measurement of a simple electrophoretic mobility, and decreased the sensitivity of the technique.

Therefore a second experiment was designed (174) using an air/liquid interface in a trough cell. Great experimental difficulties were involved but, for simple electrolytes, the authors found indications that at high pH the gas/electrolyte interface was less negatively charged than the glass/electrolyte interface, and more negatively charged at pH 3. This was consistent with their previous experiment which suggested a point of zero charge (p.z.c.) around pH 1-2.

Despite these problems (174), McShea and Callaghan (212) extended the work on spinning cylinder electrophoresis, confirming the observations of Huddleston and Smith and reporting negative zeta potentials of 2-5 mV for bubbles in potassium chloride and anionic, or non ionic surfactant. Potentials of -0.6 to -74 mV were obtained in distilled water over the pH range 4-7, the unusually high potential at pH 7 being attributed to the presence of a mobile bubble interface. However, the authors' calculation of zeta potential assumed both a rigid interface and polarisation of surface charge, though the latter seems unlikely on a fixed, non conducting surface. These assumptions throw doubt on the validity of the reported zeta potentials . McShea and Callaghan also found a non-linear relationship between bubble mobility and electric field strength, in contrast to the direct proportionality predicted by conventional theory. The authors attributed this to the

influence of cell rotation on the bubble's double layer.

Matov and Okun (213,214) measured the deflection of bubbles as they rose through an electric field in aqueous solution. They concluded that bubbles were negatively charged, and that the surface charge density decreased with increasing bubble size, in agreement with the observation of Usui et al (183). However, solution purity again seems to have been ignored.

Nazarova et al (215,216) and Poberezhnyi et al (217) studied the influence of a magnetic field on rising bubbles, observing that the bubbles carried a charge of the same sign as the source electrode.

A theoretical treatment of the electric field of a moving bubble is given by Dukhin et al (218-222) who discuss the electrokinetic effect which operates when an interface containing ions of differing diffusion coefficients is extended or compressed.

3.2 Motion of Bubbles in Liquids

3.2.1 Mechanics of Motion

The velocity at which bubbles rise through a liquid is determined principally by the buoyancy force that drives it upwards, and the retarding viscous drag. When these two forces are equal the bubbles rise at a constant velocity. Similar considerations allow the calculation of the terminal falling velocity of solids, though there are three major differences between the motion of bubbles and particles (203,223):

(i) A bubble is not rigid, hence forces acting on it may deform its shape.

(ii) The tangential velocity component does not reach zero at the gas/liquid interface, unlike the solid.

(iii) Gas within the bubble may circulate, so affecting the drag force.

The behaviour of bubbles can be classified into four regions using the Reynolds number (Re), which reflects the ratio of inertial to viscous forces involved in bubble motion (203,223):

$$Re=vd\rho/\eta \qquad (3.2.1-1)$$

(a) In a clean system, such that the bubble has a mobile interface, small bubbles (Re < 1, d < 0.1 mm) rise at a terminal velocity of (203):

$$v=1/3.gr^2.(\rho-\rho')/\eta \qquad (3.2.1-2)$$

This follows from the Rybczynski-Hadamard equation (224,225) for fluid drops with η', the internal viscosity, set to zero:

$$v=2(\rho-\rho')gr^2.1/3\eta.(\eta+\eta')/(2\eta+3\eta') \qquad (3.2.1-3)$$

If sufficient contamination is present to "freeze" the bubble surface (see section 3.2.2) then Stokes law applies:

$$v=2/9.gr^2(\rho-\rho') \qquad (3.2.1-4)$$

and the bubble will rise 50 % slower than in a clean system.
(b) For intermediate size spherical bubbles (50 < Re < 400) Levich (203) obtained:

$$C_D=48/Re \quad , \quad v=1/9\eta.gr^2(\rho-\rho'). \qquad (3.2.1\text{-}5,6)$$

This was adapted by Moore (226) to allow for velocity perturbation in the bubble boundary layer, giving:

$$C_D=48/Re.(1-(2.211/\sqrt{Re})+O(Re^{-0.83})) \qquad (3.2.1\text{-}7)$$

The leading term represents the irrotational dissipation of viscous energy, the second boundary layer and wake perturbation, and the third an error term arising from the neglect of surface stress and viscous dissipation at the rear of the bubble.
(c) Ellipsoidal bubbles (400 < Re < 5000) rise in a spiral path with their maximum diameter in a horizontal plane. Generally this occurs with bubbles of 1.5-9 mm diameter.
(d) Spherical cap bubbles (Re > 5000) rise at a terminal velocity which is independent of fluid properties (227):

$$v=1.02(2gr^2)^{0.5} \qquad (3.2.1\text{-}8)$$

3.2.2 Surfactant Adsorption on Rising Bubbles

Experimental results on the motion of bubbles in fluids have shown that below a certain critical size, typically 0.5 mm,

bubbles behave as solid spheres. This has been explained as being due to contamination of the gas/solution interface by surfactant. At a critical size the bubble surface area will be such as to allow complete coverage of the bubble with surfactant, so increasing the effective interfacial viscosity and bringing surface motion nearer to that at a solid sphere. Adsorbed surfactant concentrates at the rear of a rising bubble reducing surface tension and, in turn, increasing surface tension at the front of the bubble. The ensuing surface tension gradient results in the diffusion of surfactant from the rear of the bubble to the front, and retards the interfacial motion. Therefore, surfactants have a great effect on bubble rise rate (203,223,228,229).

The dynamic effect of surfactant adsorption has been treated theoretically (203,223,230-232) with the mechanics of bubble motion, surfactant diffusion and surfactant adsorption being considered.

Pashley (233) and Anfruns and Kitchener (234) used the rise rate of a bubble in aqueous solution as a measure of the cleanliness of that solution. Even after distillation, ion exchange and activated charcoal washing, their was still evidence of contamination, illustrating the sensitivity of the technique. Similarly, Linton and Sutherland (235) observed bubbles to rise as solid spheres in the presence of only a few p.p.m. octyl alcohol, whereas the equilibrium surface tension dropped only slightly.

3.3 Mass Transfer to a Bubble

Mass transfer between bubbles and the surrounding liquid has been studied extensively (236-250). However, comparison of experimental mass tranfer coefficients ($\bar{k}$) reveals considerable scatter due to the numerous factors, such as gas circulation and bubble deformation, which can influence the mass transfer process.

Four major regions of bubble behaviour can be defined in terms of the Reynolds number (Re), the Sherwood number (Sh), and the Schmidt number (Sc):

$$Sh=\bar{k}d/D \qquad Sc=\eta/\rho D \qquad Re=vd\rho/\eta \qquad (3.3\text{-}1,2,3)$$

(a) Re < 1. For a mobile gas/liquid interface Azbel (249) gives:

$$Sh=0.65(\eta/(\eta+\eta'))^{0.5}(Re.Sc)^{0.5} \qquad (3.3\text{-}4)$$

However, in most systems surfactant contamination means that the bubble surface is immobile and mass transfer can be expressed by (240):

$$Sh=0.99(Re.Sc)^{0.33} \qquad (3.3\text{-}5)$$

(b) 1 < Re < 100. By analysis of the boundary layer around mobile spheres Chao (243) obtained:

$$Sh=1.13(1-(2.96/Re^{0.5})).(Re.Sc)^{0.5} \qquad (3.3\text{-}6)$$

If no gas circulation is assumed then (249):

$$Sh=0.56Re^{0.5}Sc^{0.33} \qquad (3.3\text{-}7)$$

(c) For bubbles in the region 100 < Re < 400, with gas circulation, mass transfer is not well defined. Many empirical and semi-empirical correlations have been proposed, and are reviewed by Azbel (249).

(d) For spherical cap bubbles (Re > 400) Takadi and Maeda (241) proposed the following correlation:

$$Sh=1.28(Re.Sc)^{0.5} \qquad (3.3\text{-}8)$$

assuming an axis ratio of 3.5.

3.4 Effect of Bubbles on Inter-electrode Properties

3.4.1 Solution Conductivity

The presence of bubbles in an electrolyte leads to a drop in conductivity relative to the gas free state (251), and hence an increase in the ohmic potential loss (168). The significant resistive contribution made by a layer of close packed bubbles adjacent to the electrode has already been discussed (section 2.5). Here, the effects of bubbles spatially distributed in the bulk electrolyte will be considered.

Three classical models exist for the case of uniformly

distributed spherical bubbles in an infinite electrolyte. The first follows from Maxwell (252):

$$K/K_0=(1+0.5\xi)/(1-\xi) \qquad (3.4.1\text{-}1)$$

the second from Bruggeman (253):

$$K/K_0=(1-\xi)^{1.5} \qquad (3.4.1\text{-}2)$$

and the third from Rayleigh (254), with a later correction by Runge (255):

$$K/K_0=\left[1+(3/2.(\xi/1-\xi))\right]^{-1} \qquad (3.4.1\text{-}3)$$

Tobias and co-workers (251,256) found equation (3.4.1-3) superior at low gas voidage ($\xi < 0.1$) whereas equation (3.4.1-2) gave a better fit at large gas volume fractions.

Empirical equations attempting to describe solution conductivity in terms of gas voidage have been collected by Meredith and Tobias (256), who concluded that all were inferior to classical theory.

Gas voidage is dependent on electrolyte flow rate, electrode structure and orientation, and current density. Numerous authors have discussed these problems, which were reviewed comprehensively by Vogt (74). More recent contributions have come from Elsner and Coeuret (257), Kreysa and Kuhn (258), Vogt (259), Hine et al (260), and Janssen et al (261,262).

From the literature it can be concluded that:

(i) Bubble induced ohmic potential losses decrease with electrolyte flow rate because of a reduced bubble residence time.

(ii) Perforated electrodes allow bubble escape if correctly designed, hence ohmic potential losses are reduced.

(iii) Horizontally mounted electrodes allow bubbles to accumulate at the upper electrode, increasing the ohmic potential loss. Losses decrease as the electrode approaches the vertical.

(iv) Gas voidage increases with height up a vertical electrode due to the non uniform distribution of bubbles with differing rise rates.

(v) Current density increases gas voidage, and consequently the ohmic potential loss, by increasing the volume of gas produced.

3.4.2 Current Density Distribution

The presence of non conducting gas bubbles between two electrodes will distort the inter-electrode current distribution. Tobias (263) characterised this by a single dimensionless parameter for a flat, vertical sheet electrode in stagnant electrolyte. This was extended by Hertwig et al (264), and Rousar and co-workers (265-267), to allow for differing bubble rise rates and electrolyte flow. Nagy (167) considered the bubble induced current distortion for an electrode built of vertical blades, whilst Hine and Murakami (170) studied the

current distribution of cells under varying flow conditions.

All authors concluded that the non uniformity of the current distribution increased with gas voidage.

3.4.3 Mass Transfer To Electrodes

The effect of gas evolution at an electrode on the mass transfer to that electrode has already been discussed (section 2.2). However, the passage of bubbles between two electrodes can also effect mass transfer through turbulent diffusion (45,53). Sigrist et al (268) considered the eddies formed in the wake of rising bubbles to be the main cause of turbulence and arrived at the empirical relationship:

$$Sh=0.19(Sc.Ar)^{0.33} \qquad (3.4.3\text{-}1)$$

where Ar= modified Archimedes number= $dg\xi/\nu^2(1-\xi)$

This model exhibits a strong similarity to the established correlation for turbulent natural convection at horizontal vertical plates (269), showing mass transfer to be controlled by the flow of a quasi-homogeneous bubble electrolyte dispersion (268). Jennings et al (270) reached a similar conclusion from work on two phase flows, showing mass transfer enhancement to arise from the increased velocity of the electrolyte due to the presence of gas.

4 Summary

The principal factors effecting bubble growth are the nature of the active sites, current density, electrolyte composition and surfactant concentration. Bubble sensitivity to surfactant is also important when determining bubble properties such as rise rate and charge. For this reason future work should be carried out with surfactant free electrolytes, a feature which has been largely ignored previously. Further complications are the disturbance of the current/potential distribution by bubbles, and characterisation of individual bubbles, though the latter may be overcome using very small electrodes to ensure single bubble growth.

Measurement of electrode charge is important in determining bubble departure diameter in a clean system, a fact ignored by recent workers, and requires knowledge of the potential of zero charge.

When measuring bubble charge, particular care must be taken in calculating zeta potential from electrophoretic mobility data, because standard theory cannot be applied to bubbles with a mobile interface. Again this has been largely neglected in previous work.

CHAPTER 2

EXPERIMENTAL DESIGN

1 Preparation Of Surfactant Free Electrolytes

1.1 Water Purification

1.2 Electrolyte Preparation

1.3 Detection Of Impurities

1.3.1 Surface Tension

1.3.2 Cyclic Voltammetry

1.3.3 Bubble Rise Rate

2 Bubble Electrophoretic Mobility and Growth Measurements

2.1 Cell Design

2.2 Electrode Preparation

3 Current, Potential, Impedance and Electrode Area Measurement

1 Preparation Of Surfactant Free Electrolytes

1.1 Water Purification

The preparation of surfactant free water was a pre-requisite for this work, so a suitable purification system was built, as shown in Fig. 2.1. The water was distilled, passed through columns of anionic (Duolite A101D) and mixed anionic/cationic (Zerolit DMF) exchange resins to remove ionic impurities, through activated charcoal to remove organics, and then re-distilled from "Analar" grade (B.D.H. Ltd.) alkaline potassium permanganate and acidified potassium dichromate to remove residual organic acids and amines respectively.

Fig. 2.2 illustrates the apparatus used for electrolyte preparation. Both this and the distillation system earlier described were constructed of glass and PTFE and kept under white spot grade nitrogen bubbled through alkaline potassium permanganate and acidified potassium dichromate. Water was directly distilled into vessel A and electrolyte added in the mixing vessels D.

All glassware was cleaned prior to use by soaking in chromic acid (CrO_3/H_2SO_4) for at least 12 hours before rinsing with triply distilled water.

1.2 Electrolyte Preparation

Whilst all electrolytes were of "ARISTAR" grade (B.D.H. Ltd.), it has nevertheless been shown (271,272) that these may contain surface active impurities. Hence, solid electrolytes

A Primary distillation: 4×1 kW heaters give an output of 8 dm^3 hr^{-1}.

B 20 dm^3 reservoir.

C PTFE lined pump.

D 0.1×0.8 m column containing anionic exchange resin.

E 0.1×0.8 m column containing mixed anionic/cationic exchange resin.

F 0.1×0.8 m column containing activated charcoal.

G Secondary Distillation: 2×1 kW heaters give an output of 4 dm^3 hr^{-1}. Contains 0.02 mol dm^{-3} potassium permanganate and 0.04 mol dm^{-3} sodium hydroxide.

H Tertiary Distillation: 2×1 kW heaters give an output of 4 dm^3 hr^{-1}. Contains 0.03 mol dm^{-3} potassium dichromate and 0.08 mol dm^{-3} sulphuric acid.

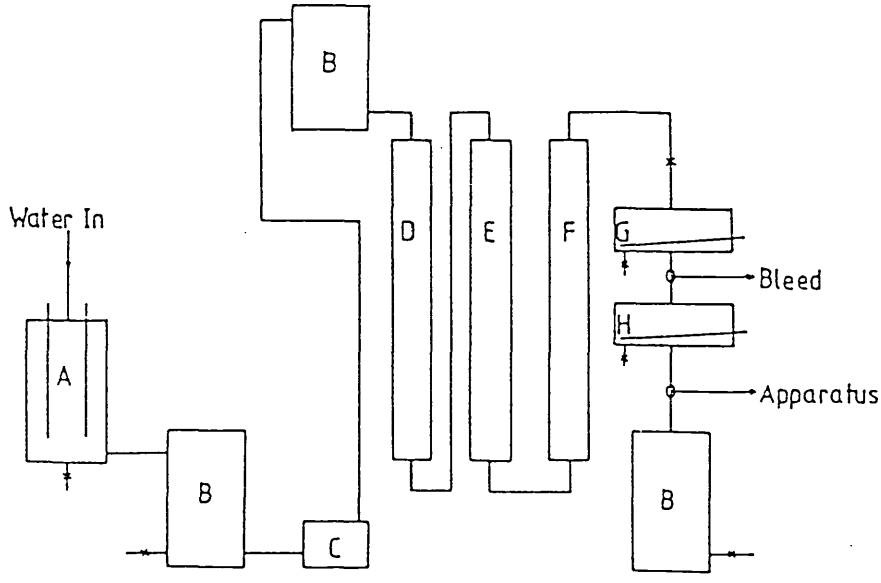


Fig. 2.1 Distillation system for the production of surfactant free water.

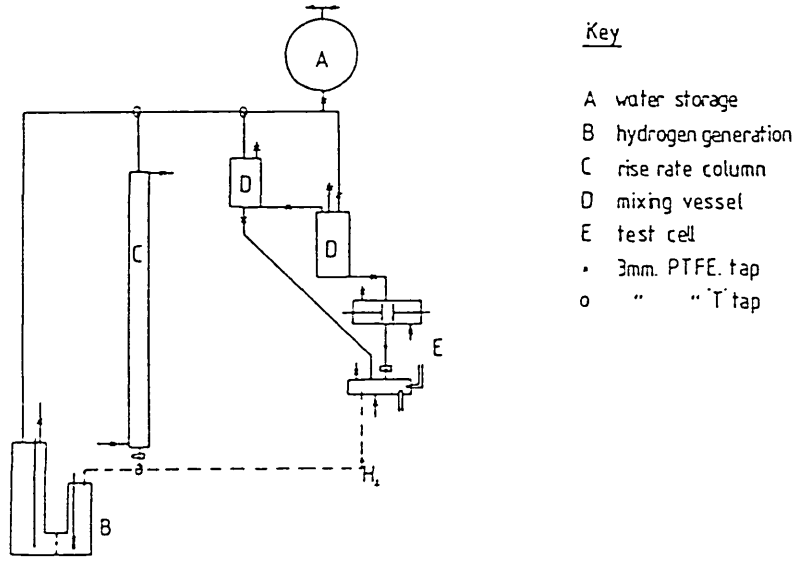


Fig. 2.2 Electrolyte preparation apparatus.

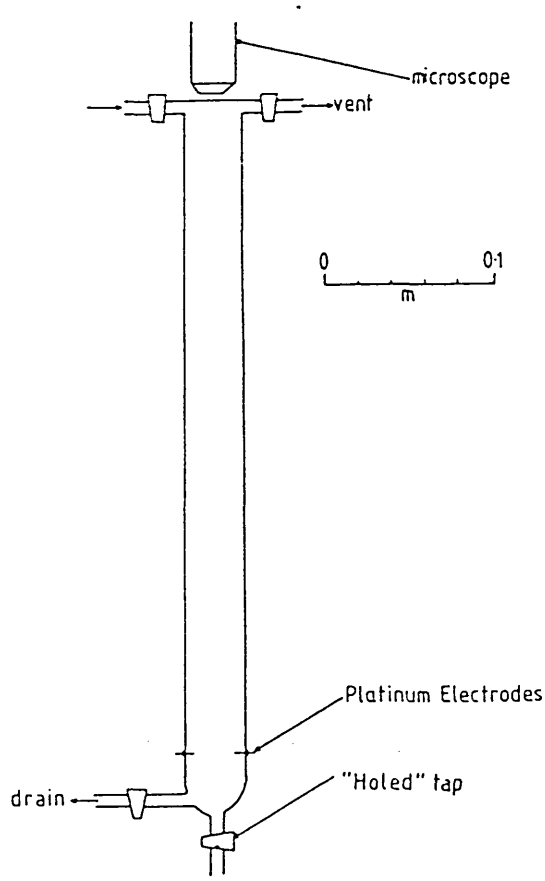


Fig. 2.3 Bubble rise rate column.

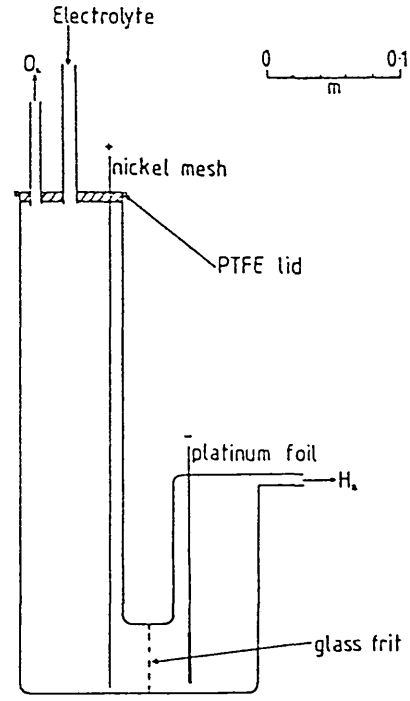


Fig. 2.4 Gas generation device.

were heated to red-heat to decompose organic impurities, sealed in glass ampoules, and broken in the apparatus under nitrogen.

To try to ensure the complete removal of surfactant, all electrolytes were purged with gas before use. Impurities concentrated at the gas/electrolyte interface (see chap.1, section 3.2.2) and were swept out of solution over a wier (273-276).

1.3 Detection Of Impurities

Three techniques were used to assess electrolyte purity.

1.3.1 Surface Tension

Impurities, both ionic and organic, affect electrolyte surface tension (273-275), which was measured using a Krüss K10 Digital Tensiometer.

1.3.2 Cyclic Voltammetry

Impurities on an electrode or in solution can be detected by sweeping the potential and monitoring the current. Conway et al (277) have characterised the voltammogram of pure platinum in a clean system and comparison can be made to this. Impurities typically block H/OH adsorption/desorption and give bigger oxidation peaks.

Voltammograms were obtained using a Hi-Tek Instruments wave-form generator, a Wenking MP81 potentiostat and a Nicolet Instrumentation Explorer 1 digital oscilloscope linked to a JJ Instruments XY/t recorder.

1.3.3 Bubble Rise Rate

Surfactants concentrate at the bubble interface, inducing surface tension gradients and lowering the rise rate (273-275). Fig. 2.3 illustrates the column used to measure bubble rise rate, the diameter of the column being at least 20 times that of the bubbles so that wall effects could be neglected. Oxygen (or hydrogen) was electrolytically generated from "clean" water plus added electrolyte (Fig. 2.4), and bubbles produced using a glass tap, modified so that by rotation of the tap a small volume of gas could be trapped, and then released to form a bubble.

Bubble velocity was measured electronically using two Centronic OSI-5K silicon photodetectors, placed 0.1 m apart, and a digital oscilloscope. Lighting was by an Allen fibre optic light source. Bubble diameter was measured at the top of the column using a calibrated microscope.

Two platinum flag electrodes were placed towards the base of the column so that the effect of electro-generated bubble cleaning could be studied.

2 Bubble Electrophoretic Mobility and Growth Measurements

2.1 Cell Design

Fig. 2.5 illustrates the apparatus used for the bulk of this work. Bubbles were generated in the lower cell at a vertically mounted electrode, and observed using a horizontally mounted microscope coupled to a Link Electronics TV camera, Sony

SL-F1UB video-recorder and Sony CVM-110UK monitor. This gave a time resolution of 20 msec and a magnification up to 1000. For better time resolution a Hadlands Ltd. Hyspeed camera (10-10 000 f.p.s.) with Kodak RAR 2479 film and L.E.D. timing light generator was used. 0.01 mol dm^{-3} sodium sulphate was used as the supporting electrolyte for hydrogen and oxygen bubble evolution, pH being varied with sulphuric acid or sodium hydroxide. Sodium sulphate was preferred to 1:1 electrolytes such as sodium perchlorate or sodium nitrate, as it could be heated to red heat to decompose organics. 0.01 mol dm^{-3} potassium chloride was used when studying chlorine bubbles, pH adjustment being made with hydrochloric acid or sodium hydroxide. It should be noted that the total ionic strength was greater than 0.01 mol dm^{-3} when operating in strongly acidic ($pH < 2$) or basic ($pH > 12$) solution. Before use, the cell was purged with gas generated at two platinum flag electrodes to remove surfactant by ion flotation (273-276), and then saturated with the gas under test, produced in the gas generation device (Fig. 2.4).

Following departure the bubble was transferred into the upper cell, using either a "holed" or standard tap, where its deflection in an electric field could be measured. Hence the electrophoretic mobility of individual bubbles of known diameter and history could be determined.

Two Roband Varex 60-5 power supplies connected in series were used to apply a potential of up to 120 V across two electrodes. Palladium plated platinum electrodes were used when studying hydrogen and oxygen bubbles, the palladium being

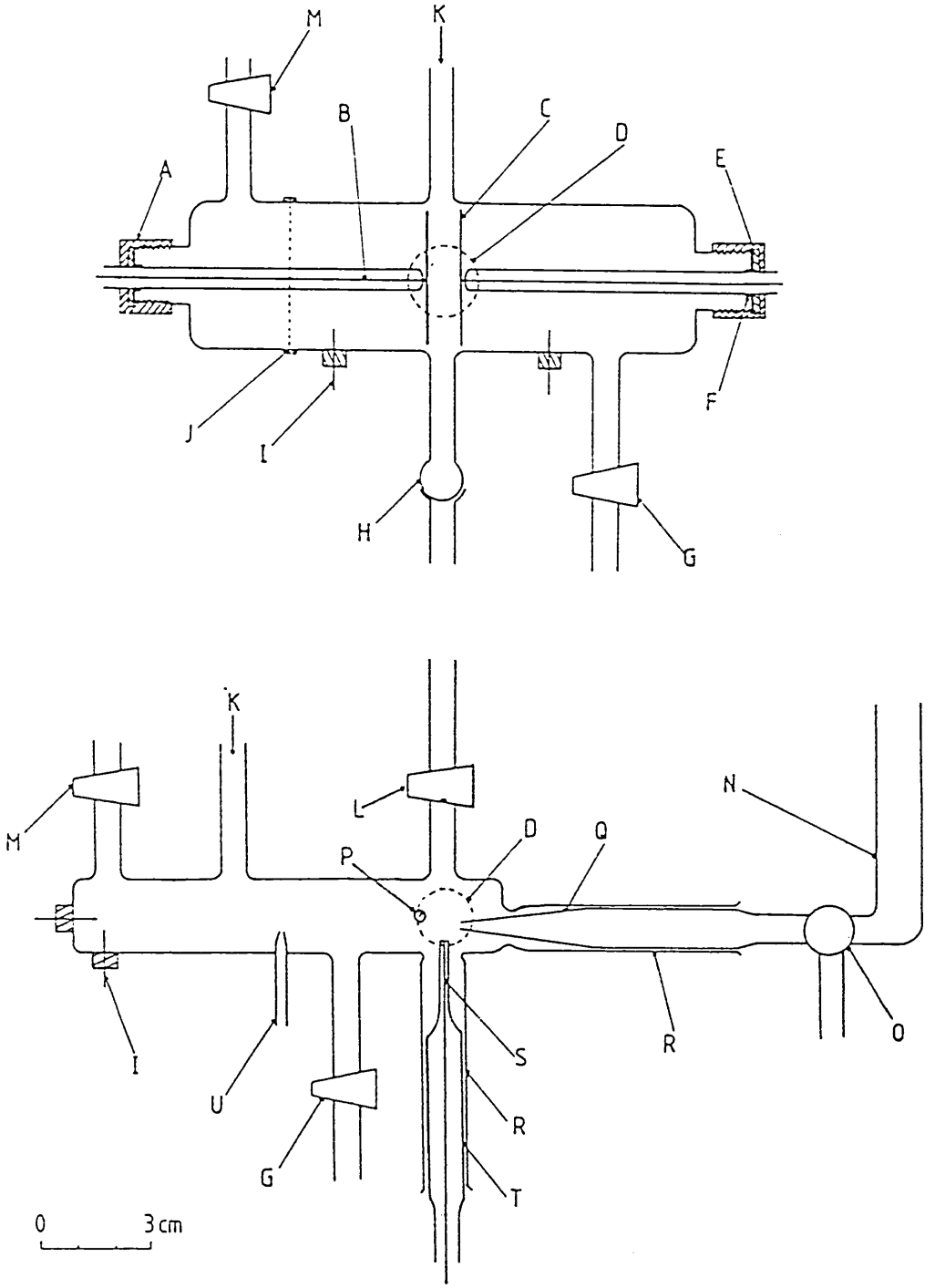


Fig. 2.5 Cell used for the measurement of bubble growth kinetics and bubble charge.

Key to Fig. 2.5

A Screw cap for electrode adjustment.

B Platinum wire sealed in glass.

C 0.02×0.03 m electrode.

D Optically flat window.

E Rubber seal.

F PTFE seal.

G 3 mm bore PTFE tap.

H Ball and socket joint.

I Platinum flag purging electrode.

J Glass flange.

K Electrolyte inlet.

L "Holed" tap.

M 3 mm bore PTFE tap to wier.

N Reference electrode.

O 3 mm bore glass 'T' tap.

P Platinum counter electrode.

Q Glass Luggin probe.

R Glass syringe barrel.

S Working electrode sealed in glass.

T Ground glass syringe plunger.

U Gas inlet.

cathodically deposited onto platinum foil at 5.5 mA cm^{-2} from a stirred solution of 2 % palladium chloride in molar hydrochloric acid (278). Silver/silver chloride electrodes were used to deflect chlorine bubbles. These were prepared by anodizing silver sheet at 0.4 mA cm^{-2} in 0.1 mol dm^{-3} hydrochloric acid for 30 minutes (279). Reversible electrodes were necessary to prevent gas formation accompanying application of the electric field.

The electrolyte was purged with gas before use and pH measured after each test using a Pye Unicam PW9418 pH meter and suitable combination glass electrode.

Bubble deflection was again studied using a microscope and TV camera. Bubble diameter was limited to the range 30-200 μm due to optical problems with either magnification or depth of field, a higher magnification giving a reduced depth of field and therefore reduced measurement time.

Milli-molar sodium sulphate or potassium chloride was used as supporting electrolyte in the upper cell, the lower ionic strength allowing high potential gradients to be used without unwanted gas evolution. The ionic strength limit also restricted the pH range to 2-10.

The design of the upper cell, whereby bubble deflection was measured over a short time and in the centre of a relatively large volume, meant that electro-osmotic flow at the cell walls could be ignored. This assumption was checked by measuring the mobility of glass spheres whose charge had been previously determined using a Rank Bros. microelectrophoresis apparatus.

It was important to avoid heating of the electrolyte during the measurement of bubble charge, as this led to convection currents and decreased the experimental accuracy. Therefore, measurements of the temperature change were made, and showed that heating of the electrolyte by the TV camera light source was negligible (< 1 K), as was electrical heating arising from the passage of current with application of the electric field.

All reported electrophoretic mobility data are the mean of 10-20 measurements and have a typical error of ±10-20 %, the error increasing with bubble diameter due to the increased rate of rise, and hence reduced measurement time.

Bubble evolution at rotating electrodes was studied in a different cell to that illustrated by Fig. 2.5. Electrodes were held vertically in a rotating mount (Fig. 2.6) and driven using an Oxford Electrodes motor-controller and rotating electrode contact block. Bubbles were observed using a microscope and TV camera.

Experiments involving the deliberate addition of surfactants were left to the end of the work to prevent possible contamination. High purity dodecyltrimethyl ammonium bromide (Kodak Ltd.) and sodium dodecyl sulphate (B.D.H. Ltd.) were used. Before each experiment, glassware was washed in a dilute solution of the surfactant to be used. This "loaded" the surface of the glass with surfactant and prevented subsequent adsorption during experimentation.

Results were fitted to proposed models using non linear regression analysis.

All experiments were carried out at a temperature of 293±2 K and pressure of 101±2 kN m^{-2}.

2.2 Electrode Preparation

Wires of high purity platinum or silver (99.99 %+, Goodfellow Metals Ltd.) were used to make electrodes of 10-500 μm diameter. The wire was first sealed in glass, this being done under vacuum for wires 25μm or less in diameter to ensure a good glass to metal seal. The wire and its glass sleeve were then attached to a ground glass syringe and mercury added to make electrical contact with the wire.

Screened cable was fitted to the end of the syringe such that the central wire projected into the mercury, the plastic surround preventing the mercury from escaping. The syringe was connected to the screen wire and a "bnc" connector added. Fig. 2.7 illustrates a complete electrode.

Rotating disk and cylinder electrodes (Figs. 2.8-2.9) were constructed in a manner similar to that of the syringe mounted type. Platinum wires of 100 μm diameter were used, electrical connection being made, via mercury and a steel pin, to brass fittings.

After completion, electrodes were polished with increasingly fine grades of silicon carbide paper down to 10μm, followed by 0.3 μm alumina. In addition, silver electrodes were electrochemically polished using alkaline cyanide solutions (280).

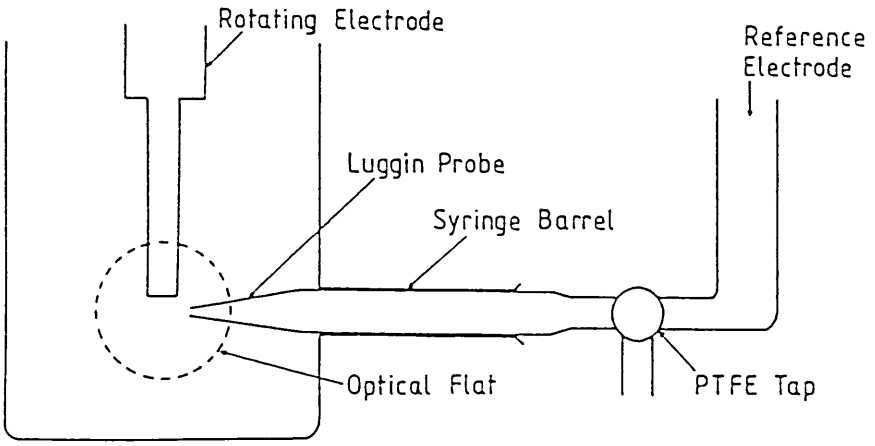


Fig. 2.6 The rotating electrode cell.

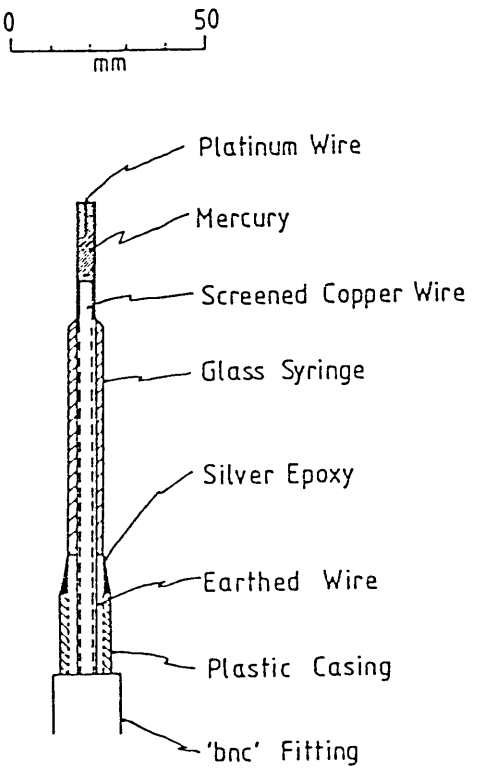


Fig. 2.7 Microelectrode construction.

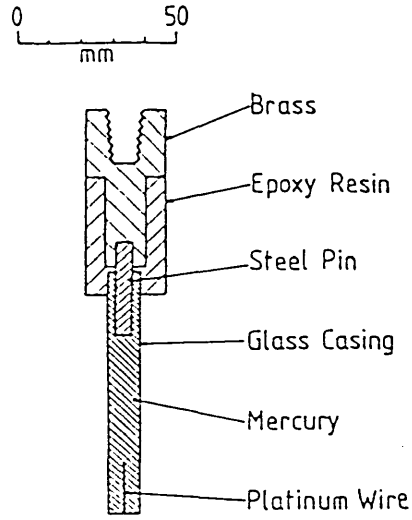


Fig. 2.8 Design of the rotating disk electrode.

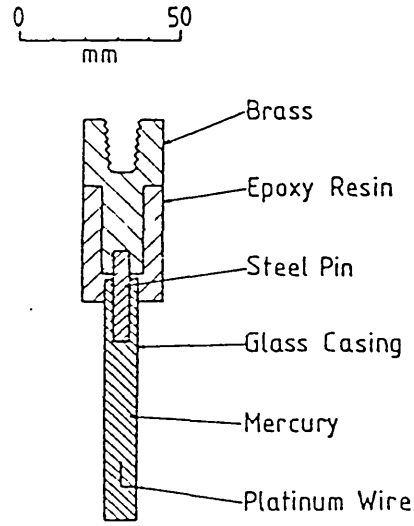


Fig. 2.9 Design of the rotating cylinder electrode.

3 Current, Potential, Impedance and Electrode Area Measurement

Current and potential transients, arising from bubble growth, were measured using a Hewlett Packard HP5420A digital signal analyser and HP54470B digital filter at both syringe-mounted microelectrodes (Fig. 2.7) and planar macroelectrodes (Fig. 2.10). 0.3 m long glass probes of 1 mm diameter, connected to reference electrodes, were used for the latter to allow potential measurement at any point(s) within the cell. A Farnell Instruments (H50/60) 50 amp power supply was used in the macro cell to give current densities of up to 10 kA m^{-2}.

Impedance measurements were made at microelectrodes, using a Solartron 1250 frequency response analyser and Solartron 1186 electrochemical interface, to determine electrode capacitance and resistance both with and without a bubble. A 10 mV peak to peak a.c. perturbation of frequency 0.1-10 000 Hz was applied, frequency being increased logarithmically at 10 steps/decade. An integration time of 30-60 sec. per point ensured a good signal to noise ratio, and a delay of 1 sec. between measurements was used to allow restabilisation.

The electrode area was calculated from measurements of the charge required to adsorb a monolayer of hydrogen on the electrode (276). By dividing that charge by the standard value of 220 μC cm^{-2}, the electrode area could be obtained.

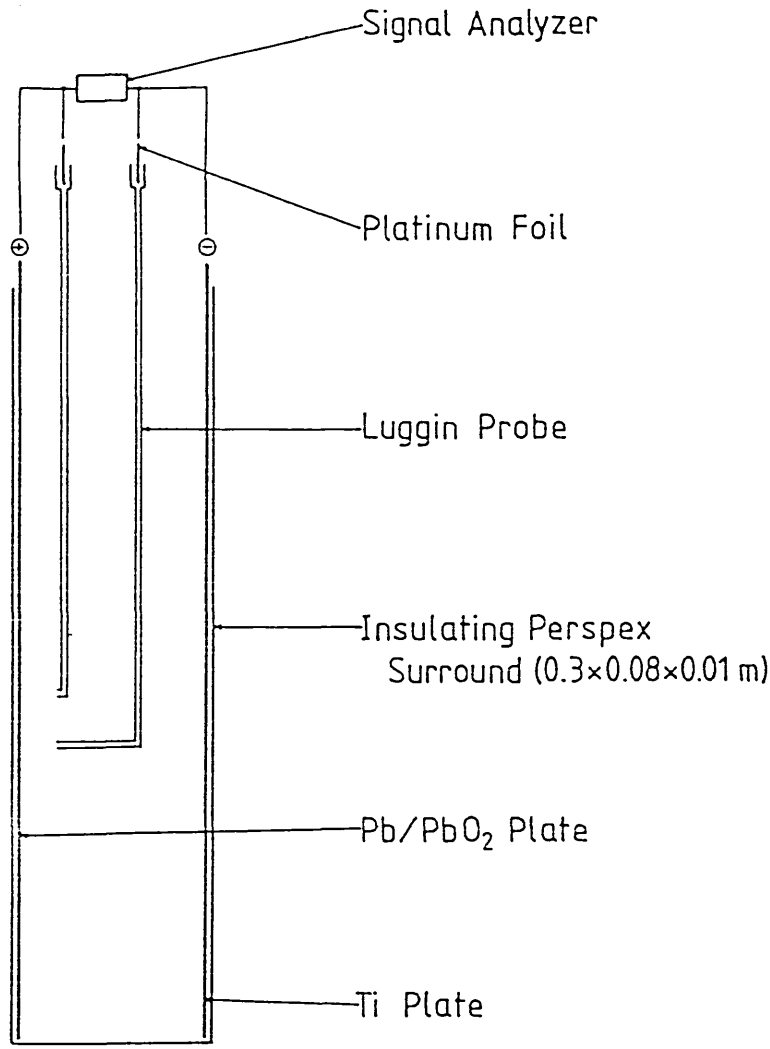


Fig. 2.10 Macroelectrode cell design.

CHAPTER 3

BUBBLE CHARGE MEASUREMENT

1 Electrolyte Purity

1.1 Surface Tension

1.2 Cyclic Voltammetry

1.3 Bubble Rise Rate

2 Bubble Electrophoretic Mobility Measurements

2.1 Bubble Mobility in Surfactant Free Electrolytes

2.2 Bubble Mobility with Added Surfactant

3 Summary

1 Electrolyte Purity

A pre-requisite for bubble charge measurement was a supply of suitably pure water, free of surfactants which concentrate at the gas/liquid interface, so lowering surface tension, inhibiting gas circulation and acting as a source of surface charge. Three techniques were used to give a semi-quantitative measure of the level of contamination.

1.1 Surface Tension

The surface tension of the triply distilled "surfactant-free" water was found to be 72.4 mN m^{-2}, as compared to the value of 69.0 mN m^{-2} obtained with singly distilled water. These measurements differ by only 5 %, showing that the technique was inadequate for the detection of low levels of contamination in water. Changes in surface tension could not be used to detect surfactant contamination arising from the addition of electrolyte, because of the inherent change in surface tension with ionic strength in addition to that arising from contamination.

1.2 Cyclic Voltammetry

Fig. 3.1 illustrates the effect of an anionic surfactant, sodium dodecyl sulphate (SDS), on the cyclic voltammogram of platinum in molar sulphuric acid. Similar results were observed with the cationic surfactant, dodecyltrimethyl ammonium bromide (DTAB). With no surfactant a voltammogram similar to that

——— "surfactant free" electrolyte

– – – – 10^{-6} mol dm^{-3} SDS

— – — 10^{-3} mol dm^{-3} SDS

sweep rate = 100 mV s^{-1}

pH = 0.1

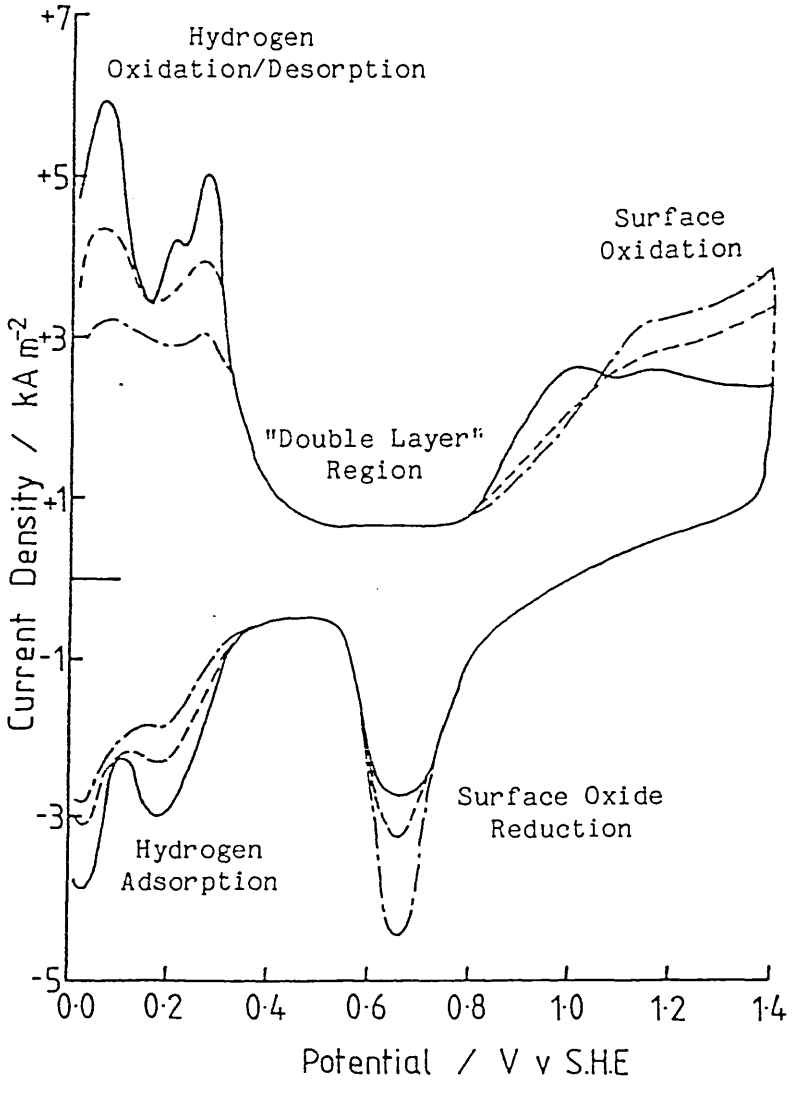


Fig. 3.1 Influence of the bulk surfactant concentration (SDS) on the cyclic voltammogram of platinum.

presented by Conway et al (277) for a clean system was obtained. Increasing surfactant concentration was indicated by:

(i) Blocking of the hydrogen adsorption/desorption peaks.

(ii) Blocking of surface oxidation at 0.8-1.0 V v SHE.

(iii) Reactivity with or on the surface oxide at high anodic potentials.

Conway et al (277) have explained the above as being typical of chemisorbed impurities and suggested cycling of the potential to remove them. However, the technique had little effect in this work, probably due to the re-adsorption of surfactant from the bulk electrolyte.

In addition to the detection of relatively low levels of electrolyte contamination ($\geq 10^{-6}$ mol dm^{-3} surfactant), cyclic voltammetry proved a useful technique for the detection of impurities present only on the electrode surface. These typically arose from inadequate electrode cleaning; though electrodes polished with diamond pastes showed long term contamination from the organic carrier fluid. Therefore, such preparation techniques were avoided.

1.3 Bubble Rise Rate

The rise rate of a bubble was particularly sensitive to surfactant contamination and proved the best method for detecting such impurities. Fig. 3.2 compares the rate of rise of bubbles in "as distilled" water with that predicted in surfactant-free water. Levich (203) gives:

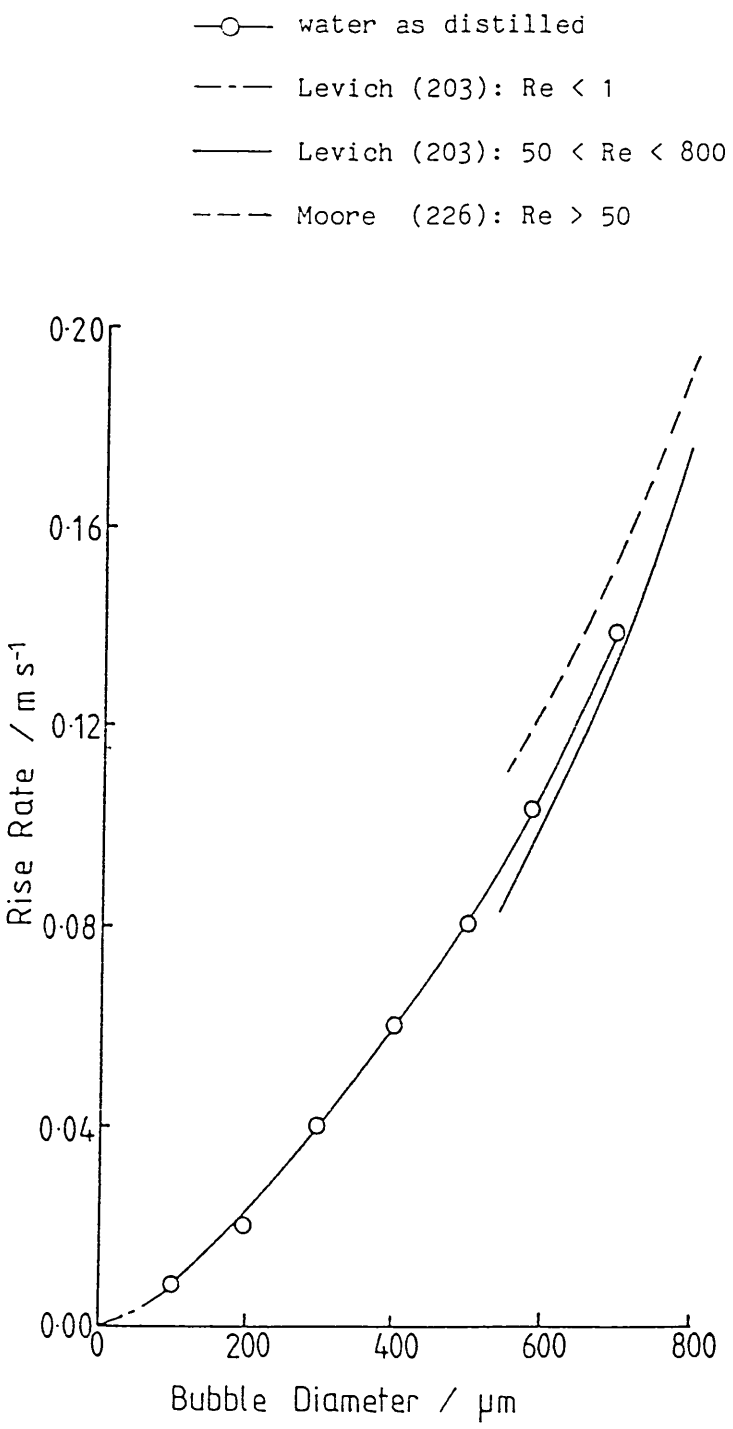


Fig. 3.2 Bubble rise rate in "as distilled" water compared with that predicted in surfactant free water.

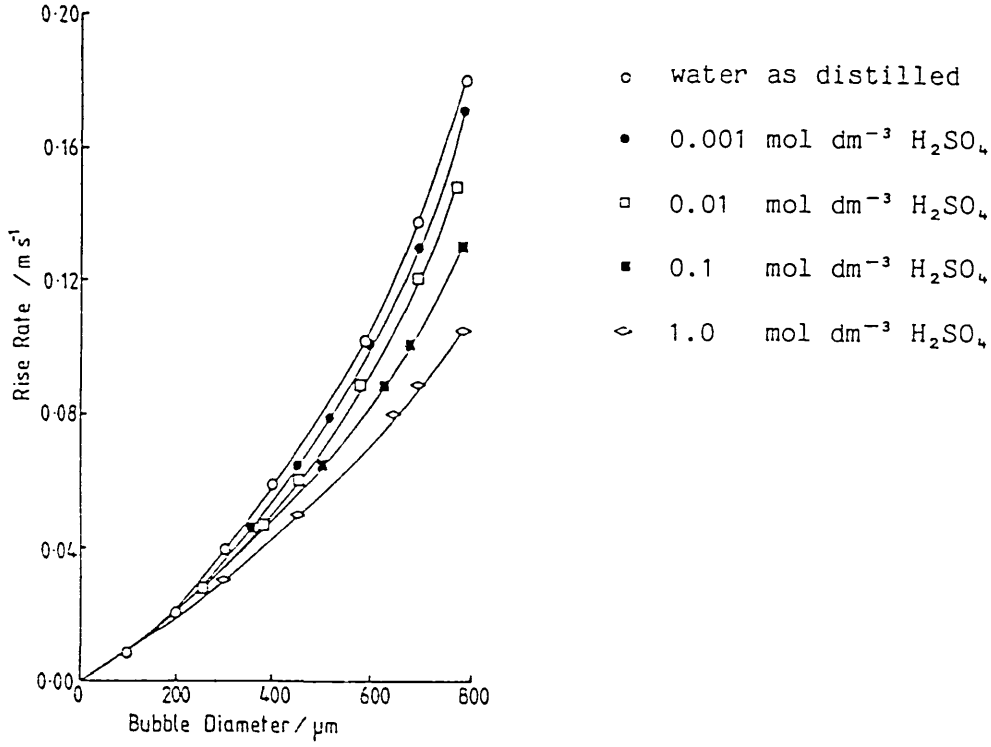


Fig. 3.3 Bubble rise rate in sulphuric acid (plus deci-molar sodium sulphate).

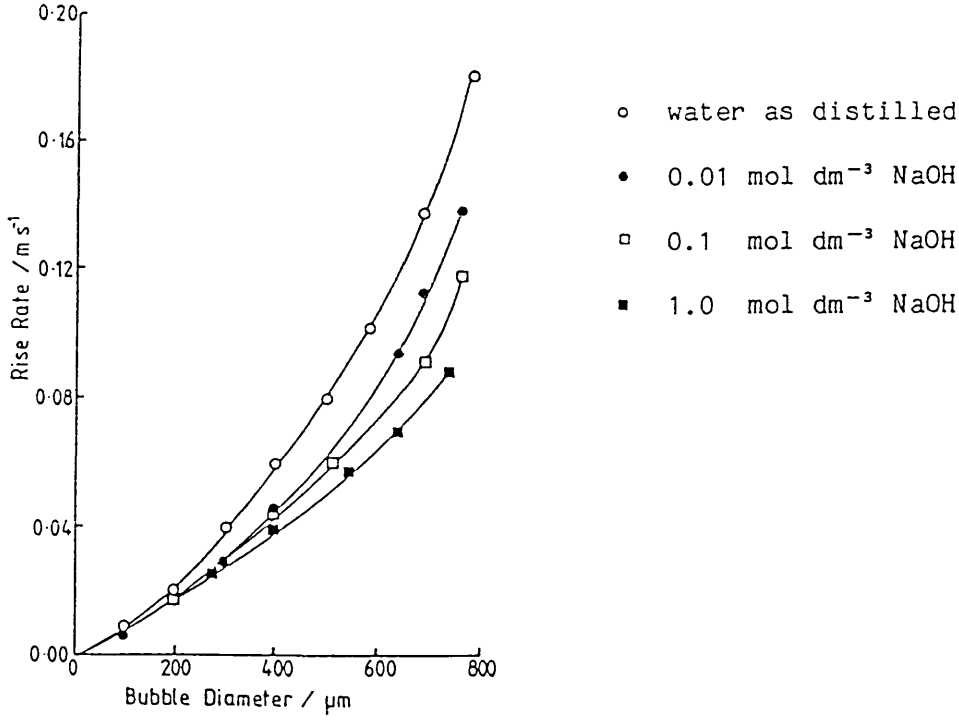


Fig. 3.4 Bubble rise rate in sodium hydroxide (plus deci-molar sodium sulphate).

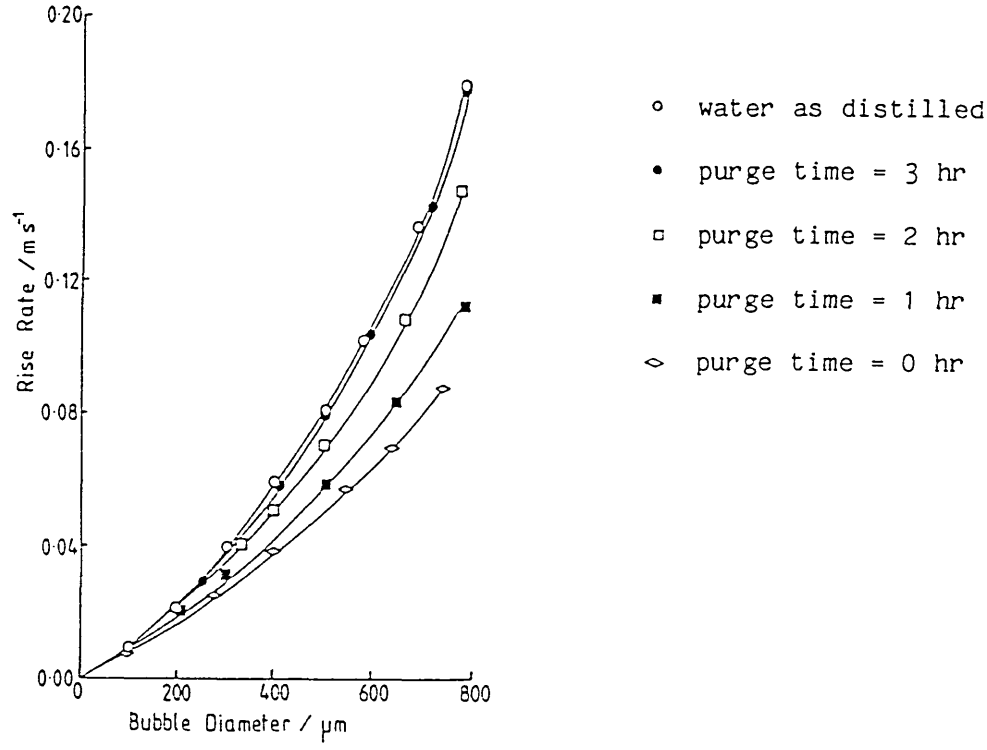


Fig. 3.5 The influence of bubble cleaning on bubble rise rate in molar sodium hydroxide (plus deci-molar sodium sulphate).

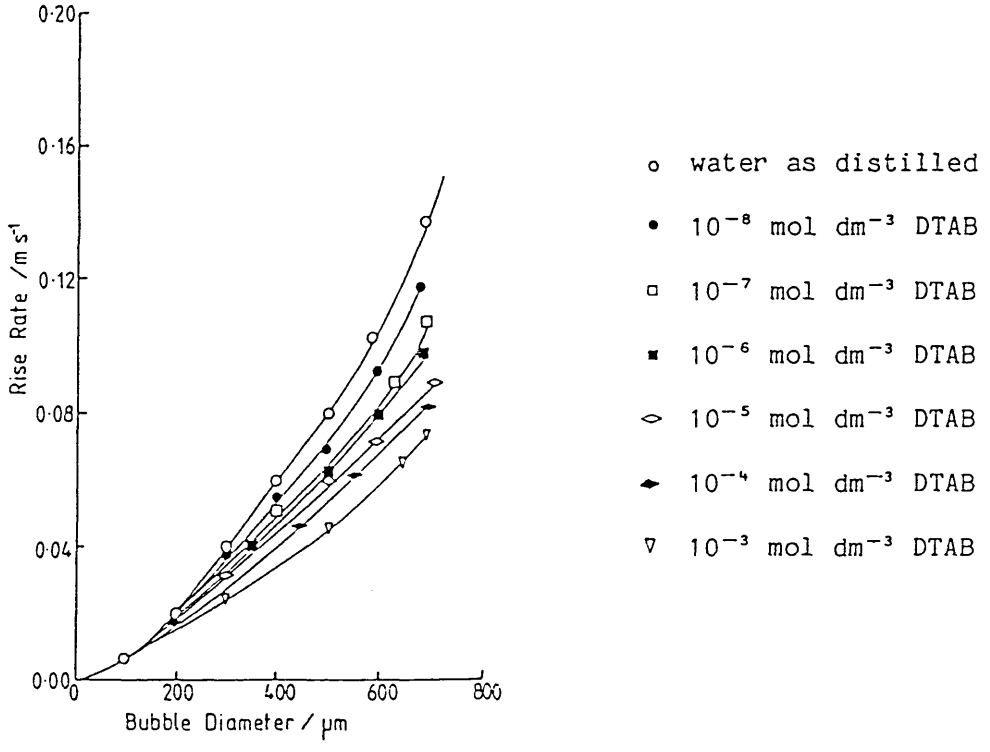


Fig. 3.6 Influence of the bulk surfactant concentration (DTAB) on bubble rise rate.

$$v=(\rho-\rho')/3\eta.r^2g \qquad \text{for } Re < 1 \qquad (1.3\text{-}1)$$

$$v=(\rho-\rho')/9\eta.r^2g \qquad \text{for } 50 < Re < 800 \qquad (1.3\text{-}2)$$

Measured data fitted the above models quite well, though for Re > 50 a better fit was given to Moore's curve (226), obtained by expanding the Levich equation to allow for boundary layer perturbation. This good fit indicated that the water produced from the purification system was essentially surfactant-free.

However, addition of electrolyte introduced further impurities, indicated by a decrease in bubble rise rate (Figs. 3.3 and 3.4). The decrease in rise rate with electrolyte concentration cannot be attributed to the accompanying change in electrolyte viscosity as this was small, e.g. the relative viscosity of both sodium hydroxide and sulphuric acid only increases from ~1.02 to ~1.2 over the range 0.1 to 1.0 mol dm^{-3} at 293 K (281). The problem of impurity addition was overcome by bubble cleaning, i.e. purging the electrolyte with a swarm of electrogenerated bubbles, the electrolyte eventually attaining the quality of "as distilled" water (Fig. 3.5). It was found that the enhanced purity achieved by prior heating of the solid electrolyte could be equalled by bubble cleaning, hence thermal pretreatment of the electrolyte was abandoned.

Fig. 3.6 illustrates the sensitivity of bubble rise rate to very low surfactant levels ($\geq 10^{-8}$ mol dm^{-3}); comparison of the data obtained with electrolytes showed molar sodium hydroxide and sulphuric acid to introduce the equivalent of 10^{-4} and 10^{-5}

mol dm^{-3} surfactant contamination respectively. However, following bubble cleaning the level of impurity dropped below 10^{-8} mol dm^{-3}.

Therefore, it can be concluded that bubble rise rate was a sensitive indicator of surfactant impurity, and that essentially surfactant-free electrolytes could be produced. Cyclic voltammetry proved useful in the detection of impurities on the electrode surface, but surface tension measurements were inadequate for the classification of "clean" electrolytes.

Following confirmation of electrolyte purity, bubble growth and charge measurements were made.

2 Bubble Electrophoretic Mobility Measurements

2.1 Bubble Mobility in Surfactant Free Electrolytes

The influence of pH on the electrophoretic mobility of electrogenerated hydrogen, oxygen and chlorine bubbles is illustrated in Figs. 3.7-3.9 respectively. Bubbles were negatively charged over most of the pH range (indicated by a negative electrophoretic mobility at pH > 3), with a point of zero charge (p.z.c.) at pH 2-3. The latter supports the conclusion of Huddleston and Smith (174) who proposed a p.z.c. at pH 1-2. Bubbles were positively charged at low pH (pH < 2), this charge reversal removing any remaining doubts that the bubble charge was induced by surfactant impurities. In the absence of such impurities, experimental data is consistent with the proposal that the preferential adsorption of OH^-/H^+ ions

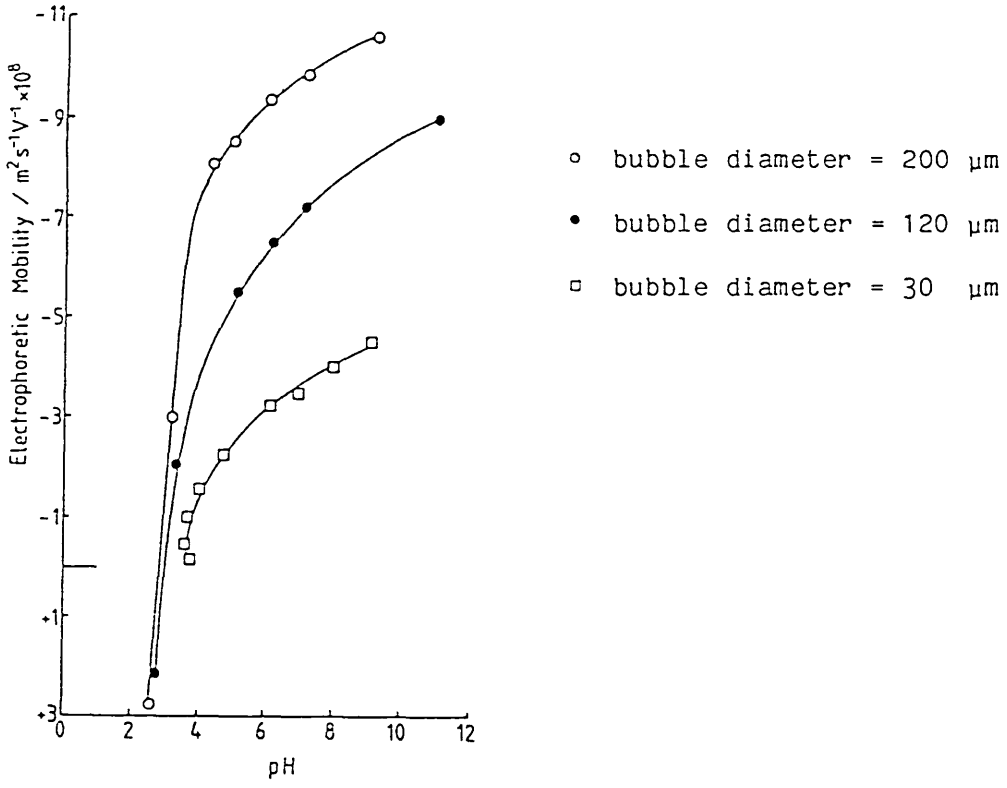


Fig. 3.7 The influence of pH on the electrophoretic mobility of hydrogen bubbles in milli-molar sodium sulphate.

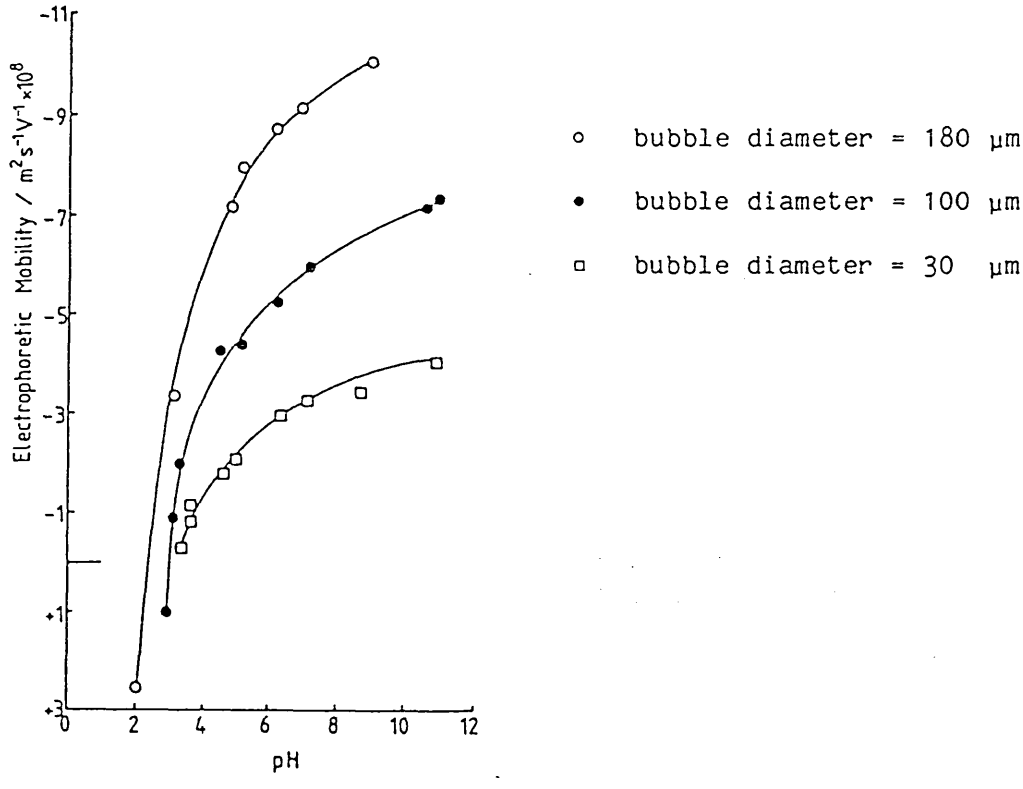


Fig. 3.8 The influence of pH on the electrophoretic mobility of oxygen bubbles in milli-molar sodium sulphate.

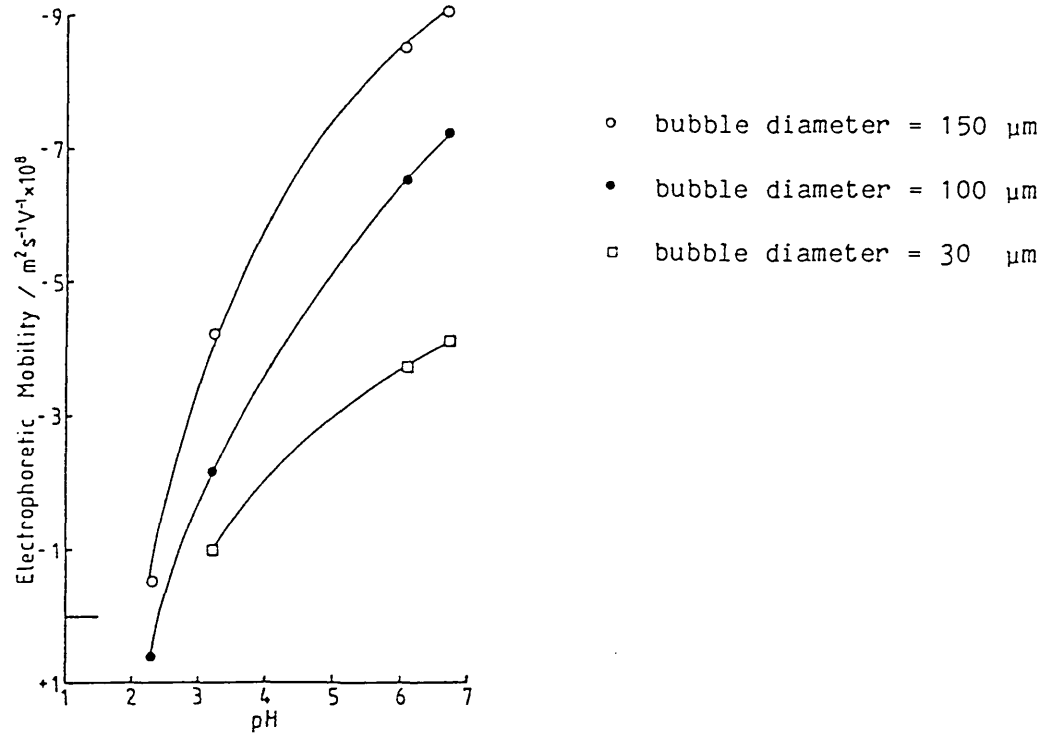


Fig. 3.9 The influence of pH on the electrophoretic mobility of chlorine bubbles in milli-molar potassium chloride.

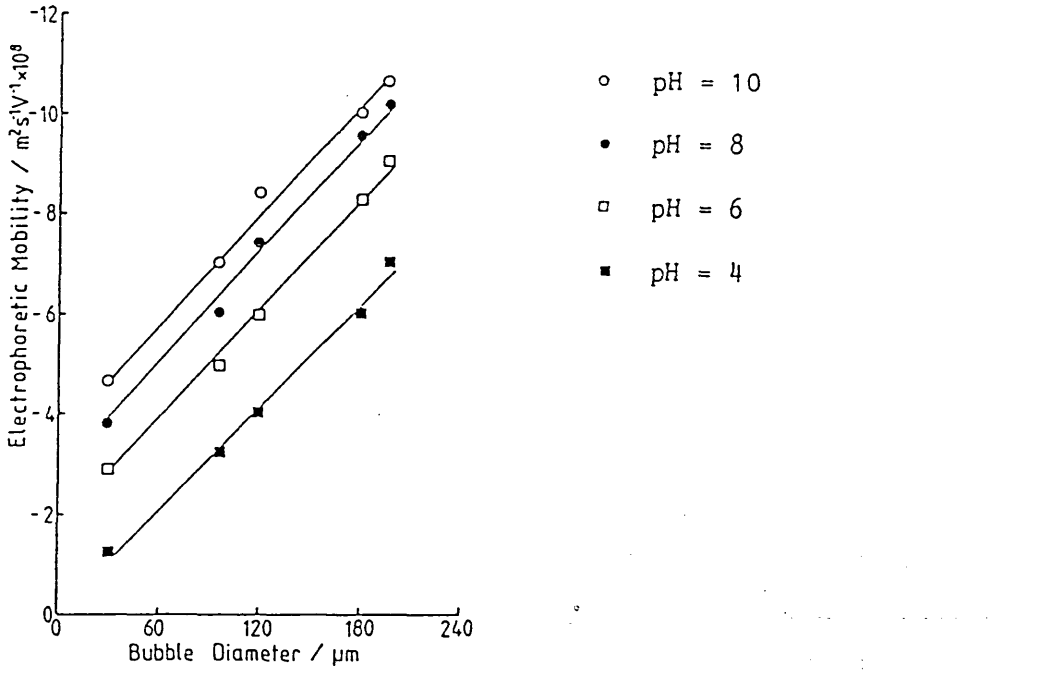


Fig. 3.10 The influence of bubble diameter on the electrophoretic mobility of bubbles in milli-molar sodium sulphate.

gives rise to a net bubble charge.

Bubble electrophoretic mobility was independent of both the type of gas and the source; bubbles of oxygen and hydrogen generated via rotation of a "holed" tap (see chap.2, section 2.1) gave identical results to those previously reported for electrogenerated bubbles (Figs. 3.7-3.9). This shows that for hydrogen, oxygen and chlorine the charge at the gas/liquid interface is determined only by the properties of the solution side of the interface.

Figs. 3.7-3.9 show that electrophoretic mobility was dependent on bubble diameter. This is better illustrated by Fig. 3.10 which shows mobility to vary linearly with bubble diameter over the pH range 4-10. Such a dependence is not predicted by the classical theory for the electrophoresis of solid particles (chap.1, section 3.1.3) and can be attributed to the mobile nature of the gas/liquid interface, which allows the separation of charge around the bubble interface through either:

(i) hydrodynamic flow induced by bubble rise.

(ii) polarisation of surface charge by the electric field.

The linear dependence of electrophoretic mobility on bubble diameter follows that predicted by Levine and O'Brien (204) for the electrophoresis of charged mercury drops, which also exhibit a mobile interface. However, the theory of the electrophoresis of mercury drops cannot be applied directly to bubbles, but can be adapted to do so. This is reported in Appendix 1, which describes the influence of a) an applied electric field, and b) bubble rise rate, on the distribution of charge around a mobile

bubble surface at small surface potentials. In the absence of an electric field equation (4-20) of Appendix 1 relates the surface charge perturbation (σ_1) to the rise rate (where the surface charge density at a given point is given by $\sigma(\theta)=\sigma_0+\sigma_1\cos\theta$):

$$\sigma_1=(3\eta v-\rho g a^2).(D\kappa/4\pi\sigma_0) \qquad (2.1\text{-}1)$$

and shows that the movement of charge around the bubble increases with rise rate. Therefore, a greater charge dipole will exist on the bubble surface as the rise rate increases, and the measured electrophoretic mobility should increase.

The electrophoretic mobility of a bubble in the absence of gravity is given by equation (3-43) of Appendix 1:

$$u_e=K/\kappa\sigma_0 \qquad (2.1\text{-}2)$$

which does not predict the experimentally observed dependence of electrophoretic mobility on bubble diameter (Fig. 3.10). However, a diameter dependence of some form would be expected since, for the extreme case where surface charge is sufficiently polarised to be represented as a point charge, the following calculation shows that the electrophoretic mobility would vary linearly with bubble diameter.

The electrostatic force (F) on a point charge (Q) is given by (252):

$$F=EQ \qquad (2.1\text{-}3)$$

where E is the electric field strength. The electrostatic force acts against the drag force (F') which, for bubbles with a mobile interface at Re < 1, is given by (203):

$$F' = 2\pi\eta du \qquad (2.1\text{-}4)$$

If Q represents the total charge (initially uniformly distributed over the bubble surface at a density of σ_0), then equating F and F' yields:

$$u = \sigma_0 Ed/3\eta \qquad (2.1\text{-}5)$$

showing electrophoretic mobility (u/E) to vary linearly with bubble diameter. Applying equation (2.1-5) to measured data (Fig. 3.8) gives extremely small surface charge densities, e.g. 20 nC cm^{-2} for 100 μm diameter bubbles at pH 10.

Equation (2.1-2) is probably not consistent with experimental observation because the influence of bubble rise on the movement of charge around the bubble was not considered in its derivation. To obtain a complete solution the influence of bubble rise on the distribution of charge would have to be coupled to the influence of an electric field applied normal to the direction of rise. This is not a trivial problem, though it would be simplified if the electric field were applied parallel to the direction of rise and the reduction or enhancement of rise rate measured. However, the small value of the

electrophoretic mobility compared to the rise rate means that great experimental difficulty would be found in measuring velocity changes. It would also be advantageous to decouple the influence of electric field and rise rate on the movement of charge around the bubble surface. In principle this may be achieved by the use of very small bubbles to give extremely low rise rates. However, this did not prove possible in this work due to difficulties in producing and observing such fine bubbles.

Equation (2.1-2) predicts that the electrophoretic mobility becomes more positive with decreasing pH, i.e. taking H^+/OH^- to be the potential determining ions at the gas/liquid interface yields:

$$d\sigma_o/dpH < 0 \qquad (2.1\text{-}6)$$

whilst from (2.1-2):

$$du_e/d\sigma_o < 0 \qquad (2.1\text{-}7)$$

Hence, combining equations (2.1-6) and (2.1-7) gives:

$$du_e/dpH > 0 \qquad (2.1\text{-}8)$$

which is inconsistent with experimental observation (Figs. 3.7 to 3.9). The answer to this discrepancy lies in the use of Levich's (203) conservation of charge condition (equation (1-8)

of Appendix 1) in the derivation of equation (2.1-2). Levich considered a mercury drop, for which σ_0 is due to electrons inside the metal, i.e. these do not enter into the conservation of charge condition which applies only to the charge density in the double layer. However, in the case of a bubble adsorbed H^+/OH^- ions, which lie within the double layer, move around the interface in addition to the movement of ions from the supporting electrolyte, giving two types of charge in the surface divergence term. Therefore, assuming a net tangential movement of negative charge in the double layer, equation (3-9) of Appendix 1 can be rewritten as:

$$3\sigma_0 u/a.f=-K(2A/a^3+E)=-3EK/\kappa a \qquad (2.1\text{-}9)$$

where f is some fraction representing the net movement of charge. Equation (2.1-2) then becomes:

$$u_e=fK/\kappa\sigma_0 \qquad (2.1\text{-}10)$$

such that $du_e/d\sigma_0 > 0$, and hence:

$$du_e/dpH < 0 \qquad (2.1\text{-}11)$$

which is consistent with experimental observation. Applying equation (2.1-10) to measured data (Fig. 3.8) yields a bubble surface charge density of 0.08 to 0.25 $\mu C\ cm^{-2}$ at pH 10 with f=-0.5 and K=0.02 $(\Omega\ m)^{-1}$ (281). This is smaller than the

corresponding charge density predicted by classical theory (0.4 to 2.8 $\mu C\ cm^{-2}$ at pH 10).

The non-linear influence of the electric field on bubble electrophoretic mobility can be seen in Fig. 3.11, confirming the observation made by McShea and Callaghan (212) using spinning cell electrophoresis. However, McShea and Callaghan attributed the non-linearity to cell rotation, whereas it would appear that enhanced polarisation of charge occurs at higher field strengths. This leads to an increased electrophoretic mobility. Evidence for this conclusion can be found by combining equations (3-34) and (3-42) of Appendix 1 to give:

$$\sigma_1 = 3D\eta EK/4\pi\sigma_0^2 \qquad (2.1\text{-}12)$$

which shows the perturbation of surface charge to be proportional to the electric field strength. Extrapolation of the curve given in Fig. 3.11 to zero field strength reveals that an electrophoretic mobility of $\sim 3.5\times10^{-8}\ m^2\ s^{-1}\ V^{-1}$ would still be expected. This represents the contribution to the net electrophoretic mobility made by bubble rise-induced hydrodynamic effects. Therefore, for field strengths of 3-18 kV m^{-1} the polarisation of charge induced by bubble rise results in 80-50 % of the measured mobility.

Fig. 3.12 describes the influence of electrolyte concentration on the electrophoretic mobility of a bubble in both 1:1 and 2:1 electrolytes. Bubbles were tap-generated since an electrolyte of high ionic strength, as would be required to

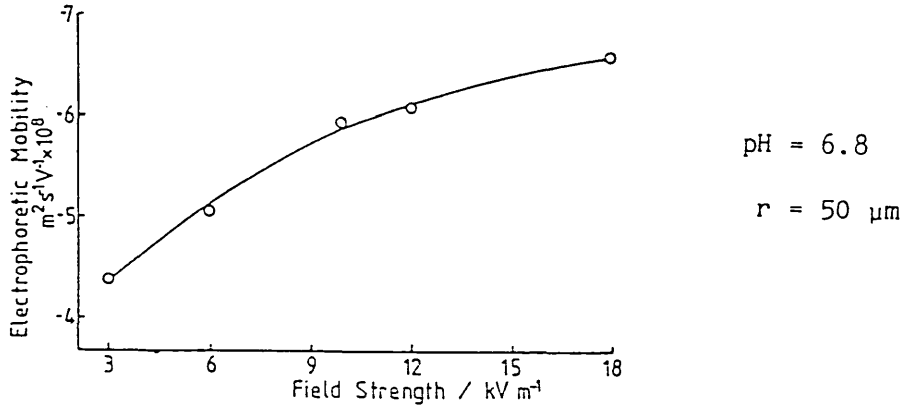


Fig. 3.11 The influence of electric field strength on the electrophoretic mobility of bubbles in milli-molar sodium sulphate.

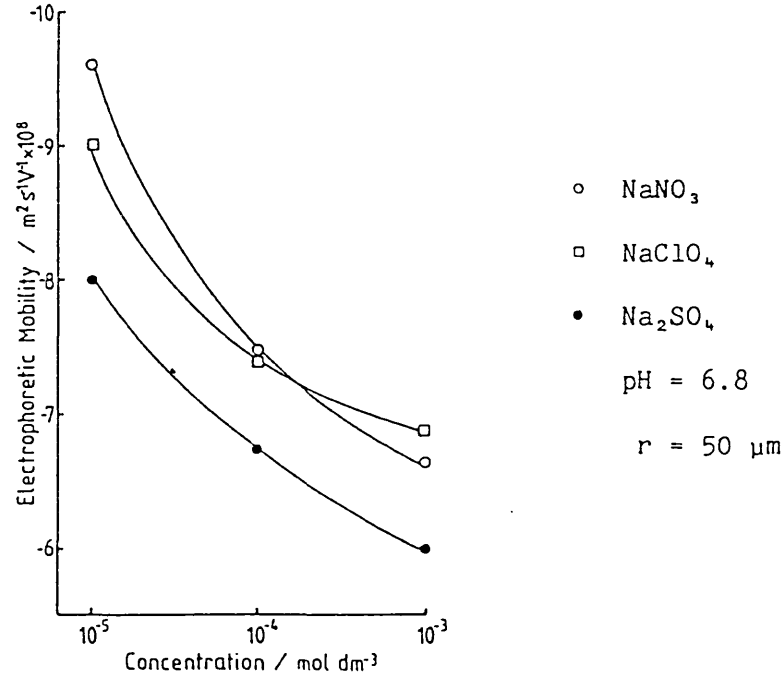


Fig. 3.12 The influence of electrolyte concentration on the electrophoretic mobility of a bubble.

generate bubbles electrolytically, was not wanted in the lower cell (so avoiding ionic diffusion from the lower to the upper cell). Electrophoretic mobility decreased with electrolyte concentration $[c]$ due to a reduced diffuse layer thickness ($1/\kappa$), the charge density remaining constant. This is in agreement with equation (2.1-2), though the influence of ionic strength on the electrophoretic mobility was not as significant as that predicted by equation (2.1-10), i.e. $u_e \propto 1/\kappa \propto [c]^{0.5}$. Electrophoretic mobility was greater in a 1:1 electrolyte, and this again follows equation (2.1-10) since a more extensive diffuse layer is obtained in a 1:1 electrolyte (173).

To confirm that results were not being influenced by the experimental design, glass spheres of known diameter were allowed to fall between the electrodes and their electrophoretic mobility measured. No diameter dependence was observed over the range 40-120 μm, as expected for solid particles. The glass spheres were then crushed and their electrophoretic mobility measured using conventional microelectrophoresis apparatus. The microelectrophoresis results can be compared to the results of Wiese et al (282) who reported mobilities of 5 and 8×10^{-8} m^2 s^{-1} V^{-1} for vitreous silica in aqueous potassium nitrate at pH 4.5 and 6.9 respectively. Table 3.1 compares the results and shows good agreement between the two techniques.

pH	u_e / $m^2\ s^{-1}\ V^{-1} \times 10^8$	
	Falling sphere	Microelectrophoresis
4.5	4.90	4.32
6.9	6.51	6.90

Table 3.1 Comparison of electrophoretic mobility measurements made using microelectrophoresis and falling sphere techniques.

2.2 Bubble Mobility with Added Surfactant

Experiments were carried out to reverse the charge on a bubble by the addition of an oppositely charged surfactant. Interpolation of the results allowed the concentration of surfactant required to give zero electrophoretic mobility, and by inference zero charge, to be determined. The results apply to all bubbles of hydrogen, oxygen and chlorine since it has been shown (section 2.1) that the electrophoretic mobility of those bubbles is determined only by the composition of the solution side of the gas/liquid interface.

Figs. 3.13 and 3.14 describe the results obtained with a cationic (DTAB) and anionic (SDS) surfactant in milli-molar sodium nitrate. Fig. 3.13 shows that DTAB concentrations of 4×10^{-6} and 8×10^{-6} mol dm^{-3} were required to neutralize the initial charge on the bubble at pH 6.9 and 10.5 respectively. Extrapolation of the adsorption isotherm for DTAB at the vapour/water interface (Fig. 3.15 (283)) gives corresponding surface concentrations (Γ) of:

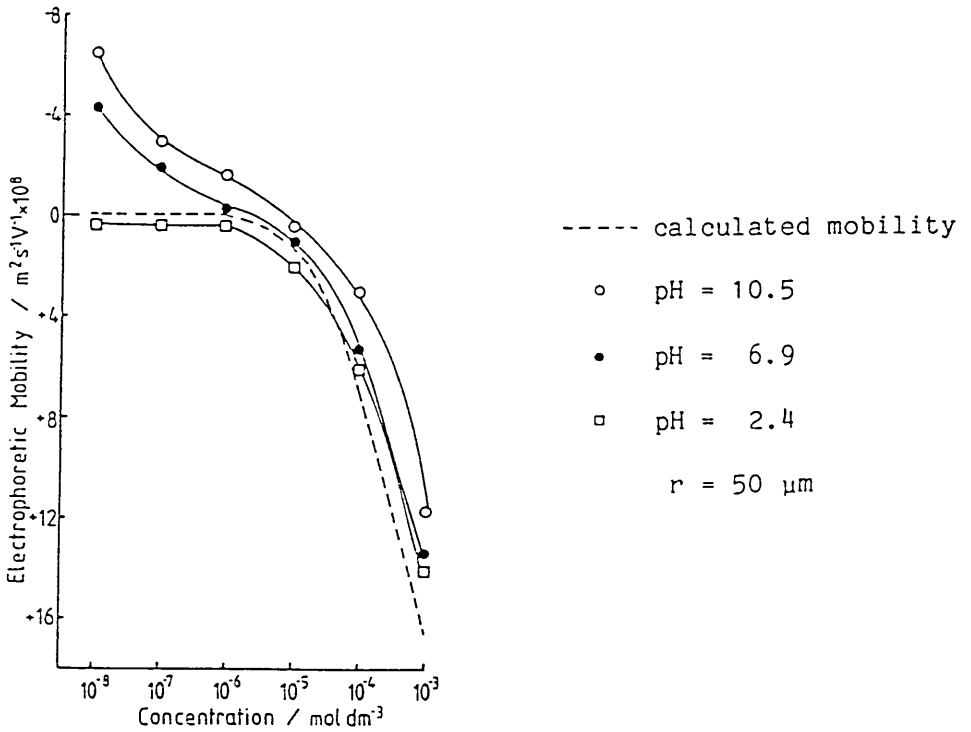


Fig. 3.13 Influence of the bulk DTAB concentration on the electrophoretic mobility of bubbles in milli-molar sodium nitrate.

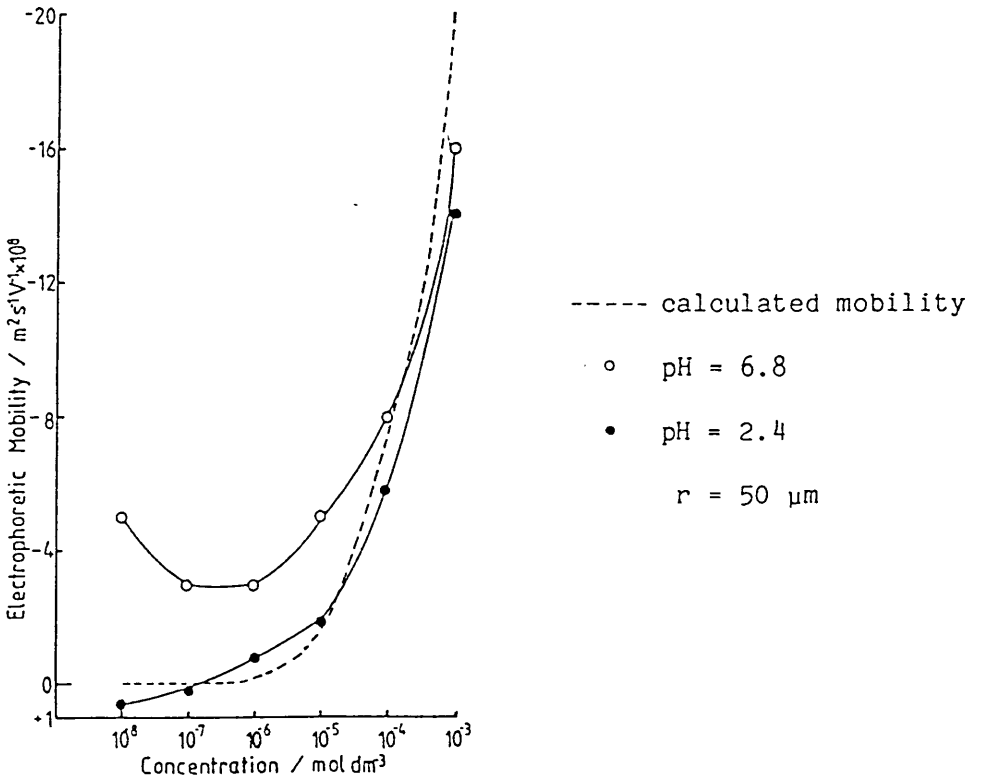


Fig. 3.14 Influence of the bulk SDS concentration on the electrophoretic mobility of bubbles in milli-molar sodium nitrate.

$\Gamma_{6.9} = 4.8\times10^{-13}$ mol cm^{-2}

$\Gamma_{10.5} = 9.6\times10^{-13}$ mol cm^{-2}

though it should be noted that Γ will be slightly higher in a milli-molar electrolyte than in water. The surface charge density can then be calculated from:

$$\sigma = \Gamma N_A e \qquad (2.2\text{-}1)$$

so that the bubble charge density at pH 6.9 and 10.5 was:

$\sigma_{6.9} = -0.046$ μC cm^{-2}

$\sigma_{10.5} = -0.093$ μC cm^{-2}

These values compare favourably with those predicted by equation (2.1-10), derived from a theoretical treatment of the electrophoresis of a bubble in an electric field (see Appendix 1).

Bubble charge at pH 2.4 was obtained using the same procedure, but required an anionic surfactant (SDS) to reverse the charge. Fig. 3.14 shows that a bulk concentration of 2×10^{-7} mol dm^{-3} was required for zero charge, corresponding to a surface concentration of 2.8×10^{-14} mol cm^{-2} (see Fig. 3.15). The surface charge density was therefore:

$\sigma_{2.4} = +0.0027$ μC cm^{-2}

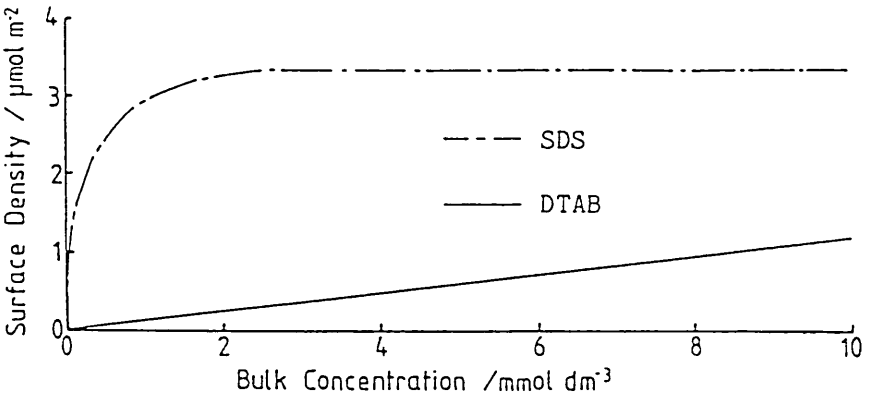


Fig. 3.15 The adsorption isotherm of SDS and DTAB in water (283).

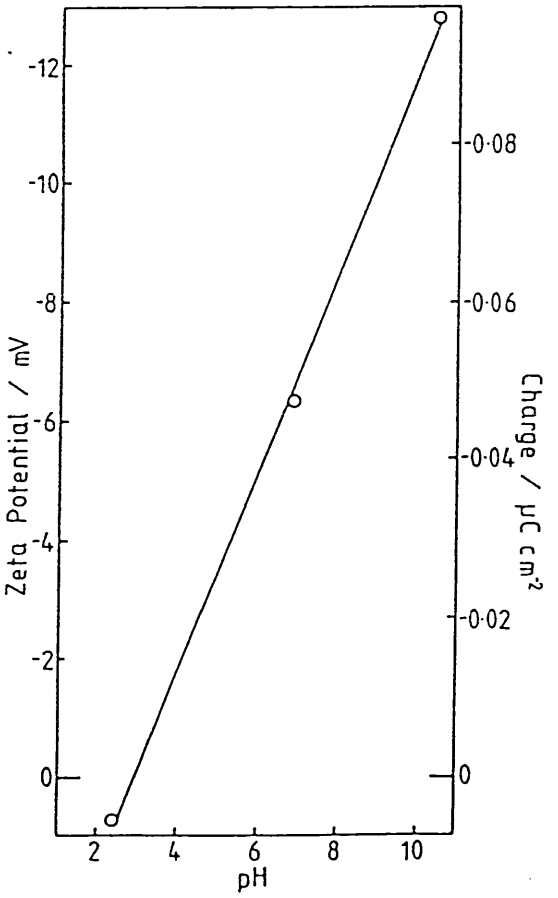


Fig. 3.16 The pH dependence of the calculated zeta potential and charge density at the gas/liquid interface.

Fig. 3.16 summarises the influence of solution pH on both the charge density of the gas/liquid interface and the corresponding zeta potentials, calculated using equation (2.2-2) (173):

$$\sigma=4n_0ze/\kappa.\sinh(ze\zeta/2kT) \qquad (2.2-2)$$

Applying Smoluchowski's theory (equation 2.2-3) to the calculated zeta potentials predicts electrophoretic mobilities of only +0.03 to -1.0×10^{-8} m^2 s^{-1} V^{-1} in a clean system. These are much lower than the values of +1 to -10×10^{-8} m^2 s^{-1} V^{-1} observed over the same pH range (Figs. 3.7-3.9), and illustrates that theories developed for solid particles cannot be applied to gas bubbles.

Figs. 3.13 and 3.14 also illustrate the influence on the electrophoretic mobility of the rigidifying of the bubble interface by surfactant (see chap.1, section 3.2.2). Low surfactant concentrations reduced the bubble electrophoretic mobility, even when bubble and surfactant were of like charge. Increasing the surfactant concentration raised the electrophoretic mobility, which tended towards that calculated for an equivalent solid particle of zero initial charge. The charge on the solid particle was assumed to derive solely from adsorbed surfactant, and the mobility calculated using Smoluchowski's equation:

$$u_e=(\varepsilon\zeta)/(4\pi\eta) \qquad (2.2-3)$$

However, equations (2.2-2) and (2.2-3) apply strictly only at small surface potentials (< 25 mV). At large potentials counter-ion adsorption becomes significant (173) so that the measured electrophoretic mobility should have been lower than that predicted by calculation. Therefore, the good correlation between measured electrophoretic mobility and that predicted by equations (2.2-2) and (2.2-3) at high surfactant concentrations (corresponding to high surface potentials) means that some sweeping of charge around the bubble surface must still have been occurring, enhancing the measured electrophoretic mobility. This arises because neither DTAB nor SDS give monolayer coverage of the vapour/water interface at the concentrations used in this work (Fig. 3.15). The decrease in mobility observed in Fig. 3.14 as the SDS concentration increased from 10^{-8} to 10^{-7} mol dm^{-3} arose from partial surface rigidifying, leading to reduced mobility of charge on the bubble surface and hence reduced electrophoretic mobility. This effect dominated the small increase in net charge with added surfactant.

Addition of milli-molar sodium tetradecyl sulphate gave monolayer coverage of the bubble by surfactant. An electrophoretic mobility of 13.6×10^{-8} m^2 s^{-1} V^{-1} was measured at pH 6.8. This is less than the mobility predicted for an equivalent solid particle, indicating that the bubble interface was immobile (i.e. the reduction in electrophoretic mobility due to counter-ion adsorption (173) was not counteracted by an enhancement due to the polarisation of charge). Under these

conditions bubble mobility was independent of the electric field strength, in contrast to the non-linear dependence observed in a clean system (Fig. 3.11). This is further evidence for the immobility of the gas/liquid interface with monolayer surfactant adsorption.

3 Summary

The use of surfactant-free electrolytes (characterised by bubble rise rate measurements) ensured that the electrophoretic mobility of a mobile gas/liquid interface was measured. The mobile nature of the interface allowed surface charge to move around the bubble due to the action of the hydrodynamic flow induced by bubble rise, and the polarisation of surface charge by the electric field through which the bubble rose.

This non uniform charge distribution resulted in the electrophoretic mobility being linearly dependent on bubble diameter, and exhibiting a non-linear dependence on electric field strength. A theoretical description of the influence of bubble rise and electric field strength on the perturbation of surface charge is reported in the Appendix, and in part explains these effects.

Bubbles exhibit a point of zero charge at pH 2-3. Consequently the gas/liquid interface is negatively charged at pH > 3 and positively charged at pH < 2. The charge on the bubble was dependent only on the composition of the solution side of the interface, the probable origin of the charge being preferential OH^-/H^+ adsorption.

Addition of sufficient oppositely charged surfactant to bring the bubble to zero charge allowed the charge density in the absence of surfactant to be calculated. The low values obtained (< 0.1 μC cm^{-2}) showed that the electrophoretic mobilities measured in a clean system were far greater than that predicted by applying classical theory to the calculated charge densities. This is again due to the mobile nature of the bubble interface.

Bubbles tend to behave as solid spheres with increasing surfactant concentration. This is due to the rigidifying of the bubble interface by adsorbed surfactant.

CHAPTER 4

BUBBLE GROWTH KINETICS AND DEPARTURE DIAMETER

1 Bubble Growth Kinetics

1.1 Bubble Induction Time

1.2 The Growth Coefficient

1.3 The Time Coefficient

2 Electrode Charge

3 Bubble Departure Diameter

3.1 Influence of pH

3.2 Influence of Electrode

3.3 Influence of Electrolyte

3.4 Influence of Hydrodynamics

4 Summary

1 Bubble Growth Kinetics

Following nucleation the growth kinetics of a bubble was described using the following relationship:

$$r=\beta t^{x} \qquad (1\text{-}1)$$

where β represents the growth coefficient and x the time coefficient, these two parameters allowing the growth kinetics of individual bubbles to be described. Typical bubble growth curves are illustrated by Fig. 4.1.

1.1 Bubble Induction Time

A linear relationship was observed between applied potential (which included an uncompensated ohmic potential loss) and the reciprocal of the induction time (τ) required for bubble nucleation (Fig. 4.2), in agreement with the observations of Fahidy and Abdo (108). The induction time represents the time required for the supersaturation of electrolyte in the vicinity of the electrode and can be approximated using equation (1.1-7), derived as follows.

For the simple electrode reaction:

$$2H^{+} + 2e \rightarrow H_2$$

at a planar macroelectrode in the absence of convection, linear diffusion can be assumed. Hence Fick's second law (150) gives:

$$\partial C_{H^+}(x,t)/\partial t = D_{H^+}(\partial^2 C_{H^+}(x,t)/\partial x^2) \qquad (1.1\text{-}1)$$

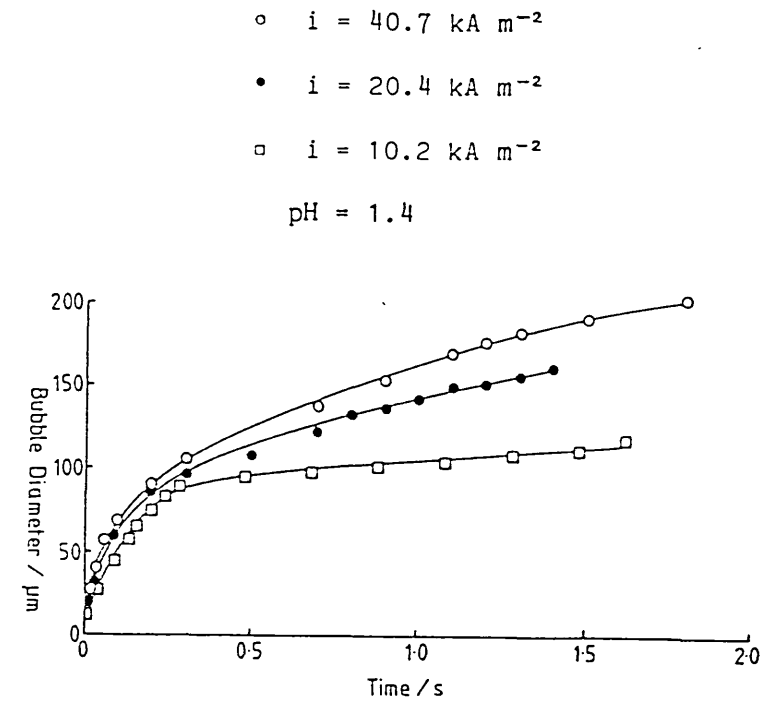


Fig. 4.1 Typical bubble growth curves, observed during hydrogen evolution at a 25 μm diameter platinum electrode.

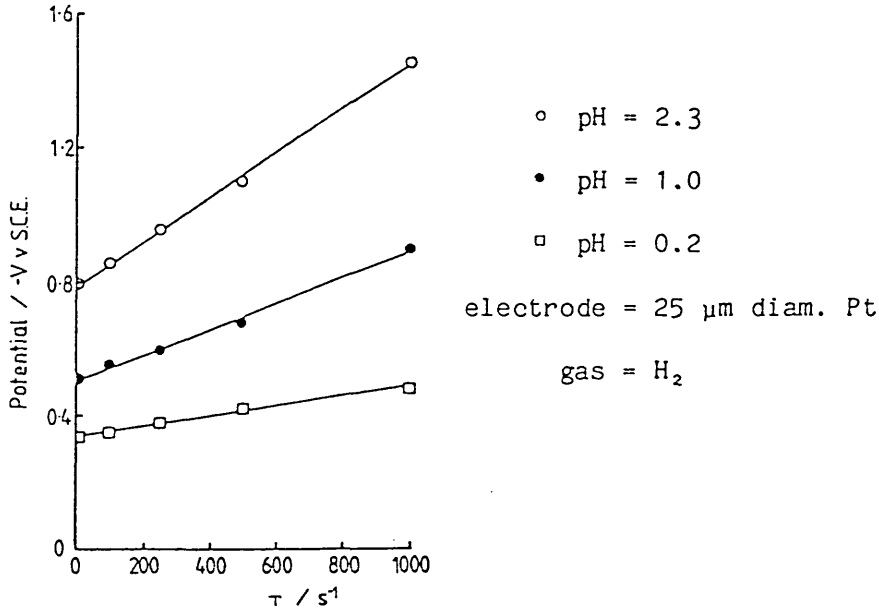


Fig. 4.2 The influence of applied potential on the reciprocal of the induction time required for bubble nucleation (τ).

$$\partial C_{H_2}(x,t)/\partial t = D_{H_2}(\partial^2 C_{H_2}(x,t)/\partial x^2) \qquad (1.1\text{-}2)$$

with the initial conditions (t=0) at all x being:

$$C_{H^+}(x,0) = C_{H^+,\infty} \qquad C_{H_2}(x,0) = C_S \qquad (1.1\text{-}3)$$

and the semi-infinite boundary conditions ($x \to \infty$ for all t) of:

$$C_{H^+}(x,t) = C_{H^+,\infty} \qquad C_{H_2}(x,t) = C_S \qquad (1.1\text{-}4)$$

where $C_{H^+,\infty}$ represents the initial bulk proton concentration. Total transport control is implicit in the above starting and boundary conditions, though a proton migration term would have to be added if no supporting electrolyte were used.

Therefore, since the condition of conservation of matter yields:

$$D_{H^+}(\partial C_{H^+}(x,t)/\partial x) + D_{H_2}(\partial C_{H_2}(x,t)/\partial x) = 0 \text{ at } x=0 \qquad (1.1\text{-}5)$$

and the flux equation:

$$D_{H^+}(\partial C_{H^+}(x,t)/\partial x) = i(t)/zF \qquad (1.1\text{-}6)$$

it can be shown (150) that equation (1.1-7) describes the concentration of dissolved gas in the electrolyte immediately adjacent to the electrode.

$$C_{H_2}(0,t)=2i/zF.\sqrt{(t/\pi D_{H_2})}=\varepsilon\sqrt{(t/t)}.C_{H^+,\infty} \quad (1.1\text{-}7)$$

where:

$$\varepsilon=\sqrt{(D_{H^+}/D_{H_2})} \quad (1.1\text{-}8)$$

and t represents a transition time.

The above relationship can only be approximate since edge effects increasingly influence the current distribution, and hence the source of evolved gas, as the electrode diameter decreases; indeed hemispherical diffusion becomes dominant as the electrode diameter tends towards zero (see chap.1, section 2.3.3). Additionally electrolyte flow induced by bubble growth and departure would disturb the supersaturated layer. However, equation (1.1-7) embodies the principal terms which influence supersaturation.

If a given supersaturation must be attained for bubble nucleation then equation (1.1-7) shows that the induction time will decrease with increasing current. This is illustrated in Fig. 4.2 by an increase in τ with potential, and hence current. The linear relationship between τ and potential may be due to the inclusion of uncompensated ohmic losses in the reported potentials because, since $i \propto \exp(\eta)$ (2), it would be expected from equation (1.1-7) that $\tau \propto \exp(2\eta)$.

The reduced induction time at lower pH can be attributed to two accompanying effects:

(i) A decrease in the hydrogen diffusion coefficient ($D_{H_2O}=7.38\times10^{-9}$ m^2 s^{-1}, $D_{\text{molar } H_2SO_4}=4.2\times10^{-9}$ m^2 s^{-1} at 298 K (76)) shown by equation (1.1-7) to lower the time required to attain a given supersaturation.

(ii) An increase in the bulk proton concentration ($C_{H^+,\infty}$), shown by equation (1.1-7) to decrease the induction time.

Short induction times were observed in this work due to the relatively high current densities used ($\geq$ 2 kA m^{-2}).

Use of equation (1.1-7) and the data reported in Fig. 4.2, for which i=2-20 kA m^{-2}, gave C_{H_2}=5-500 mol m^{-3} in the electrolyte immediately adjacent to the electrode. Taking the saturation value of hydrogen in water as 0.75 mol m^{-3} at 298 K (284) gave relative supersaturations of 7-700. These exceed the values of 20-160 given by Shibata (69-72) for the relative supersaturation in the immediate vicinity of hydrogen and oxygen evolving electrodes, probably because of:

(i) The extremely high current densities used in this work.

(ii) The likely greater supersaturation required to nucleate a bubble on a clean, hydrophilic surface than on a contaminated, hydrophobic electrode.

(iii) The simplifying assumptions made in deriving equation (1.1-7).

During continuous bubble evolution, induction times of less than 10 msec were observed, indicating rapid formation of a supersaturated layer. However, lower supersaturations may occur during continuous bubble growth due to the possibility of

undissolved gas being trapped in crevices on the electrode surface and acting as preferential nuclei (chap.1, section 2.3.1).

1.2 The Growth Coefficient

The growth coefficient (β) represents the rate of bubble growth and was primarily dependent on current density and the Faradaic charge per mole requirement of the evolved gas. An increase in current density gave an increase in β through a corresponding increase in $(C_\infty - C_s)$, the driving force for bubble growth. This is shown in Fig. 4.3 where the growth coefficient of hydrogen and oxygen evolution is compared to that predicted by the "total gas production model" (22,23) i.e.

$$r(t) = \beta t^{0.33} \qquad (1.2\text{-}1)$$

where $$\beta = \left[(3\hat{R}TI\Sigma)/(4\pi PzF)\right]^{0.33} \qquad (1.2\text{-}2)$$

A current efficiency (Σ) of 100 % was assumed in the calculation of the curves given in Fig. 4.3.

A good fit was obtained between experimental and theoretical data, indicating a current/growth coefficient relationship of the form $\beta \propto I^{0.33}$. The best fit was observed at high current densities, corresponding to large bubble to electrode diameter ratios and high current efficiencies (see section 1.3), where the "total gas production model" was more likely to apply (chap.1, section 2.3.3). Bubbles of oxygen grew slower than

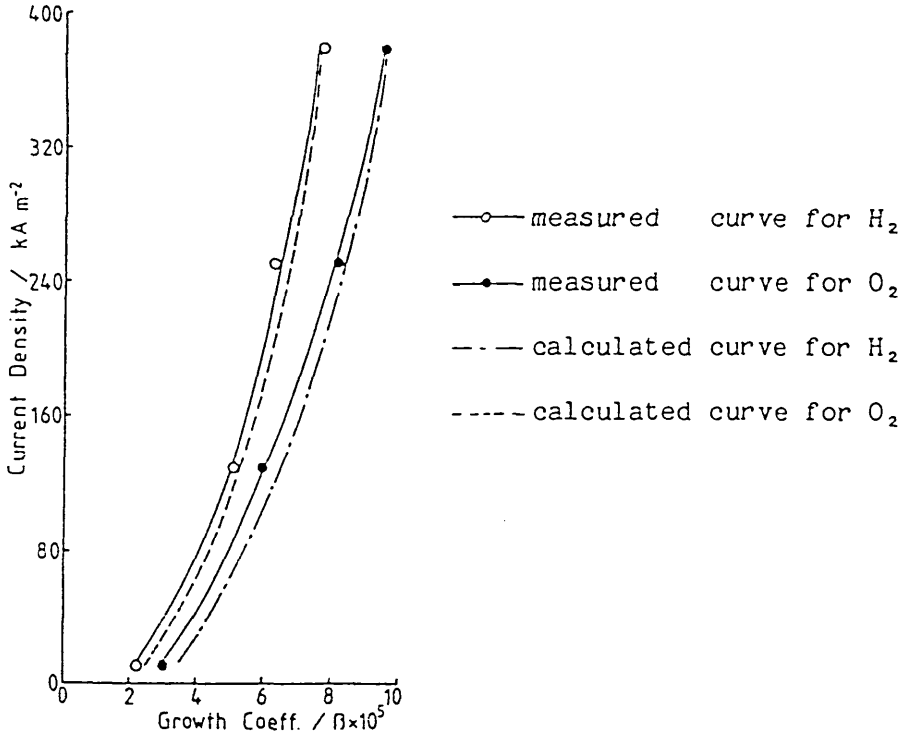


Fig. 4.3 The influence of current density on the growth coefficient of a bubble.

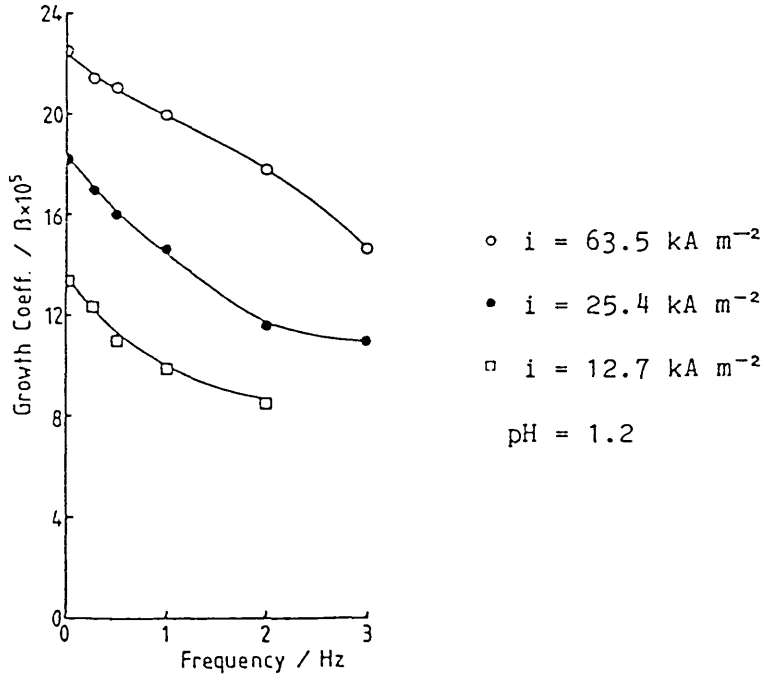


Fig. 4.4 The influence of rotation frequency on the growth coefficient during hydrogen evolution at a rotating disk electrode.

those of hydrogen or chlorine because only half the volume of gas was generated per unit charge.

Solution pH had no effect on the growth coefficient during hydrogen or oxygen evolution. However, the rate of growth of chlorine bubbles decreased at high pH due to the corresponding increase in the hydrolysis of chlorine to hypochlorite:

$$Cl_2 + 2OH^- \rightarrow ClO^- + H_2O + Cl^-$$

The growth coefficient of all gases decreased with increasing rotation frequency at both rotating disk (Fig. 4.4) and cylinder electrodes. This was due to enhanced gas transport away from the electrode at higher frequencies, leaving less gas available for bubble growth. However, accurate measurements were difficult to make as the bubble could be viewed only once per revolution.

Other variables studied were:

(i) Applied potential. Other than through its influence on current density, potential did not effect β

(ii) Electrolyte. Added surfactant (10^{-8} to 10^{-3} mol dm^{-3} DTAB or SDS) had no influence on β, showing growth rate to be independent of the mobility of the bubble interface.

(iii) Electrode material/pretreatment. β was the same for hydrogen bubbles generated on either platinum or silver electrodes. Therefore, though hydrogen adsorption by each electrode may have differed, it did not have a significant effect on β over the lifetime of a bubble. No difference in β was observed between bubbles grown on mechanically or electrochemically polished (280) silver electrodes.

Results obtained on different electrodes of the same diameter and material showed good agreement. This also applied to measurements of the time coefficient and bubble departure diameter.

1.3 The Time Coefficient

The time coefficient (x) allowed the mode of bubble growth to be determined, as will be shown later. Fig. 4.5 shows that the time coefficient changed during the lifetime of a bubble, tending towards 1.0 at very short times, dropping through 0.5 during the mid period of its growth, and tending towards 0.33 at long times. This was due to the corresponding increase in bubble diameter with time, the ratio of bubble to electrode diameter determining the time coefficient. This is more clearly shown by Fig. 4.6 where the influence of electrode diameter (d) on the time coefficient, for a given bubble diameter (d'), can be seen:

$$x \to 1.00 \text{ as } d'/d \to 0$$

$$x \to 0.33 \text{ as } d'/d \to \infty$$

Three modes of bubble growth can be defined. Immediately following nucleation a high supersaturation existed and bubble growth was hydrodynamically controlled, being governed by liquid inertia. The Rayleigh equation (18) describes this case when the time coefficient equalled unity.

$$r(t)=\left[(2\Delta P)/(3\rho)\right]^{0.5}.t \qquad (1.3\text{-}1)$$

In effect the bubble "exploded", with growth being driven

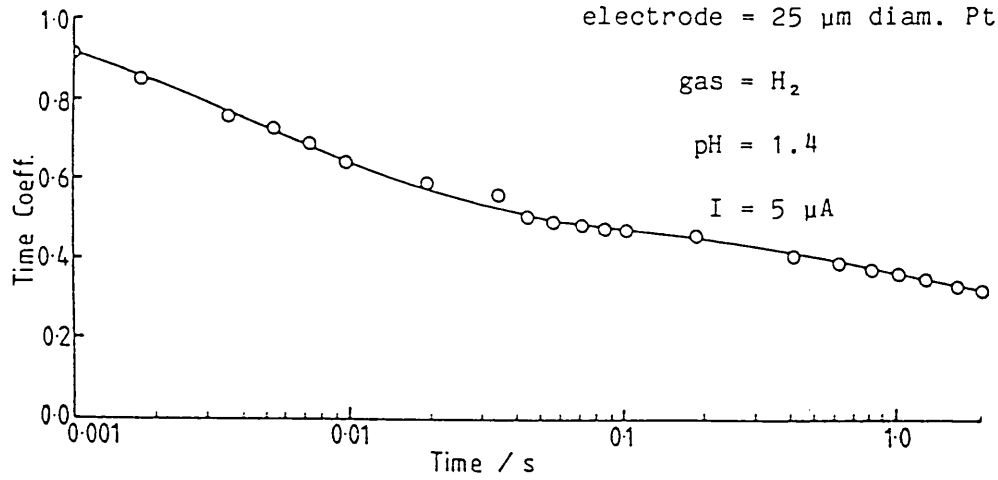


Fig. 4.5 The change in time coefficient during the lifetime of a bubble.

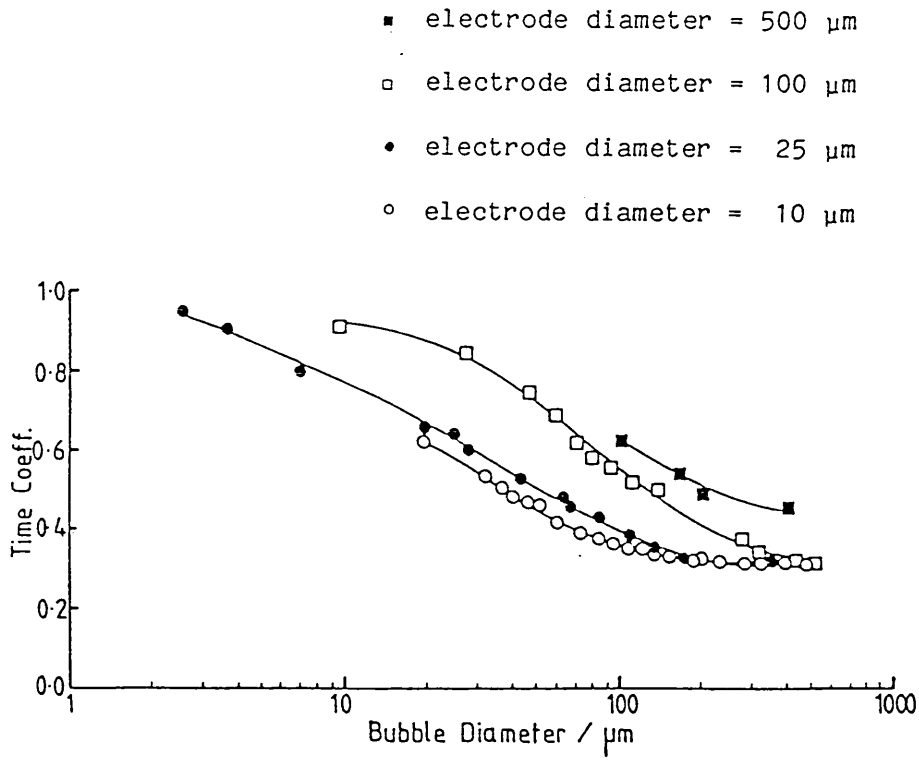


Fig. 4.6 The influence of bubble and electrode diameter on the time coefficient.

by the high internal excess pressure (ΔP) of the small bubble.

$$\Delta P = 2\gamma/r \qquad (1.3\text{-}2)$$

and with the supersaturated layer acting as a source of gas.

A rapid decrease in supersaturation at the bubble interface resulted from this high initial growth rate coupled with a low rate of gas diffusion. Growth was no longer inertia controlled but, with a time coefficient of one half, the growth kinetics were well described by an equation analogous to that derived by Scriven (16) for diffusion controlled spherical phase growth in an infinite, incompressible fluid:

$$r(t) = 2B\sqrt{(Dt)} \qquad (1.3\text{-}3)$$

(Note that if measured values of β (Fig. 4.3) are compared with the constant $2B\sqrt{D}$ in equation (1.3-3), where B is reported to be about 1 by Buehl and Westwater (17), diffusion coefficients of order 10^{-9} m^2 s^{-1} are obtained, in agreement with those reported in the literature (284)).

As the bubble diameter exceeded that of the electrode, steep dissolved gas concentration gradients were set up between the base of the bubble and the electrode. Gas effectively became "directly injected" into the bubble and Janssen's "total gas production model" (23) applied, giving a time coefficient of one third (see equations (1.2-1) and (1.2-2)). This mode of growth became increasingly dominant as the ratio of bubble to electrode

diameter increased.

The above results expand upon those presented by earlier workers (see chap.1, section 2.1.2), who reported a time coefficient of either one half or one third without allowing for it changing during growth (though the magnitude of the change is dependent upon the ratio of bubble to electrode diameter).

The relationship between bubble and electrode diameter for a given time coefficient is further described in Fig. 4.7. This shows that a given ratio of bubble to electrode diameter always resulted in the same time coefficient, and again illustrates the significance of that ratio in determining bubble growth kinetics.

The ratio of bubble to electrode diameter was also significant in determining bubble current efficiency (Σ), i.e. that proportion of the current which resulted in bubble growth. Assuming an initially saturated electrolyte:

$$\Sigma=(zF/it\bar{V}).(4\pi r^3/3) \qquad (1.3\text{-}4)$$

Fig. 4.8 illustrates the change in current efficiency during bubble growth at electrodes of 10-100 μm diameter. The greater the ratio of bubble to electrode diameter the greater was the current efficiency since less gas diffused into the bulk solution (though this was sensitive to the hydrodynamic regime (see section 3.4)). In addition the "mopping up" of dissolved gas by the bubble at long growth times may have been significant. The efficiencies reported here exceed those

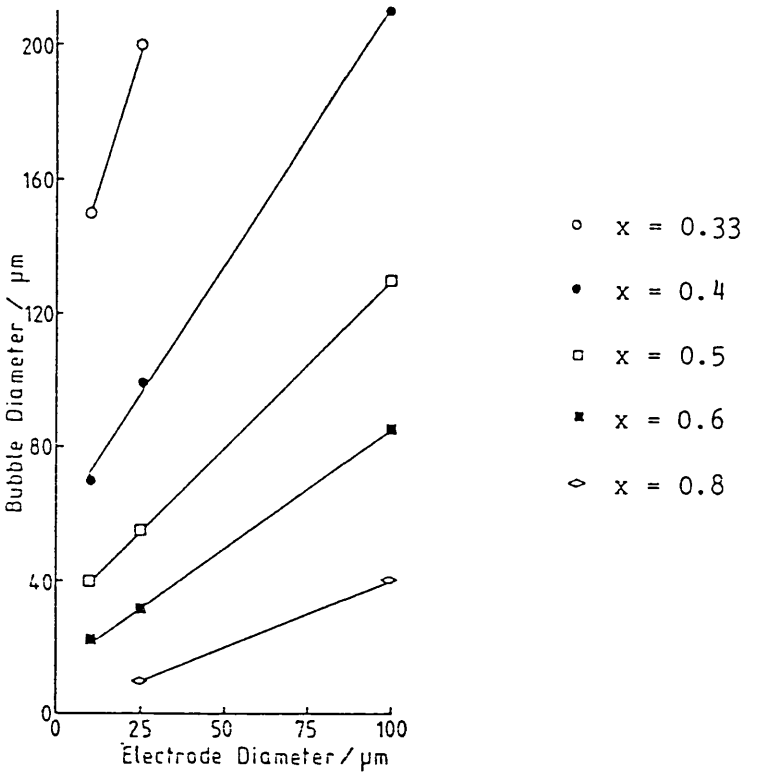


Fig. 4.7 The relationship between bubble and electrode diameter at differing time coefficients.

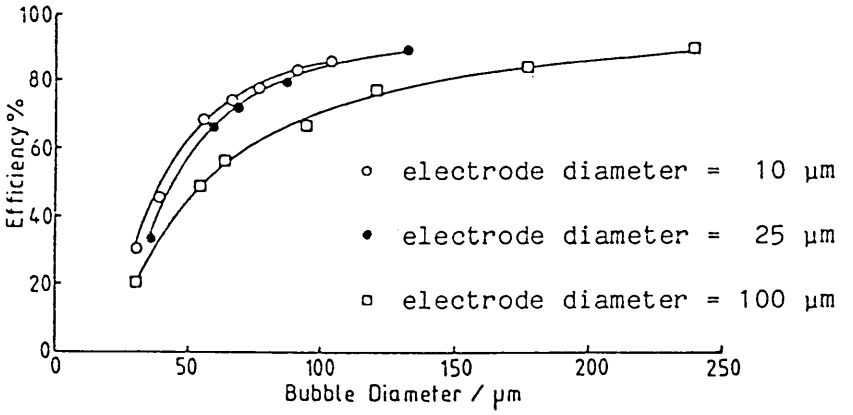


Fig. 4.8 The change in current efficiency during bubble growth at microelectrodes.

calculated by Vogt (77) for the "efficiency of gas evolution" because Vogt considered only multiple bubble growth at large electrodes, where much gas can be lost into solution.

Neither potential, current density, electrolyte, electrode material/pretreatment, hydrodynamics or pH had any effect on the time coefficient other than through their influence on the ratio of bubble to electrode diameter.

2 Electrode Charge

Characterisation of the electrode/electrolyte interface was important if full understanding of the factors influencing bubble growth was to be obtained. In particular the electrode charge was significant in determining bubble departure diameter (see section 3.1).

Information concerning electrode charge can be obtained from double layer capacitance measurements, made by previous workers for well defined platinum surfaces at potentials lying in the double layer region (see chap.1, section 2.1.3). However, in this work it was required to extend the potential range so that the charge on platinum oxide and platinum hydride could be measured, these surface phases being present during bubble growth experiments, as well as looking at the influence of electrolyte pH and the non-electrochemical adsorption of ionic surfactants on electrode charge.

The double layer capacitance of a platinum electrode was measured as a function of potential using a.c. impedance techniques (285). Following each potential step the current was

allowed to decay before making a measurement. At high anodic potentials (≥ 0.7 V v S.C.E.) this allowed oxide growth to essentially come to completion, so reducing time dependent effects on the measurements. At low anodic potentials (≤ 0.5 V v S.C.E.) the delay allowed oxide removal, shown by Gilroy (30,31) to occur in short times (< 50 msec at 0.2 V v S.C.E.), so ensuring that the capacitance of platinum alone was determined. Holding the electrode cathodic led to the possibility of it becoming hydrogen loaded, so the electrode was held for 12 hours at a potential in the double layer region to allow complete oxidation of adsorbed hydrogen.

Plots of real versus imaginary impedance resulted in semicircles (Fig. 4.9) characteristic of the following model (285), the equivalent circuit for which is given in Fig. 4.10:

$$Z(f)=R_1+(1/R_2+j\omega(C_1+C_2))^{-1}+R_3 \qquad (2\text{-}1)$$

$$Z(f)^2=Z_R{}^2+Z_I{}^2 \qquad (2\text{-}2)$$

R_1 represents the electrode resistance (≈2 Ω for a microelectrode), R_2 a faradaic reaction resistance, R_3 the resistance between luggin probe tip and electrode, C_1 double layer capacitance and C_2 a pseudo-capacitance arising from the ability of platinum to adsorb hydrogen, or from surface oxide phase growth during the period of measurement (C_2 was minimised by the experimental procedure). From the impedance plot in the complex plane (Fig. 4.10) it is possible to determine the double layer capacitance ($C=C_1+C_2$) as follows, where the plot is assumed to be a perfect semicircle:

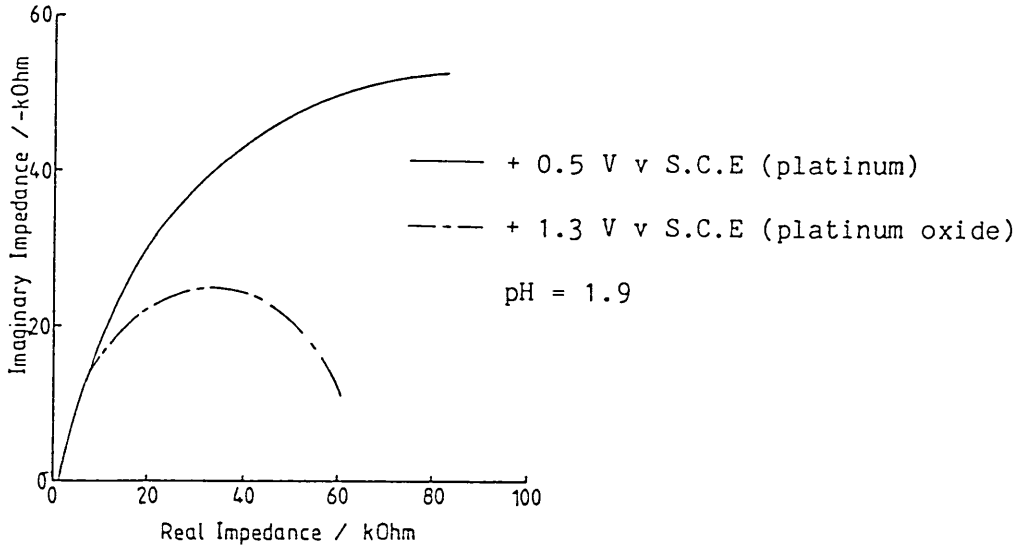
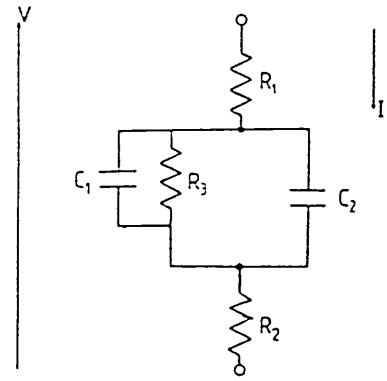
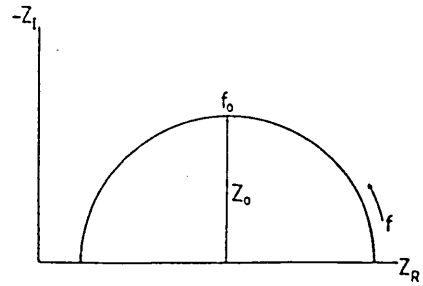


Fig. 4.9 Complex plane impedance plot for platinum and platinum oxide at a 100 μm diameter electrode.



A. Equivalent Circuit.



B. Complex Plane Impedance Plot.

Fig. 4.10 The equivalent circuit and ideal complex plane impedance plot of a platinum electrode.

$$C=(2\pi f_0 Z_0)^{-1} \qquad (2-3)$$

The double layer capacitance of platinum as a function of potential and solution pH is given in Fig. 4.11. Capacitance values of 11-30 μF cm^{-2} were observed in acid solution over the potential range -0.2 to +0.6 V v S.C.E., the so called double layer region, and compare favourably with the values of 14-20 μF cm^{-2} reported in the literature (25). The two minima observed in each curve arose at the potential of zero charge (p.z.c.) of the metal, the more anodic being the p.z.c of platinum oxide (PtO_x) which exists at potentials anodic of 0.2 to 0.7 V v S.C.E. at pH 12 to 1 (286). A high Faradaic current coupled with oxygen bubble evolution were observed above +1.6 V v S.C.E., limiting measurements to below this potential. However, at low pH a third minimum is perhaps indicated by the continuing decrease in capacitance with potential. This minimum could be attributed to the p.z.c. of PtO_2, which is the dominant surface phase at such high anodic potentials (37), or it may be due to a low space charge capacitance of the oxide phase dominating the double layer capacitance (287). Double layer capacitance increased rapidly at cathodic potentials due to the adsorption pseudo-capacitance associated with hydrogen evolution, which made measurements at strongly cathodic potentials impossible.

Fig. 4.12 summarises the influence of pH on the p.z.c. of platinum and platinum oxide, the results on platinum showing good agreement with those of Gileadi et al (38).

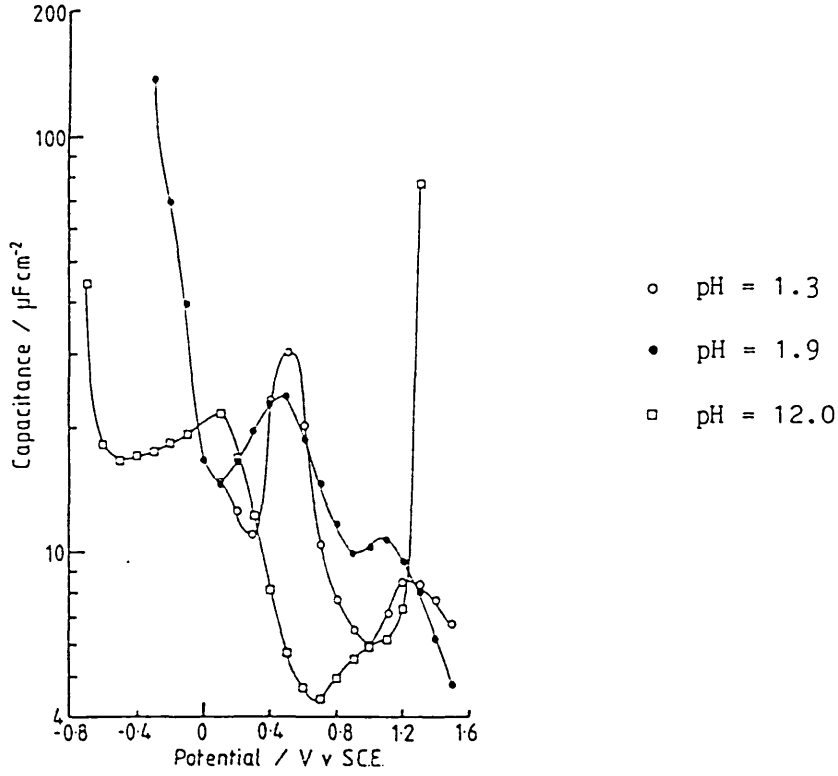


Fig. 4.11 The influence of pH on the double layer capacitance of a platinum/platinum oxide electrode.

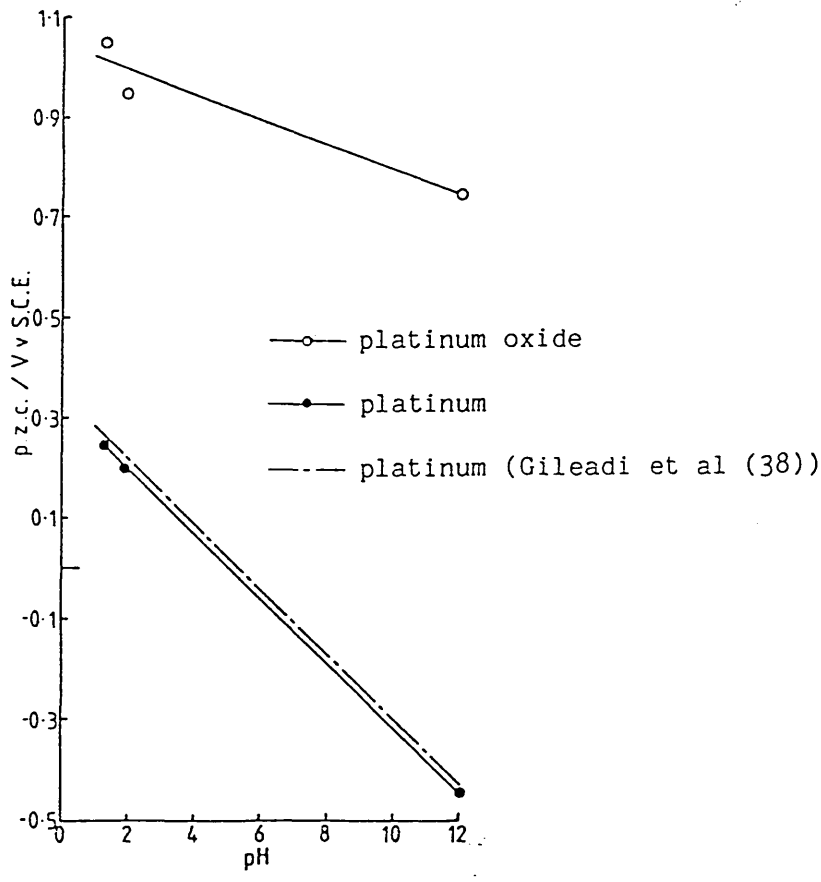


Fig. 4.12 The influence of pH on the potential of zero charge of platinum and platinum oxide.

The double layer capacitance of platinum in the double layer region increased with the addition of cationic (DTAB) and anionic (SDS) surfactant, as shown in Figs. 4.13 and 4.14, due to an increase in the total charge at the interface. The general shape of the capacitance curves followed that seen on platinum in surfactant-free electrolytes, but with a slight shifting of the p.z.c. of both platinum and platinum oxide. The latter is better illustrated by Figs. 4.15 and 4.16, which show DTAB to decrease the p.z.c. (by counteracting the negative charge on the electrode) and SDS to increase the p.z.c. (by enhancing the negative electrode charge). Alteration of the p.z.c. probably arose through hydrophobic interaction between surfactant and electrode. Electrostatic interaction would not be expected to make a significant contribution since such interaction reaches a minimum at the p.z.c.

The differential charge (Q) of the electrode at a given potential (E) was calculated from:

$$\partial Q = C\partial(E - E_{p.z.c.}) \qquad (2\text{-}4)$$

The results for platinum are presented in Fig. 4.17 as the modulus of charge versus potential. Consequently, values of charge lying cathodic of the p.z.c. are negative and those anodic are positive. Charge reversal occurred on sweeping the potential due to the formation of a new surface phase ($Pt \leftrightarrows PtO_x$). The decrease in charge at potentials anodic of 1.5 V v S.C.E. is again indicative of either the p.z.c. of PtO_2, or the

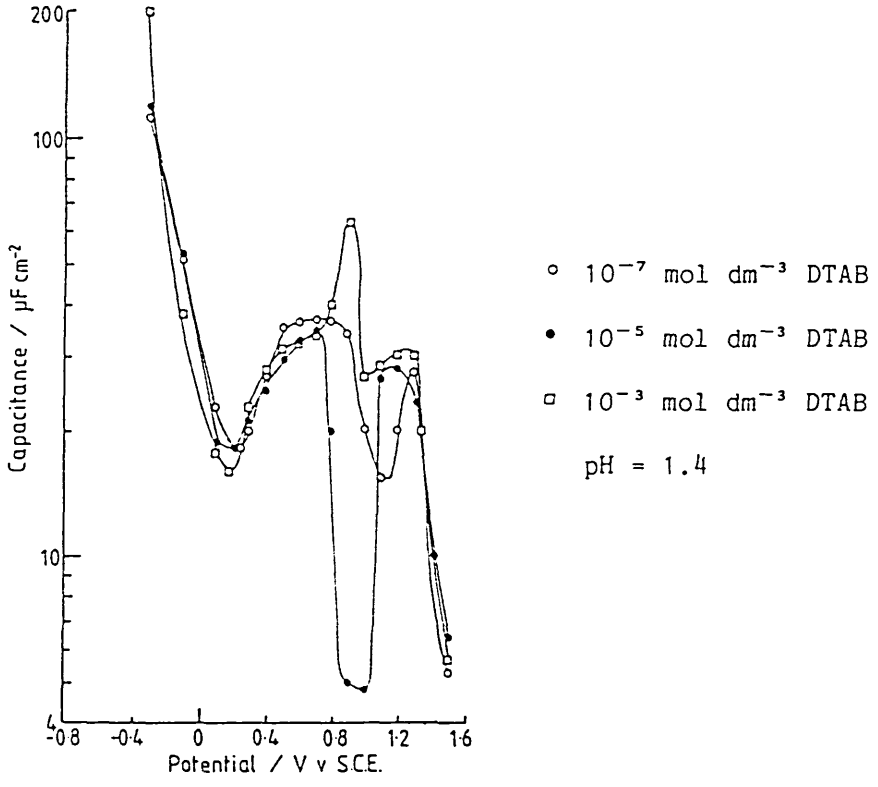


Fig. 4.13 Influence of the bulk DTAB concentration on the double layer capacitance of a platinum/platinum oxide electrode.

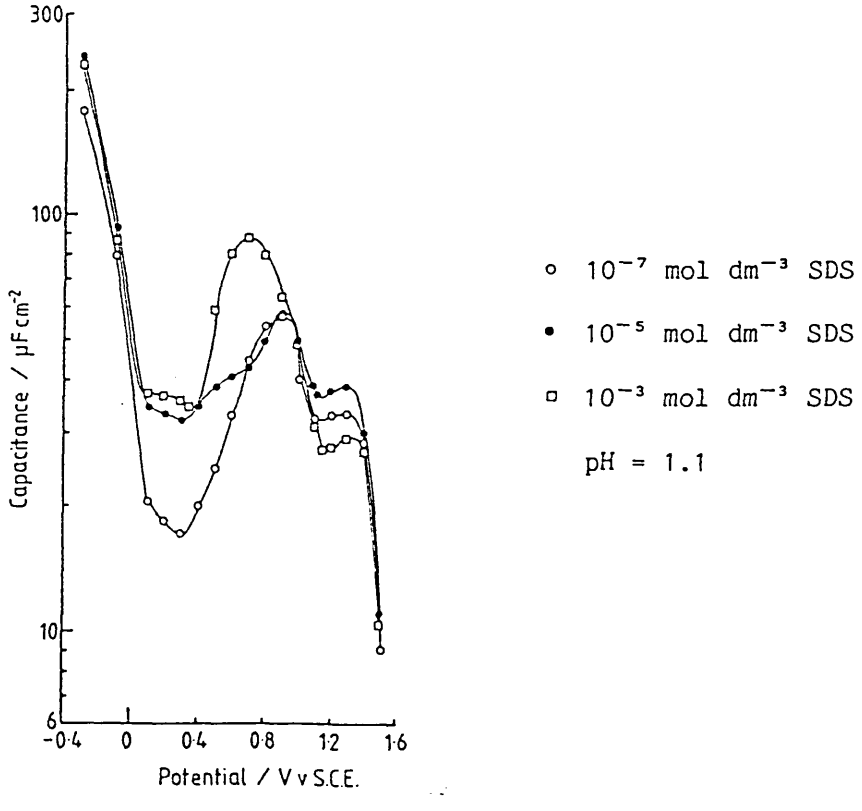


Fig. 4.14 Influence of the bulk SDS concentration on the double layer capacitance of a platinum/platinum oxide electrode.

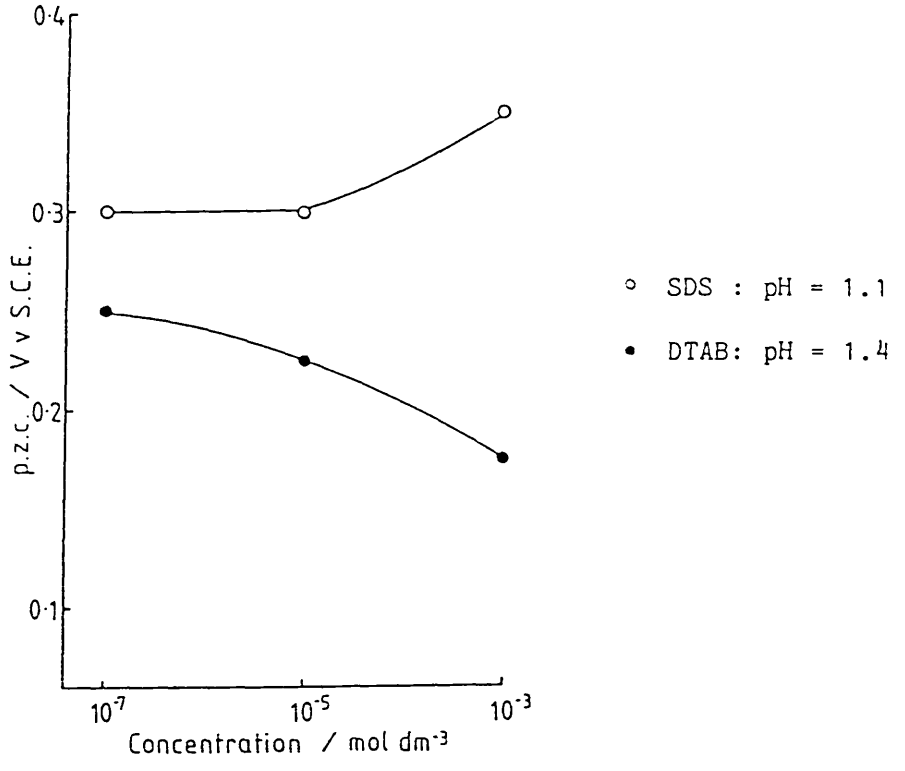


Fig. 4.15 Influence of the bulk surfactant concentration on the potential of zero charge of platinum.

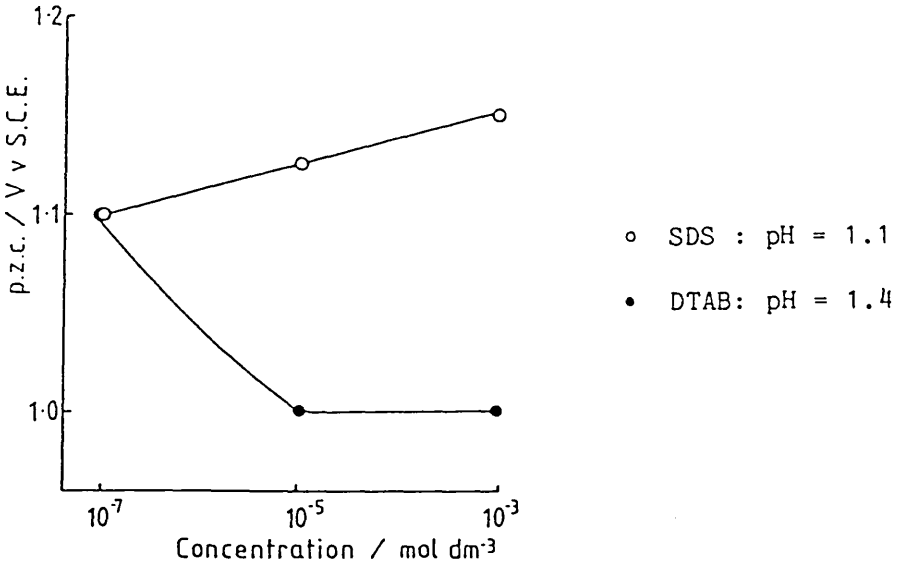


Fig. 4.16 Influence of the bulk surfactant concentration on the potential of zero charge of platinum oxide.

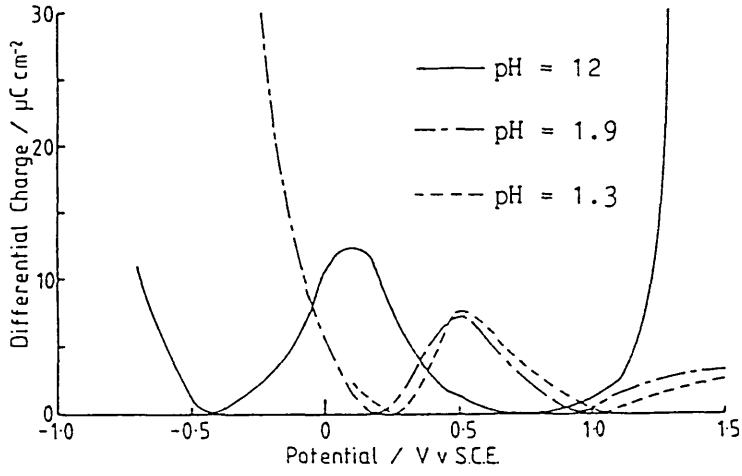


Fig. 4.17 The influence of pH on the differential charge of a platinum/platinum oxide electrode.

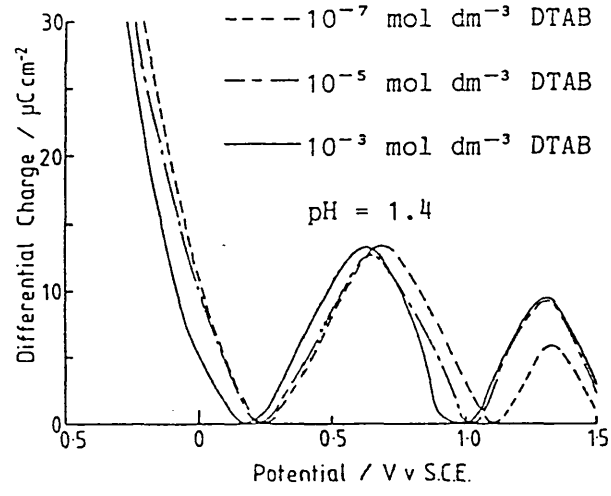


Fig. 4.18 Influence of the bulk DTAB concentration on the differential charge of a platinum/platinum oxide electrode.

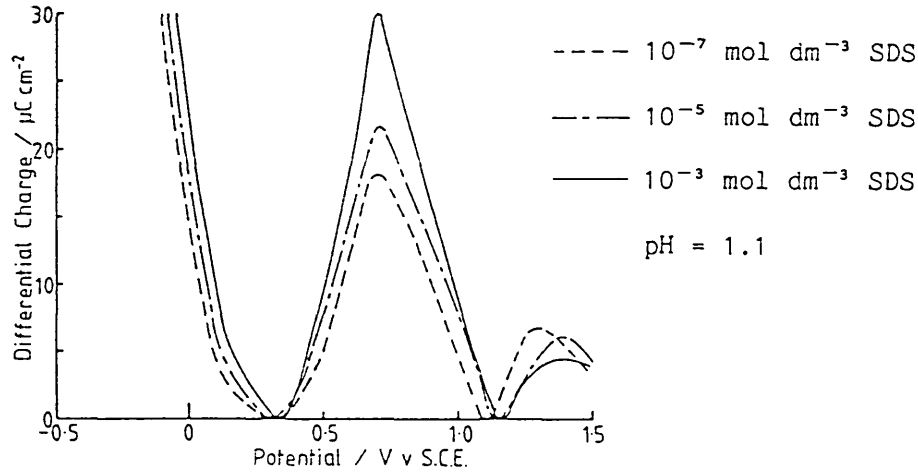


Fig. 4.19 Influence of the bulk SDS concentration on the differential charge of a platinum/platinum oxide electrode.

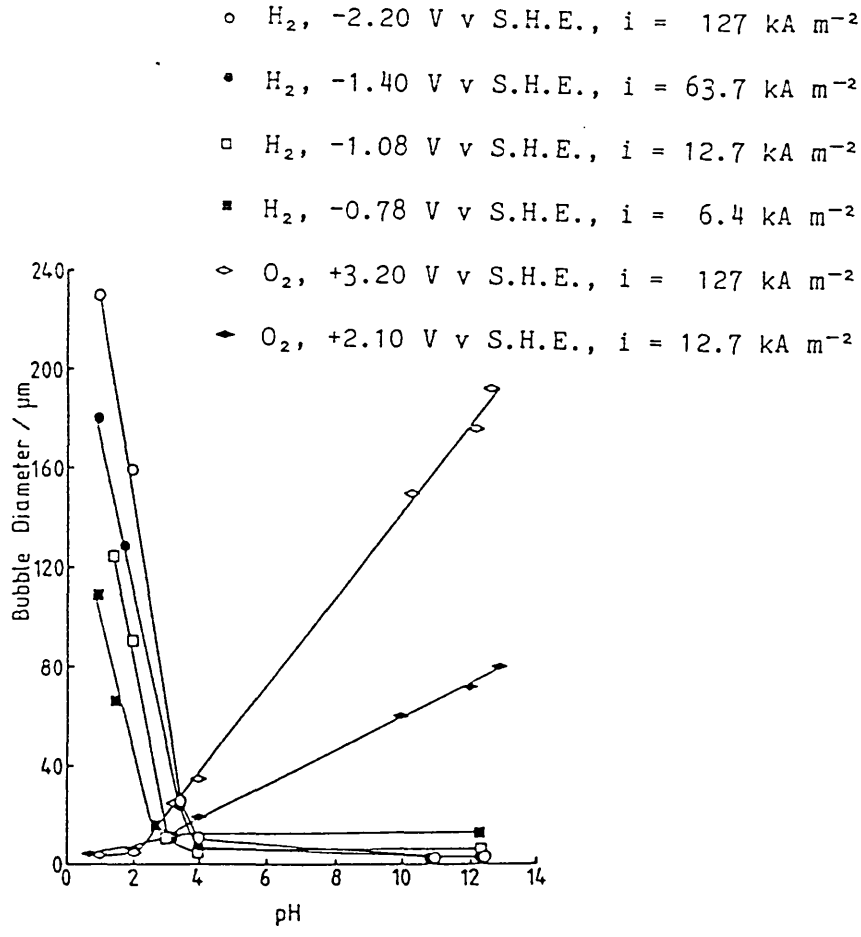


Fig. 4.20 The influence of pH on the departure diameter of hydrogen and oxygen bubbles at a 10 μm diameter platinum electrode.

influence of a space charge capacitance of the oxide phase.

The influence of DTAB on electrode charge is illustrated by Fig. 4.18. When the electrode was positively charged interaction between electrode and surfactant was probably via chemisorption and/or hydrophobic interaction, electrostatic interaction becoming significant only with a negatively charged electrode.

Fig. 4.19 shows SDS to have a greater effect on electrode charge than DTAB, perhaps because the better separation of polar and organic groups within the SDS molecule allowed greater interaction with the electrode surface. This is shown further by calculation of the fraction of the electrode surface covered by surfactant. Taking the area of an SDS molecule to be 25×10^{-20} m^2 (288) and that of DTAB as 26×10^{-20} m^2 (289), then Figs. 4.17-4.19 show that a maximum fractional coverage of 0.37 was obtained in milli-molar SDS, as compared to only 0.11 in milli-molar DTAB.

3 Bubble Departure Diameter

Bubbles appeared to be spherical at all times and did not exhibit a perceptible contact angle.

3.1 Influence of pH

Solution pH had a significant effect on bubble departure diameter (Figs. 4.20-4.23). At departure, hydrogen bubbles were large at low pH but small at high pH, the converse being observed during oxygen and chlorine evolution. These trends confirm the observations of earlier workers (95,111), though the marked change in the slope of the bubble diameter/pH curve at pH

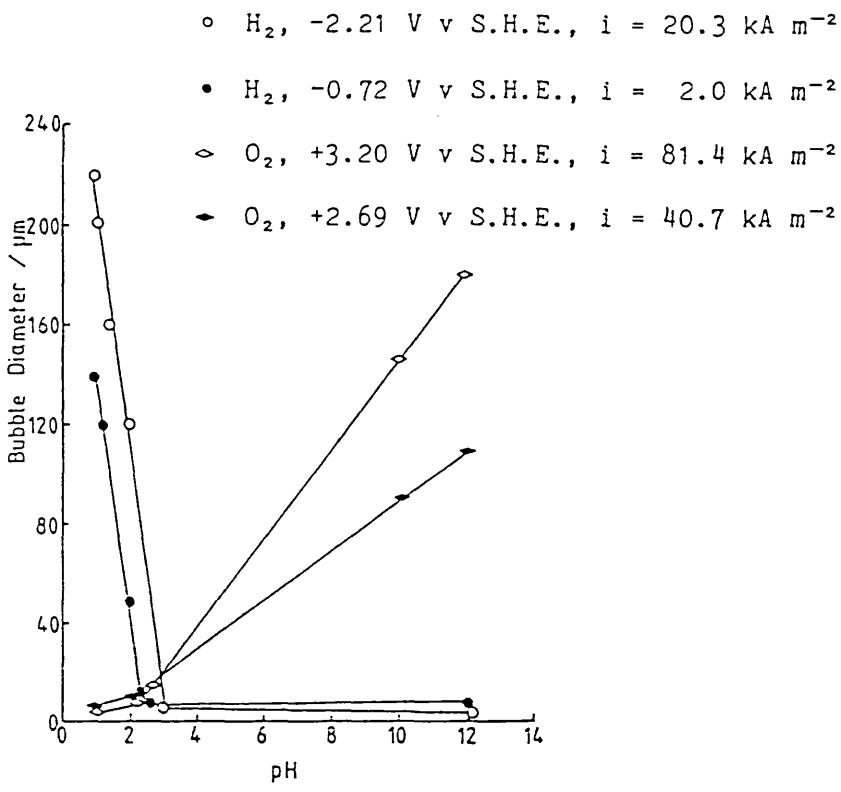


Fig. 4.21 The influence of pH on the departure diameter of hydrogen and oxygen bubbles at a 25 µm diameter platinum electrode.

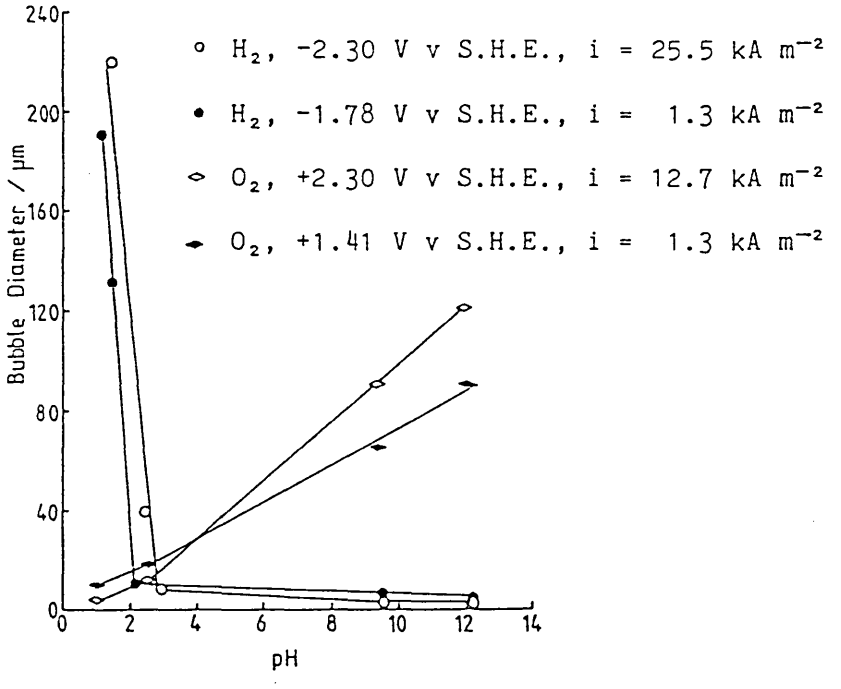


Fig. 4.22 The influence of pH on the departure diameter of hydrogen and oxygen bubbles at a 100 µm diameter platinum electrode.

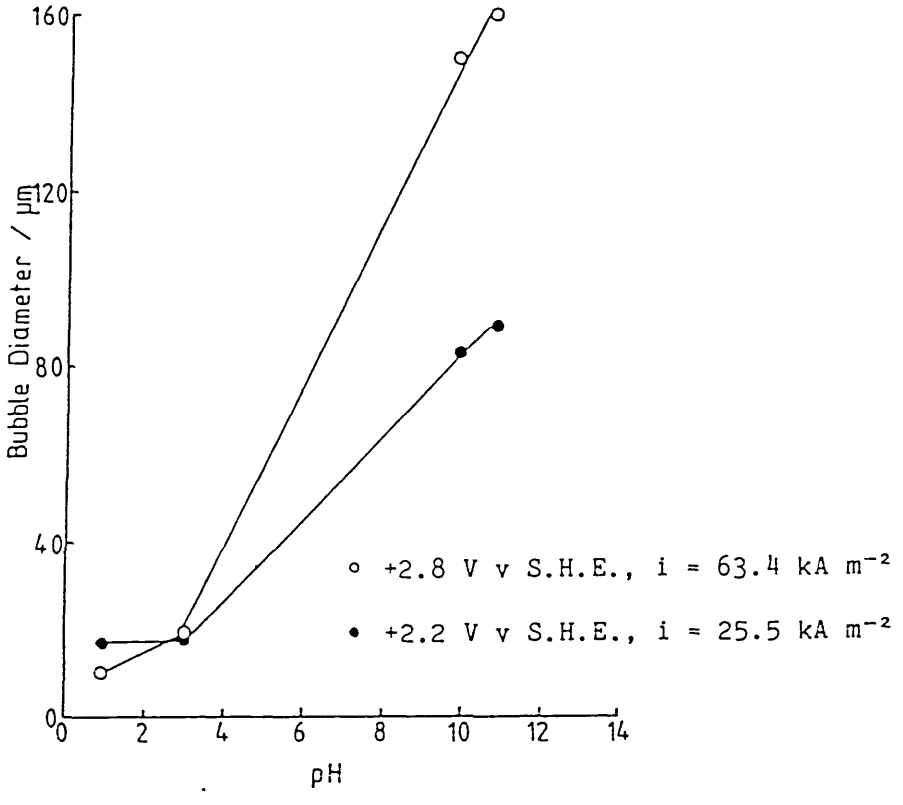


Fig. 4.23 The influence of pH on the departure diameter of chlorine bubbles at a 10 μm diameter platinum electrode.

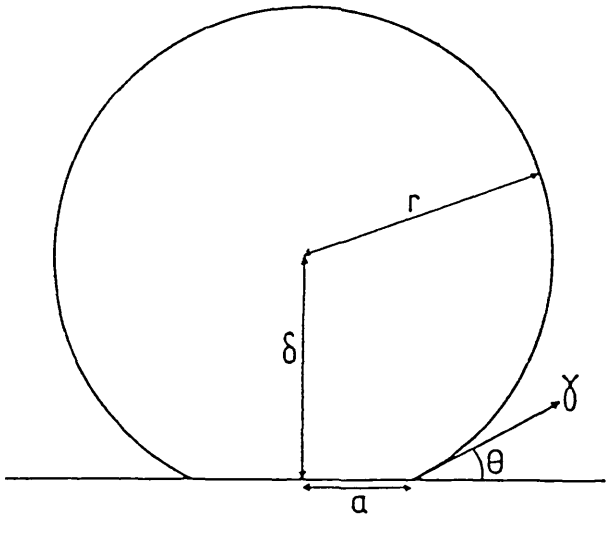


Fig. 4.24 Bubble as a segment of a sphere.

2-3 has not been reported previously.

As discussed earlier (chap.1, section 2.3.6) recent workers have considered only the bubble/electrode contact angle to be significant in determining bubble departure diameter. Indeed the following calculation shows that contact angles of only 3° would have been sufficient to hold bubbles of less than 400 μm diameter in place:

When a bubble exhibits a contact angle it is assumed to become a segment of a sphere (Fig. 4.24) and hence:

$$\cos\theta=\delta/r \qquad (3.1\text{-}1)$$

$$\sin\theta=a/r \qquad (3.1\text{-}2)$$

The volume of gas (V') within the bubble is:

$$V'=(4/3.\pi r^3)-(1/3.(r-\delta)(3r-(r-\delta)) \qquad (3.1\text{-}3)$$

Equating (3.1-1), (3.1-2) and (3.1-3) yields:

$$V'=r^3\left[(4\pi/3)-(\pi/3.(2-3\cos\theta+\cos^3\theta))\right]$$

$$=\pi r^3/3.(2+3\cos\theta-\cos^3\theta) \qquad (3.1\text{-}4)$$

The surface area of the bubble (S') is given by:

$$S'=4\pi r^2-2\pi r(r-\delta)=2\pi r^2(1+\cos\theta) \qquad (3.1\text{-}5)$$

If static equilibrium is assumed at the moment of bubble

departure then the following force balance can be drawn up:

$$F_B+F_P=F_T \qquad (3.1\text{-}6)$$

where F_B represents the buoyancy force acting on the bubble, F_P the force due to the excess pressure inside the bubble, and F_T the surface tension force. Consider first the buoyancy force.

If the top of the bubble is taken to be a distance H below the air/liquid interface, then the vertical component of the buoyancy force acting on a segment of the upper half of the bubble surface (at an angle σ from the vertical and of area $2\pi r\sin\sigma.rd\sigma$) is given by:

$$dF=\rho g(H+r(1-\cos\sigma))\cos\sigma.2\pi r^2\sin\sigma.d\sigma \qquad (3.1\text{-}7)$$

where $\rho=\rho_G-\rho_L$. Therefore, the total buoyancy force acting on the upper surface of the bubble is equal to the sum of the forces on each segment of that surface:

$$F\uparrow=2\pi r^2\rho g\int_0^{\pi/2}(H+r(1-\cos\sigma))\cos\sigma\sin\sigma.d\sigma$$

$$=\pi r^2\rho g(H+r/3) \qquad (3.1\text{-}8)$$

The vertical component of the buoyancy force acting on the lower half of the bubble is similarly given by:

$$F\uparrow=2\pi r^2\rho g\int_{\pi/2}^{\pi-\theta}(H+r(1+\sin\sigma))\sin\sigma\cos\sigma.d\sigma$$

$$=\pi r^2\rho g(H\sin^2\theta+r\sin^2\theta+2r/3.\sin^3\theta-H-5r/3) \quad (3.1\text{-}9)$$

Therefore, the net upward, vertical component of the buoyancy force acting on the bubble is:

$$F_B=F\downarrow+F\uparrow$$
$$=\pi r^2(\rho_L-\rho_G)g[r(4/3-\sin^2\theta-2\sin^3\theta/3)-H\sin^2\theta] \quad (3.1\text{-}10)$$

Note that in the absence of a contact angle equation (3.1-10) reverts to the well known relationship for the buoyancy of a sphere; $F=4/3.\pi r^3(\rho_L-\rho_G)g$.

The excess pressure inside the bubble (ΔP) can be derived by equating the decrease in surface free energy to the increase in (PV) energy when the bubble radius changes from r to $(r-\partial r)$. From equation (3.1-5) the decrease in surface free energy (F(s)) as $r\rightarrow(r-\partial r)$ is:

$$\partial F(s)=-4\pi\gamma r\partial r(1+\cos\theta) \quad (3.1\text{-}11)$$

where second order terms of ∂r are taken to be negligible. From equation (3.1-4) the change in (PV) energy as $r\rightarrow(r-\partial r)$ is, retaining only first order terms of ∂r:

$$\Delta(PV)=-\pi r^2\partial r(2+3\cos\theta-\cos^3\theta) \quad (3.1\text{-}12)$$

Therefore, equating (3.1-11) and (3.1-12) yields:

$$\Delta P=4\gamma/r.\left[(1+\cos\theta)/(2+3\cos\theta-\cos^3\theta)\right] \qquad (3.1\text{-}13)$$

In the absence of a contact angle, equation (3.1-13) is consistent with the conventional equation for the excess internal pressure of a spherical droplet; $\Delta P=2\gamma/r$.

The internal pressure of the bubble is dissipated over the area of the bubble foot (πa^2), so that the force acting on the bubble becomes:

$$F_P=4\pi\gamma r\sin^2\theta\left[(1+\cos\theta)/(2+3\cos\theta-\cos^3\theta)\right] \qquad (3.1\text{-}14)$$

The vertical component of the surface tension force is dependent on the circumference of the bubble foot ($2\pi a$) and takes the form:

$$F_T=2\pi\gamma r\sin^2\theta \qquad (3.1\text{-}15)$$

Therefore, substituting (3.1-10), (3.1-14) and (3.1-15) into (3.1-6) yields:

$$r(\rho_L-\rho_G)g\left[r(4/3-\sin^2\theta-2\sin^3\theta/3)-H\sin^2\theta\right]$$
$$=2\gamma\sin^2\theta\left[1-2\left\{(1+\cos\theta)/(2+3\cos\theta-\cos^3\theta)\right\}\right] \qquad (3.1\text{-}16)$$

Expressing (3.1-16) as a quadratic allows r to be given as:

$$r=(A+\sqrt{B})/C \qquad (3.1\text{-}17)$$

where, letting $\mu=\cos\theta$ and $\omega=\sin\theta$:

$$A=H\omega^2 \qquad (3.1\text{-}18)$$

$$B=A^2+8\gamma\omega^2/(\rho_L-\rho')g.\left[1-2\left\{(1+\mu)/(2+3\mu-\mu^3)\right\}\right].$$
$$(4/3-\omega^2-2\omega^3/3) \qquad (3.1\text{-}19)$$

$$C=2(4/3-\omega^2-2\omega^3/3) \qquad (3.1\text{-}20)$$

Therefore, for H=0.1 m and $\theta=3°$, equation (3.1-17) gives a bubble departure diameter of ~400 μm.

However, particularly for the case of fast growing bubbles, the inertia of the liquid surrounding the bubble (F_I), and the viscous drag acting on the growing gas/liquid interface (F_D) may also influence the bubble departure diameter, i.e. a dynamic equilibrium must be assumed. The force balance then becomes:

$$F_B+F_P=F_T+F_I+F_D \qquad (3.1\text{-}21)$$

The inertial force retarding bubble departure can be expressed as:

$$F_I=d/dt(Mv) \qquad (3.1\text{-}22)$$

where v is the rate of bubble growth (dr/dt) and M the virtual mass of the bubble, shown by Milne Thompson (290) to be:

$$M=w'+w/2+3wa^3/16b^3 \qquad (3.1\text{-}23)$$

for inviscid liquids (for viscous liquids equation (3.1-23) is only approximate). For the geometry considered here:

$$a=r \qquad b=r\cos\theta \tag{3.1-24}$$

so that, from (3.1-4):

$$M=\pi r^3/3.(2+3\cos\theta-\cos^3\theta).(\rho'+\rho/2+3\rho/16\cos^3\theta) \tag{3.1-25}$$

Therefore, introducing the bubble growth equation (see section 1):

$$r=\beta t^x \tag{3.1-26}$$

gives, from (3.1-22):

$$F_I=\pi/3.(2+3\cos\theta-\cos^3\theta)\beta^4x(4x-1)t^{4x-2} \tag{3.1-27}$$

The drag force acting on a bubble in a clean system at Re < 1 is given by (203):

$$F_D=4\pi\eta rv \tag{3.1-28}$$

Therefore, from (3.1-26):

$$F_D=4\pi\eta\beta^2t^{2x-1} \tag{3.1-29}$$

Values of x, β and t can be obtained from Figs. 4.3 and 4.6, and substitution of this data into equations (3.1-27) and (3.1-29) showed that the force due to either drag or inertia was several orders of magnitude less than that due to surface tension under the same conditions. Therefore, drag and inertia can be taken to make a negligible contribution to the force of bubble attachment in the presence of a bubble/electrode contact angle.

However, the presence of a contact angle would not explain the marked influence of pH on departure diameter. In addition, all bubbles immediately left the electrode following either current interruption or a sufficient reduction in applied potential, indicating that they were not being held by a surface tension force. Instead, it is proposed that electrostatic interaction between the bubble and electrode double layers controls bubble departure diameter, and that bubbles were tangential to the electrode with a thin liquid film separating the two phases. In the absence of a contact angle a thin film must exist; indeed, the bubble/electrolyte interface itself can be considered to be a thin film (291). Experimental evidence for the existence of such a film is given in section 1.1 of chapter 5.

Electrostatic attraction between bubble and electrode occurred when they were oppositely charged. For example, during oxygen or chlorine evolution at high pH the electrode was positively charged, applied potentials being strongly anodic of the p.z.c. of platinum oxide (Fig. 4.12), and the bubble

negatively charged, as shown by electrophoretic mobility measurements (Fig. 3.8). Consequently at high pH, oxygen and chlorine bubbles were held strongly to the electrode, and exhibited large departure diameters. Departure diameter decreased with decreasing pH due to a corresponding decrease in bubble charge (Fig. 3.16) and increase in the p.z.c. of the electrode (Fig. 4.12), so decreasing electrode charge at a given potential. Below pH 2-3 bubbles were positively charged (Fig. 3.16) and electrostatic repulsion led to small departure diameters. Indeed, bubbles may have departed from the electrode immediately following nucleation, growing to the observed departure diameter (~10μm at pH 12) within the first period of measurement ($\leq$ 20 msec), whilst still appearing to reside on the electrode due to the correspondingly small distance of rise.

During hydrogen evolution the electrode was strongly cathodic of the p.z.c. of platinum (Fig. 4.12) and hence negatively charged. Therefore, positively charged bubbles (pH $\leq$ 2-3) were held and negatively charged ones (pH $\geq$ 2-3) repelled.

The validity of the above explanation can be examined by the following calculation. Under conditions of bubble/electrode electrostatic attraction the departure diameter of the majority of bubbles greatly exceeded the electrode diameter. Therefore, the small curvature of the bubble interface over the electrode allows a plane/plane model of double layer interaction to be assumed. Hogg et al (292) give:

$$V=\varepsilon\kappa/8\pi.\left[(\psi_1^2+\psi_2^2)(1-\coth(2\kappa\partial))+2\psi_1\psi_2\,\mathrm{cosech}(2\kappa\partial)\right] \quad (3.1\text{-}30)$$

for the potential energy of interaction (V) between two parallel, flat double layers. Hence, since P, the disjoining pressure across the thin film of thickness ∂ which separates bubble and electrode, is given by (291):

$$P=-dV/d\partial \qquad (3.1\text{-}31)$$

it follows from equation (3.1-30) that:

$$P=\varepsilon\kappa^2/4\pi.\mathrm{cosech}(2\kappa\partial).\left[(\zeta_1^2+\zeta_2^2)\mathrm{cosech}(2\kappa\partial)-2\zeta_1\zeta_2\coth(2\kappa\partial)\right] \qquad (3.1\text{-}32)$$

where a positive pressure indicates electrostatic attraction. ζ_1 and ζ_2 are taken to represent the zeta potential of the electrode and bubble respectively, though they are more accurately the potential at the outer Helmholtz plane of the respective double layers. Equation (3.1-32) assumes the Debye-Huckel approximation to hold true, i.e. small zeta potentials (typically < 25 mV), and the use of a 1:1 electrolyte.

κ, the inverse Debye length, can be calculated from the following equation (173):

$$\kappa=\left[(1\times10^3F^2.\textstyle\sum c_i z_i^2)/(\varepsilon\hat{R}T)\right]^{0.5} \qquad (3.1\text{-}33)$$

which gives values of 0.1-3.3 $(nm)^{-1}$ for κ in 0.001-1.0 mol dm^{-3} 1:1 electrolyte at 298 K.

ζ_1 and ζ_2 were calculated from measured values of electrode and

bubble surface charge density (Figs. 4.17 and 3.16) using equation (3.1-34) (173):

$$\sigma=\{2\kappa kT\sum n_i[\exp(-z_i e\zeta/kT)-1]\}^{0.5} \qquad (3.1-34)$$

This shows zeta potential to be influenced by κ, and hence ionic strength.

Using measured data for the influence of electrolyte concentration on bubble departure diameter (Fig. 4.32), equations (3.1-32) to (3.1-34) can be used to calculate the thickness of the thin film between bubble and electrode. Assuming dynamic equilibrium at the moment of bubble departure, a force balance gives:

$$F_B=F_E+F_I+F_D \qquad (3.1-35)$$

where F_B, F_E, F_I, and F_D represent the forces due to buoyancy, electrostatic interaction, inertia and drag respectively. The buoyancy force acting on a spherical bubble is given by:

$$F_B=4\pi r^3(\rho-\rho')g/3 \qquad (3.1-36)$$

and F_I and F_D have been defined previously (see equations (3.1-27) and (3.1-29)). Therefore, assuming the disjoining pressure to be uniformly distributed over the electrode area (S) yields:

$$P=(F_B-F_I-F_D)/S \qquad (3.1\text{-}37)$$

Table 4.1 summarises the thickness (∂) of the thin film between bubble and electrode calculated from experimental data (Fig. 4.32) using equation (3.1-37). Values for β and x were taken from Figs. 4.3 and 4.6, and σ_1 and σ_2 were taken to be about 30 and -0.05 $\mu C\ cm^{-2}$ from Figs. 4.17 and 3.16.

$[c]$ mol dm^{-3}	∂ / (nm)
10^{-3}	135
10^{-2}	49
10^{-1}	16
10^{0}	5

Table 4.1 The influence of electrolyte concentration on the thickness of the thin film between bubble and electrode during oxygen evolution at a 25 µm diameter platinum electrode.

It should be noted that the thin film does not rupture under the action of a positive disjoining pressure due to the presence of 'dispersive' Van der Waals forces, which stabilise the thin film at the thickness given above.

The values of ∂ reported in Table 4.1 are of the same order as those typically reported in thin film work (291,293-296), indicating that, in the absence of a bubble/electrode contact

angle, the force of electrostatic attraction between the bubble and electrode double layers is sufficient to hold bubbles at the electrode (if this was not the case then the value of ∂ calculated using equation (3.1-37) would be much smaller than expected). However, the values of ∂ reported above cannot be exact because the following assumptions were made in their calculation.

(i) The calculated zeta potential of the electrode in some cases exceeded 25 mV, particularly at low ionic strengths, so introducing a small error term in equation (3.1-32) due to counter ion adsorption.

(ii) The distance ∂ may more accurately represent the mean distance between the curved bubble interface and the plane electrode. This would be greater than the thin film thickness and therefore reduce the force of attraction. To account for this effect a plate/sphere model of double layer interaction could be used.

(iii) The mobility of the bubble interface would allow the presence of a charged electrode to polarise charge on the bubble surface. This would be expected to enhance the net attractive force.

(iv) The dielectric constant of the double layer is less than that of the bulk electrolyte (typically 6-8 as opposed to ~80 (297)). This decreases the disjoining pressure.

Despite the above assumptions equation (3.1-32) predicts the experimentally observed trends of reduced electrostatic attraction with reduced ζ_1 and ζ_2, and electrostatic repulsion when

bubble and electrode are of like charge. The minimum force of attraction occurs at the p.z.c. of bubble or electrode; therefore the marked change in the departure diameter of hydrogen, oxygen and chlorine bubbles around pH 2-3 is further evidence that the p.z.c. of the gas/liquid interface occurs at that pH. However, local pH changes must be calculated (perhaps by numerically solving the Laplace equation to give the distribution of OH^-/H^+ ions) before the actual pH at the electrode can be stated confidently.

Figs. 4.20-4.23 illustrate the influence of electrode potential on bubble departure diameter. A higher applied potential gave significantly greater departure diameters when bubble and electrode were oppositely charged, and marginally smaller departure diameters when bubble and electrode were of like charge. This follows from the increase in electrode charge with potential, and consequently the increase in electrostatic attraction or repulsion. The influence of potential on departure diameter is better illustrated by Fig. 4.31 which indicates a linear relationship between applied potential (which includes an uncompensated ohmic potential loss) and bubble departure diameter. However, the reported potentials are only modal values since the bubble itself distorts the potential distribution (see chap.5, section 1.1).

3.2 Influence of Electrode

Bubble growth was studied on 25 μm diameter electrodes of platinum (Fig. 4.21) and silver (Fig. 4.25), with reduced hydrogen (at low pH) and increased oxygen (at high pH) bubble departure diameters being observed on silver. This follows from the different p.z.c. of the metals, e.g. at pH 7 the p.z.c of platinum equals -0.13 V v S.C.E. (Fig. 4.12), whilst the p.z.c. of silver equals -0.74 V v S.C.E. (298), the more negative p.z.c. of silver giving the electrode a reduced differential charge during hydrogen evolution, and an increased charge during oxygen evolution. Consequently, this influenced bubble departure diameter through the parameter ζ_1 in equation (3.1-32).

Electrode diameter had no influence on bubble departure diameter during individual bubble growth. However, at large electrode diameters ($\geq$ 100 μm) multiple bubble growth often occurred due to the greater number of nucleation sites, this becoming more prevalent with increasing electrode diameter. During multiple bubble growth the mean bubble size was smaller, perhaps because of increased hydrodynamic flow (due to turbulence induced by growing and departing bubbles) and inter-bubble repulsion forces. However, similar trends in mean bubble departure diameter with pH and potential were observed.

3.3 Influence of Electrolyte

The influence of electrolyte pH on bubble departure diameter has already been discussed (section 3.1). Here, the effect of added surfactant, and electrolyte symmetry and

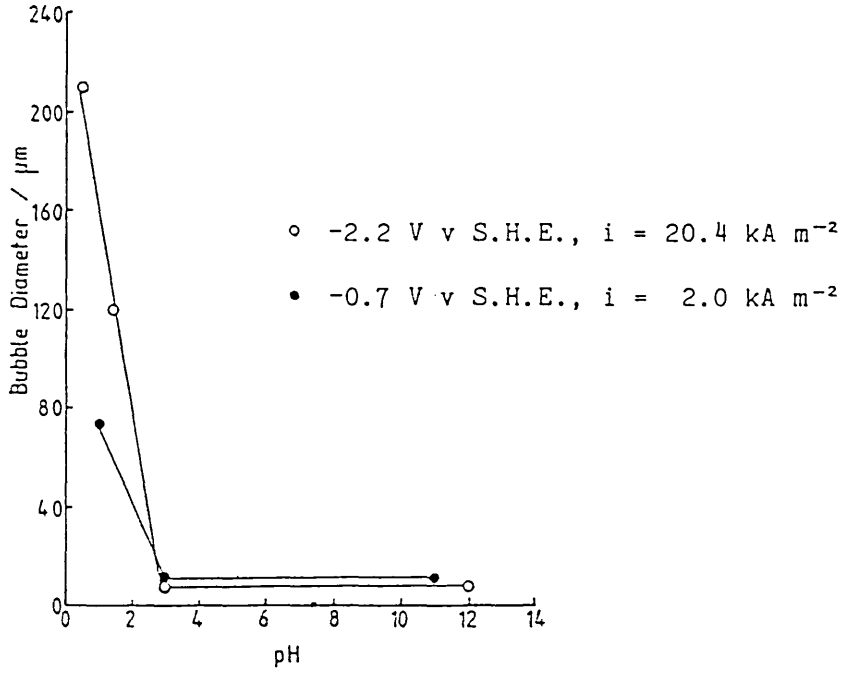


Fig. 4.25 The influence of pH on the departure diameter of hydrogen bubbles at a 25 μm diameter silver electrode.

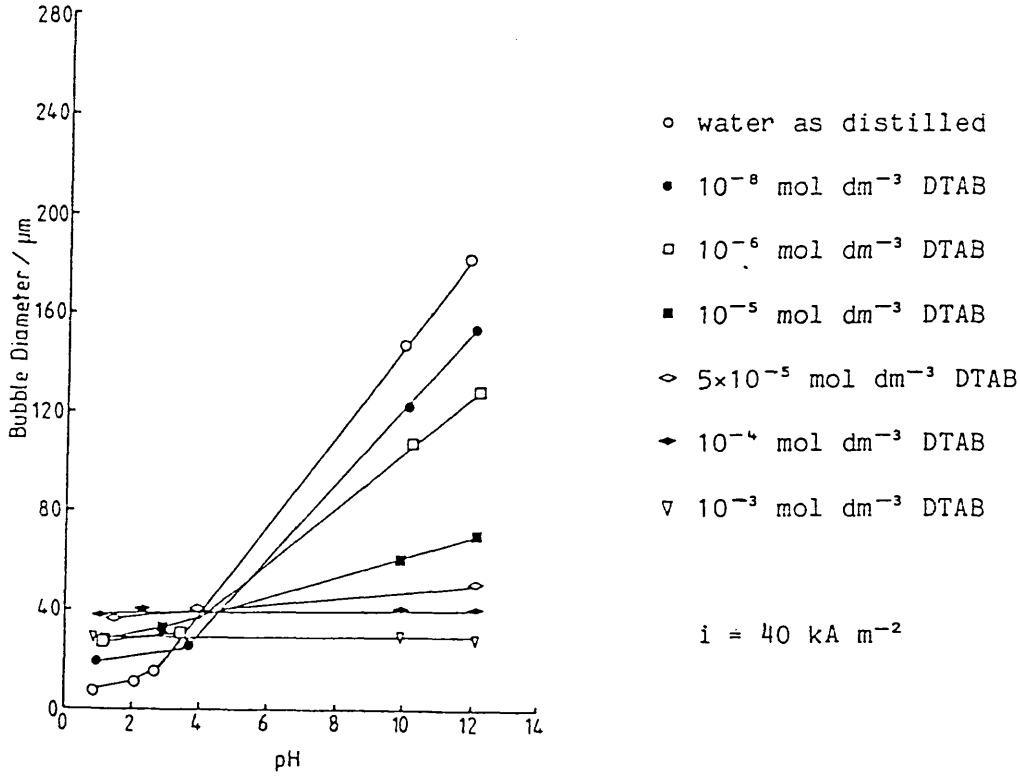


Fig. 4.26 Influence of the bulk DTAB concentration on the departure diameter of oxygen bubbles at a 25 μm diameter platinum electrode.

concentration will be considered.

Figs. 4.26 and 4.27 show the influence of a cationic surfactant (DTAB) on bubble departure diameter during oxygen and hydrogen evolution. There was a gradual equalizing of diameter across the pH range, and at differing current densities (Fig. 4.28), as the surfactant concentration was increased. This cannot be solely attributed to a decrease in surface tension since this was less than 8 % over the concentration range used (283). Instead it can be explained as the influence of the positively charged surfactant on bubble/electrode double layer interaction since it has been shown, by an increase in double layer capacitance with added DTAB (Fig. 4.13), that DTAB adsorbed on the electrode surface through a possible combination of chemisorption, hydrophobic interaction and electrostatic attraction (section 2). Similarly DTAB adsorbed at the bubble interface to give an increasingly positive electrophoretic mobility (Fig. 3.13) and, by inference, charge (Fig. 3.15 describes the adsorption isotherm). Therefore, the adsorption of positively charged surfactant onto both bubble and electrode led to electrostatic repulsion between the like charged surfactant species, decreasing bubble departure diameter. The significance of this effect increased with added DTAB, eventually masking the influence of pH and potential and giving a uniform bubble diameter.

Very small bubbles ($\leq$ 60 μm diameter) did not depart from the electrode following current interruption at DTAB concentrations greater than 10^{-4} mol dm^{-3}. This was attributed to the presence of

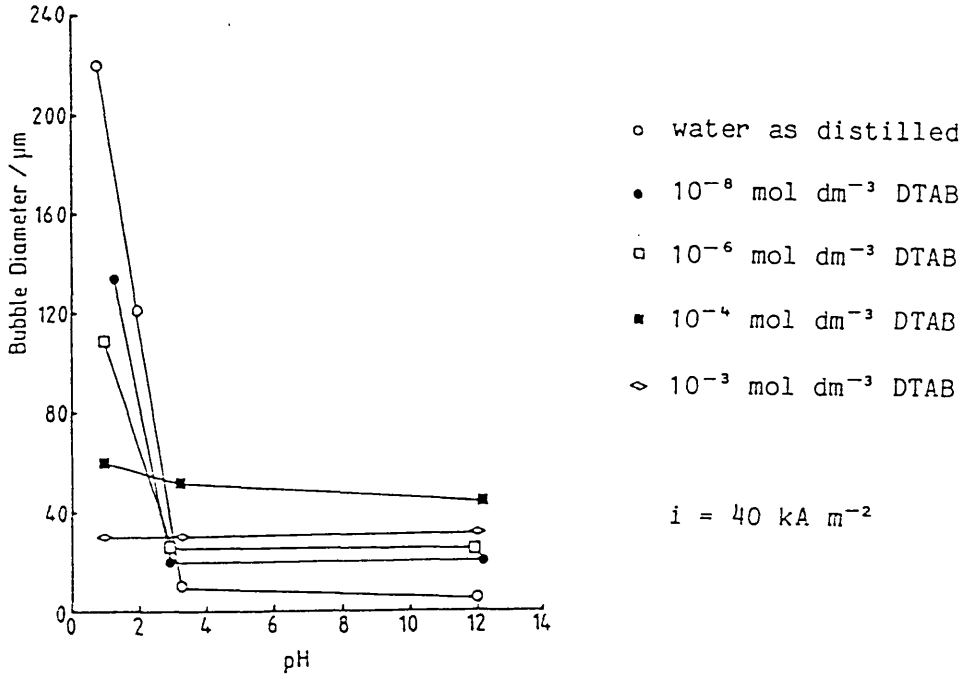


Fig. 4.27 Influence of the bulk DTAB concentration on the departure diameter of hydrogen bubbles at a 25 µm diameter platinum electrode.

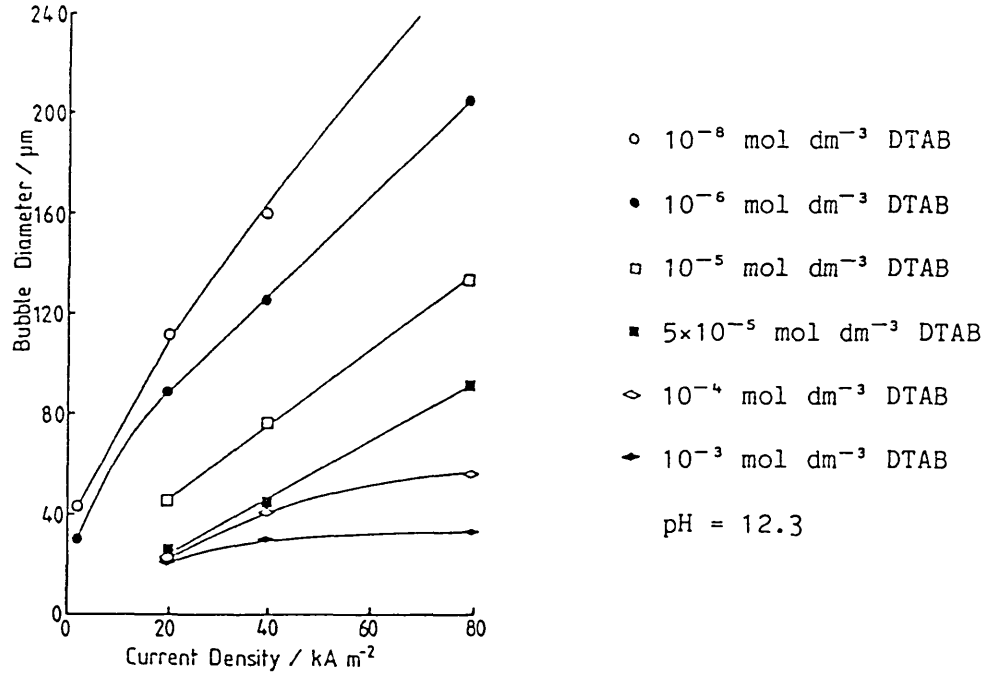


Fig. 4.28 Influence of the bulk DTAB concentration on the departure diameter of oxygen bubbles at a 25 µm diameter platinum electrode, with varying current density.

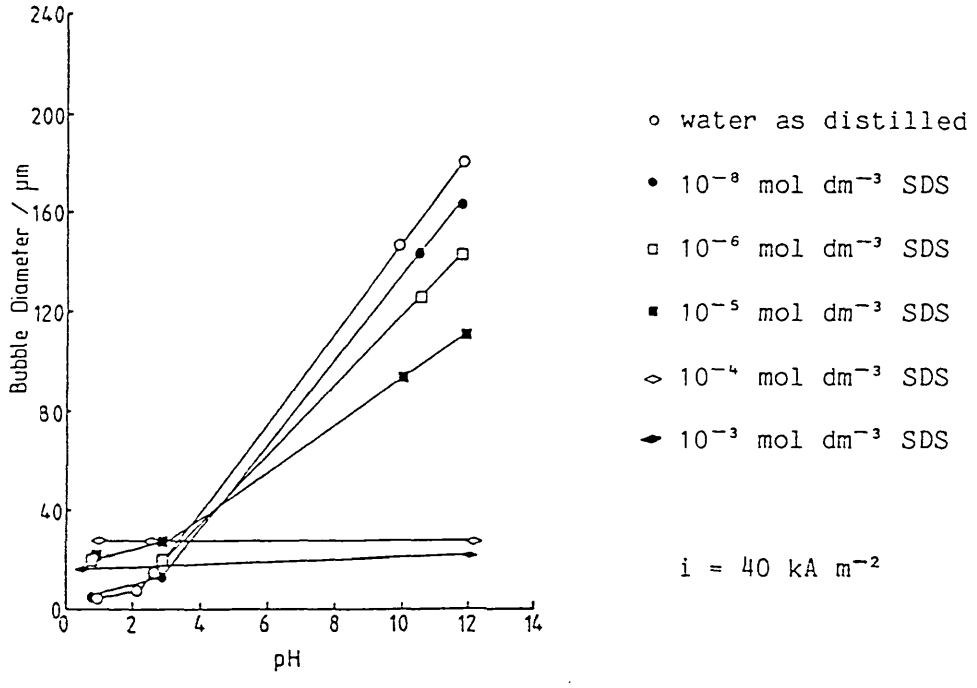


Fig. 4.29 Influence of the bulk SDS concentration on the departure diameter of oxygen bubbles at a 25 µm diameter platinum electrode.

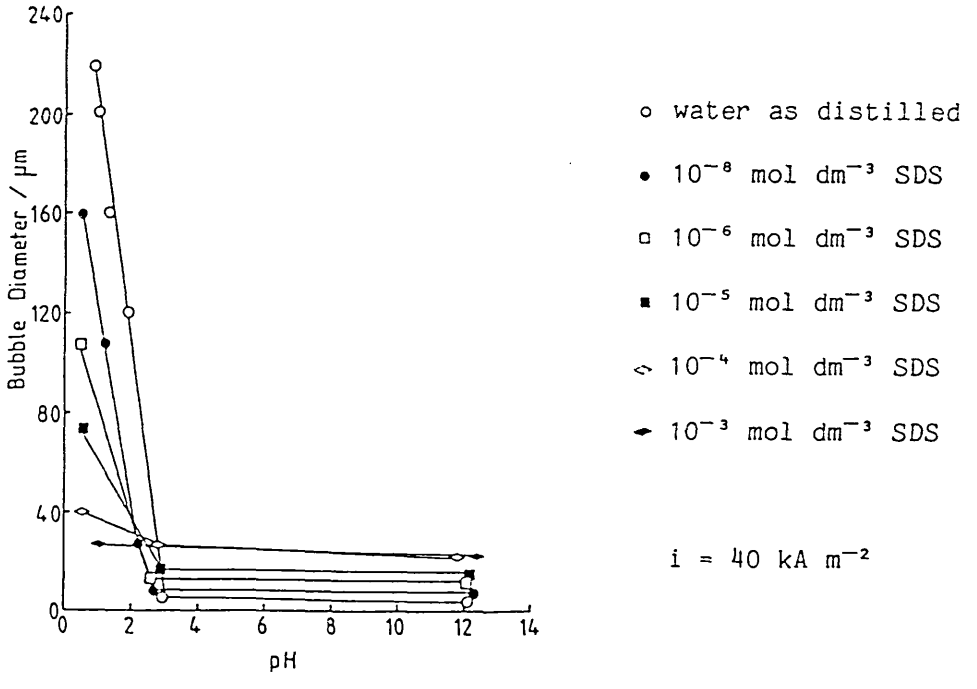


Fig. 4.30 Influence of the bulk SDS concentration on the departure diameter of hydrogen bubbles at a 25 µm diameter platinum electrode.

a very small bubble/electrode contact angle (< 1°) and explained the observed increase in the lower limit of bubble departure diameter at high DTAB concentrations. The absence of large contact angles can be attributed to the low fractional coverage of the electrode by surfactant (see section 2).

The rigidifying of the otherwise mobile bubble interface by surfactant adsorption may also have been significant in decreasing bubble departure diameter. This is indicated by electrophoretic mobility measurements (see chap.3, section 2.2) which show that such adsorption reduces the degree of polarisation of charge on the bubble surface, so negating any enhancement of the force of electrostatic interaction between the bubble and electrode double layers arising from that polarisation.

Addition of a negatively charged surfactant (SDS) also reduced the departure diameter of oxygen (Fig. 4.29) and hydrogen (Fig. 4.30) bubbles. The reason for this is identical to that given above for the addition of DTAB, SDS having been shown to adsorb onto both bubble (Fig. 3.14) and electrode (Fig. 4.14). Consequently, this led to enhanced electrostatic repulsion, reduced polarisation of bubble charge, and decreased bubble departure diameter.

Comparison of the influence of 1:1 and 2:1 supporting electrolytes is given in Fig. 4.31, which shows bubble departure diameter to be slightly greater in a 1:1 electrolyte. This follows from the influence of electrolyte symmetry on κ, ζ_1, and ζ_2 in equation (3.1-32), a 1:1 electrolyte giving a greater double

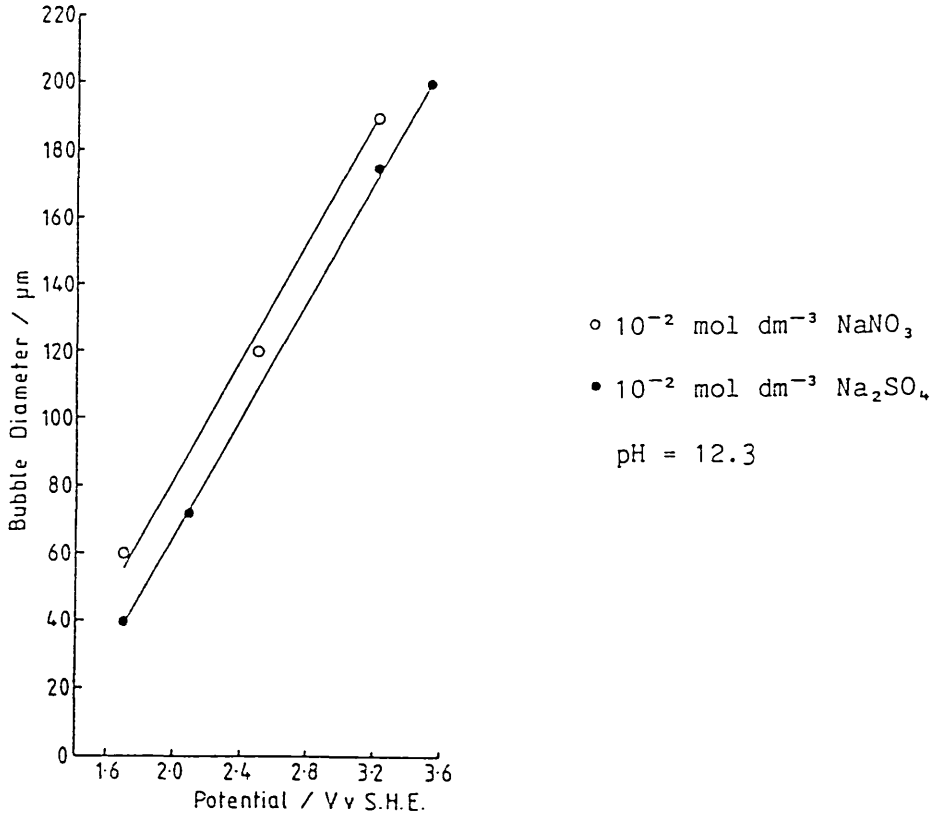


Fig. 4.31 The influence of applied potential and electrolyte symmetry on bubble departure diameter during oxygen evolution at a 10 µm diameter platinum electrode.

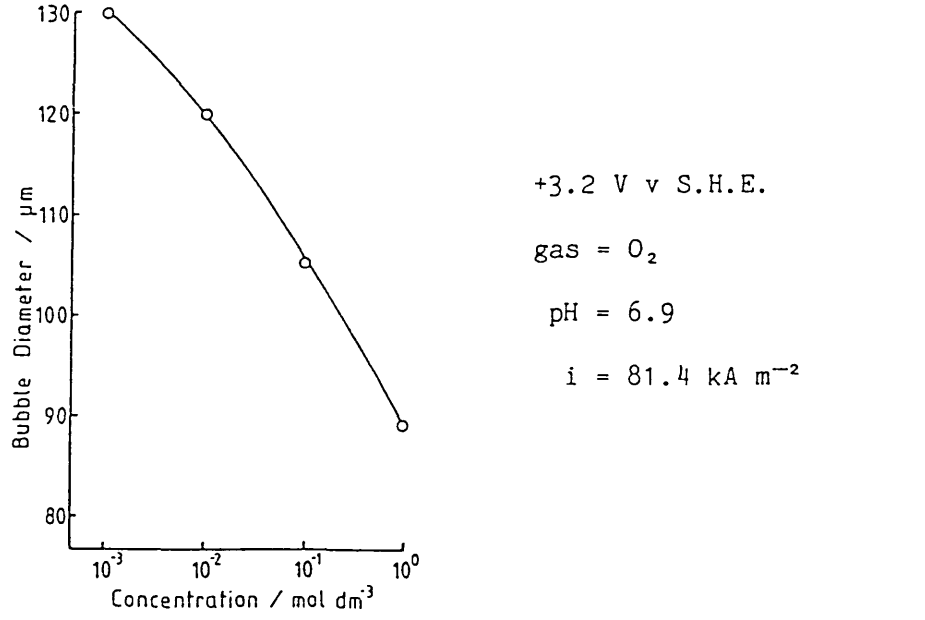


Fig. 4.32 The influence of electrolyte concentration (sodium nitrate) on bubble departure diameter at a 25 µm diameter platinum electrode.

layer thickness, increased zeta potentials, and consequently enhanced bubble/electrode electrostatic interaction. This is further illustrated by Fig. 4.32 which describes the decrease in bubble departure diameter with increasing electrolyte concentration. However, changes in local ionic stength during bubble evolution meant that the effective electrolyte concentration was unknown.

3.4 Influence of Hydrodynamics

Fig. 4.33 describes the influence of rotation frequency on bubble departure diameter at a rotating disk electrode. Large departure diameters were observed at low rotation rates due to the inability of bubbles to escape from the downward facing electrode. Departure diameter decreased with increased rotation frequency because bubbles were more easily swept off the electrode.

Current efficiency decreased with rotation frequency (Fig. 4.34) due to enhanced dissolved gas dispersion into the bulk electrolyte. Current efficiency was further lowered by the decrease in bubble diameter with frequency (Fig. 4.33), as it has been shown (Fig. 4.8) that current efficiency is decreased by a reduction in the ratio of bubble to electrode diameter.

Bubble departure diameter measurements were extremely difficult to make at a rotating cylinder electrode for frequencies greater than 0.5 Hz. However, measurements at zero frequency (Fig. 4.35), where the electrode can be represented as a microelectrode with a vertical surface, showed departure

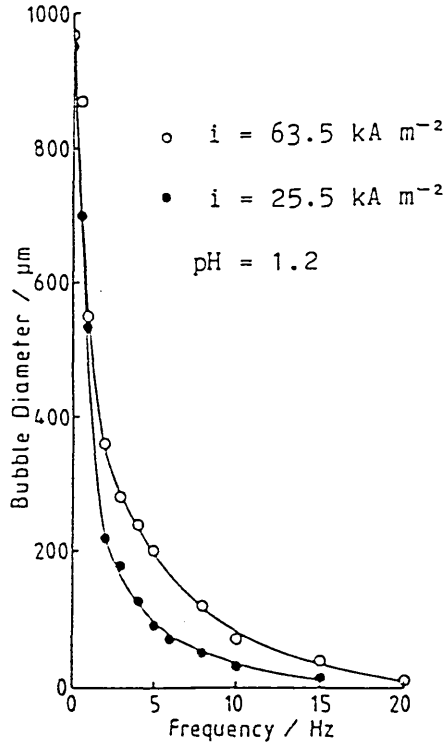


Fig. 4.33 The influence of rotation frequency on bubble departure diameter during hydrogen evolution at a rotating disk electrode.

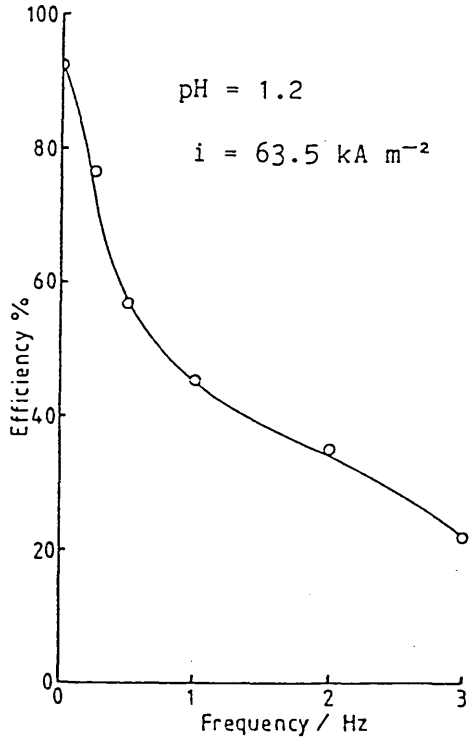


Fig. 4.34 The influence of rotation frequency on the current efficiency of hydrogen evolution at a rotating disk electrode.

o -2.0 V v S.H.E., i = 12.7 kA m^{-2}

• -1.8 V v S.H.E., i = 1.3 kA m^{-2}

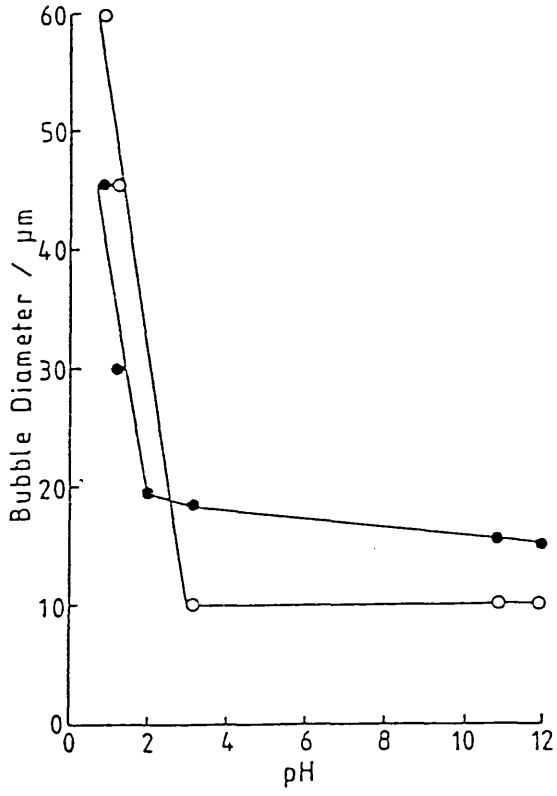


Fig. 4.35 Bubble departure diameter during hydrogen evolution at a vertical surface (100 µm diameter platinum electrode).

diameter to be far less than for the corresponding case of a stationary, upward facing disk electrode (Fig. 4.22). This was due to the small vertical component of the electrostatic interaction force having to oppose the full buoyancy force, bubble departure diameter therefore being reduced.

4 Summary

Bubble growth kinetics have been characterised as a function of current density, potential, pH, electrolyte, evolved gas, hydrodynamics and electrode material/pretreatment. Bubble growth rate was controlled primarily by current density, hydrodynamics and the faradaic charge required to generate one mole of gas, while bubble departure diameter was controlled by electrostatic interaction between the bubble and electrode double layers. Therefore, electrode charge, controlled by applied potential and electrolyte pH, and bubble charge, determined by pH alone, controlled bubble departure diameter.

Charged surfactants adsorbed onto both bubble and electrode, electrostatic repulsion between the like charged surfactant species reducing bubble departure diameter. The departure diameter was also decreased by sweeping electrolyte past the electrode, or by the use of a horizontally mounted electrode.

Three regimes of growth existed during the lifetime of a bubble. At small times $r \propto t$ and growth was controlled by inertial forces. After ~10 msec growth became diffusion controlled and $r \propto \sqrt{t}$, with this mode of growth dominating until

the bubble diameter exceeded that of the electrode. Steep dissolved gas concentration gradients then existed at the bubble/electrode contact point and $r \propto t^{0.33}$ (i.e. the bubble volume increased linearly with time as expected from Faraday's law), this becoming the dominant mode of growth at longer times.

Bubbles were spherical at all times and sat tangent to the electrode, separated by a thin film of electrolyte.

CHAPTER 5

POTENTIAL/CURRENT DISTRIBUTION and "NOISE" MEASUREMENT

1 Potential/Current Distribution

1.1 Potential/Current Transients

1.2 Electrode Resistance

2 "Noise" Measurement

2.1 Microelectrodes

2.2 Macroelectrodes

3 Summary

1 Potential/Current Distribution

The presence of dielectric bubbles at an electrode distorts the potential and current distribution as dicussed earlier (chap.1, section 2.5); the magnitude of that disturbance will be considered here.

1.1 Potential/Current Transients

Fig. 5.1 illustrates a typical potential transient, in which the dimensionless potential perturbation ($\Delta V=(V-V_0)/V_0$) increases with bubble diameter. The relationship between bubble diameter and potential is further illustrated by Fig. 5.2 where the addition of surfactant, shown earlier to give a reduced departure diameter (Figs. 4.26-4.30), decreased the modal electrode potential under galvanostatic control. Therefore, any accompanying increase in potential with added surfactant due to an enhanced contact angle, and hence decreased electrode area, was not significant.

The significant influence of the ratio of bubble to electrode diameter on electrode potential can be illustrated by the following calculation. For the geometry illustrated in Fig. 5.3 the electrode area available for the passage of current can be approximated as being dependent on the distance x, where x is given by:

$$x=(r^2+R^2)^{0.5}-r \qquad (1.1\text{-}1)$$

Assuming constant current (I) yields a current density of:

o ΔV

• bubble diameter

electrode = 25 μm Pt.

gas = H_2

i = 81 kA m^{-2}

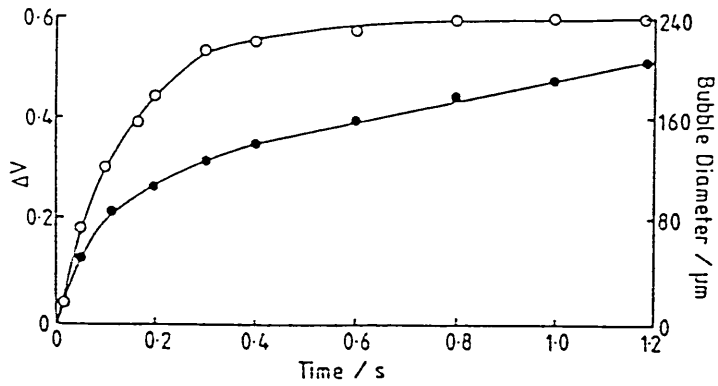


Fig. 5.1 Typical potential transient observed during bubble growth under galvanostatic control.

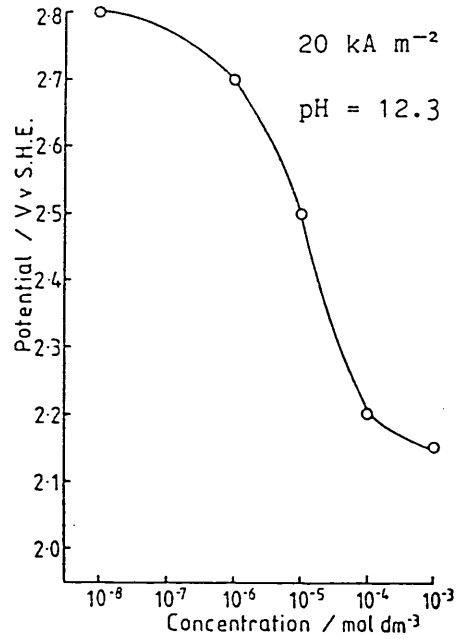


Fig. 5.2 Influence of the bulk surfactant concentration (DTAB) on electrode potential during oxygen evolution at a 25 μm diameter platinum electrode.

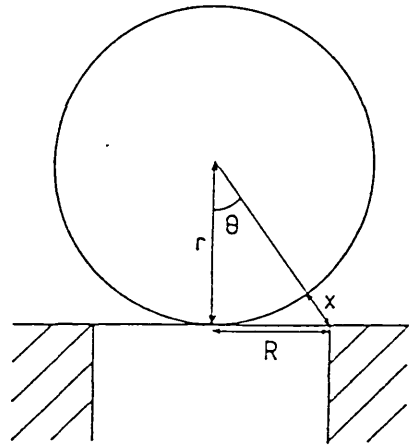


Fig. 5.3 Schematic illustration of a spherical bubble tangent to a planar disk electrode.

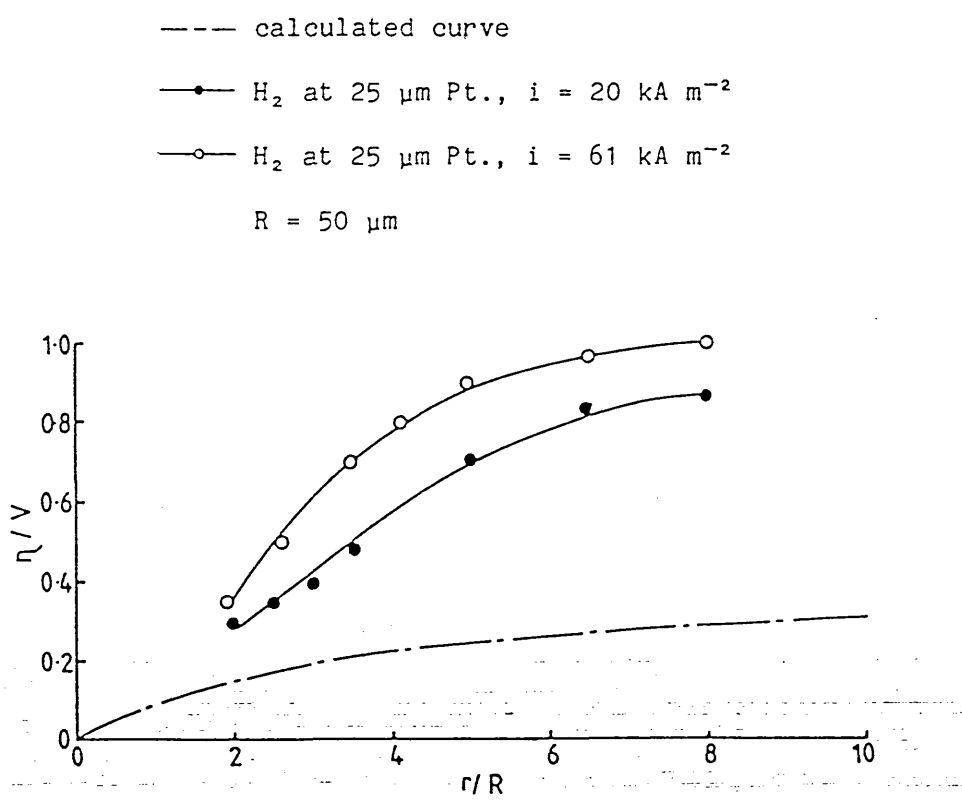


Fig. 5.4 Comparison of measured electrode potential with that predicted by calculation.

$$i=I/S \qquad (1.1\text{-}2)$$

where S represents the effective electrode area. At the large potentials used in this work, the Tafel equations (3) describe the relationship between overpotential (η) and current density, i.e. for high cathodic overpotentials:

$$\eta=RT/\alpha nF.\ln(i_o)-RT/\alpha nF.\ln(i) \qquad (1.1\text{-}3)$$

and for high anodic overpotentials:

$$\eta=RT/(1-\alpha)nF.\ln(i_o)-RT/(1-\alpha)nF.\ln(i) \qquad (1.1\text{-}4)$$

where i_o is the exchange current density and α the transfer coefficient. Therefore, for hydrogen evolution:

$$\eta_1=b.\ln(i_o)-b.\ln(i_1) \qquad (1.1\text{-}5)$$

$$\eta_2=b.\ln(i_o)-b.\ln(i_2) \qquad (1.1\text{-}6)$$

where $b=RT/\alpha nF$, η_2 and i_2 are the overpotential and current density during bubble growth, and η_1 and i_1 the corresponding terms in the absence of a bubble. Subtracting equation (1.1-5) from (1.1-6) yields:

$$\eta_2-\eta_1=b.\ln(i_1/i_2) \qquad (1.1\text{-}7)$$

where $(\eta_2-\eta_1)$ gives the change in overpotential due to the presence of a bubble (η_b). Therefore, taking η_b to be negative for a cathodic process, and substituting (1.1-2) into (1.1-7), yields:

$$\eta_b=b.\ln(S_1/S_2) \qquad (1.1-8)$$

where S_2 and S_1 represent the effective electrode area with and without a bubble, respectively. If the distance x (given by equation (1.1-1)) is projected onto the electrode then the area ratio is given by:

$$S_1/S_2=R^2/\left[(r^2+R^2)^{0.5}-r)\right]^2 \qquad (1.1-9)$$

The Tafel constant b is given by the slope of the Tafel plot and is 120 mV for hydrogen evolution on platinum at high overpotentials (303). Fig. 5.4 compares the potential predicted by equation (1.1-8) with potentials measured during hydrogen evolution, and shows the calculated values to lie below those measured. This is because equation (1.1-8) considers overpotential to arise solely from local current density enhancement, whereas concentration overpotentials and iR losses may also be significant. The concentration overpotential can be calculated from the Nernst equation (3):

$$E=-0.059pH-0.0295\log(p_{H_2}) \qquad (1.1-10)$$

where p_{H_2} represents the supersaturation of dissolved hydrogen in

the thin film separating bubble and electrode, the approximate thickness of which (∂) is given in Table 4.1. Assuming dissolved gas to diffuse linearly across the thin film in time t, where $t=\partial^2/2D$ (150), equation (1.1-7) of chap.4 gives relative thin film supersaturations of 60-180. From equation (1.1-10) these correspond to a decrease of 52-66 mV in the reversible potential, and hence an equivalent increase in the measured electrode potential. The added resistance (ΔR) due to the presence of a bubble can be estimated from the work of Sides and Tobias (see chap.1, equation (2.5-1) (154)), with the bubble population density defined as $n=S/\pi r^2$. Hence:

$$\Delta R=1.803r/K.p \qquad (1.1-11)$$

where p is a pinching factor, estimated by Sides and Tobias (156) to be as high as 5 for a close packed bubble array. Therefore, with p=5 and K=0.187 $(\Omega\ m)^{-1}$ for 0.01 mol dm^{-3} Na_2SO_4 (281), equation (1.1-11) predicts iR losses of less than 10 mV for the current densities reported in Fig. 5.4. Thus, ohmic potential losses apparently account for only little of the discrepancy between measured and calculated electrode potential. However, equation (1.1-11) cannot be considered an accurate guide to the resistance increase arising from bubble growth at microelectrodes because it was derived for an electrode of infinite dimensions.

A solution for the potential distribution may be obtained by solving the Laplace equation for the geometry of a spherical

insulating sphere tangent to a planar disk electrode, using numerical techniques (155) and allowing for proton migration and the diffusion of dissolved hydrogen. This would enable the current distribution along the electrode, and hence the distribution of the source of dissolved gas, to be calculated.

Fig. 5.4 illustrates that electrode potential decreases with a decrease in the ratio of bubble to electrode diameter. Therefore, potential could be reduced not only by adding surfactants, but also by control of electrolyte pH or by sweeping electrolyte past the bubble, both of which reduce the ratio of bubble to electrode diameter (see Figs. 4.20-4.23 and Fig. 4.33).

Albeit at large potentials, current passed even when the bubble diameter exceeded that of a 10 μm diameter electrode by a factor of up to forty. This indicated the presence of a thin conducting film between bubble and electrode since, if a contact angle of only 1.5° were present, the electrode would have been completely obscured by the bubble foot and no current could flow (this follows from the geometry reported in chap.4, section 3.1, which shows that if $\sin\theta > R/r$, the electrode is completely masked by gas).

1.2 Electrode Resistance

A.C. impedance techniques (see chap.2, section 3) were used to determine the increase in electrode resistance due to bubble shielding. Bubbles were grown in a 'dirty' system to give a contact angle sufficient to hold the bubble on the electrode

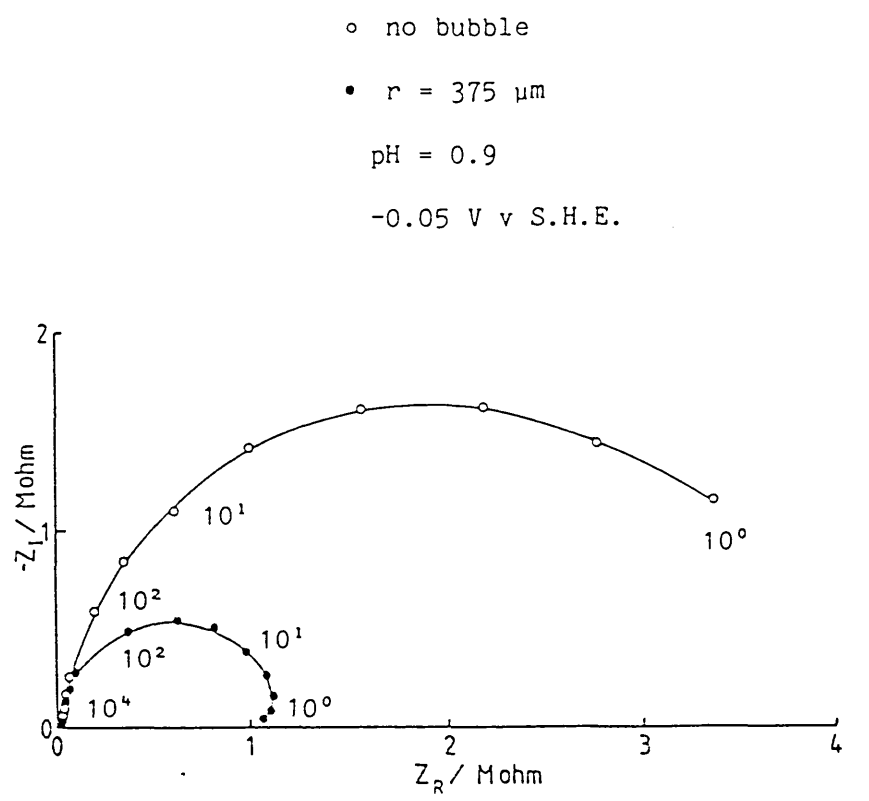


Fig. 5.5 Typical complex plane impedance plots at a 100 μm diameter platinum electrode, both with and without a bubble.

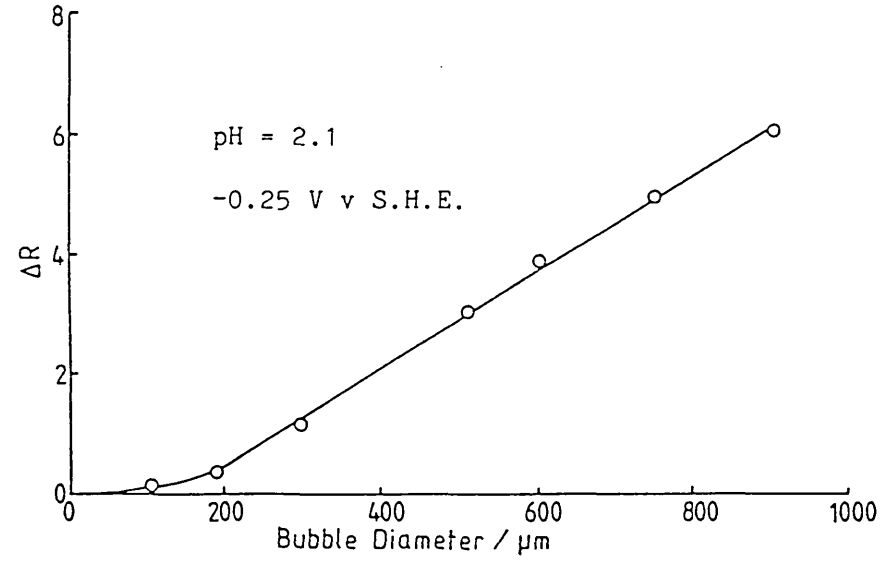


Fig. 5.6 The influence of bubble diameter on the resistance of a 100 μm diameter platinum electrode.

when the d.c. potential was lowered. Impedance measurements were then made; typical results are given in Fig. 5.5. The form and interpretation of the impedance spectra have been discussed in section 2 of chap.4, from which it can be seen that electrode resistance (R) is given by the high frequency intercept on the real (resistive) axis of the complex plane impedance plot.

Fig. 5.6 describes the increase in dimensionless resistance ($\Delta R=(R-R_0)/R_0$) with bubble diameter at a 100 μm diameter platinum electrode, and illustrates that a reduced bubble departure diameter lowers the ohmic potential loss.

2 "Noise" Measurement

As discussed earlier (section 1.1), the growth of a bubble disturbs the potential and current distribution, the frequency of the disturbance being characteristic of the rate of bubble generation. Therefore, by analysis of the current and potential transients it should be possible to identify the rate of bubble departure.

The potential was sampled at a frequency satisfying the Nyquist criteria (i.e. at least twice that corresponding to the maximum signal frequency) and analysed in the amplitude, time and frequency domains (301). Equation (2-1) defines the autocorrelation function:

$$R(\tau)=\lim_{T\to\infty}.1/T.\int_0^T x(t).x(t+\tau)dt \qquad (2\text{-}1)$$

and taking the real part of its Fourier transform gives the

power spectral density function:

$$G(f)=4\int_0^{\infty} r(\tau).\cos(2\pi f\tau)dt \qquad (2\text{-}2)$$

For purely random sources the correlation function consists of one or more decaying exponentials, the time constant of the decay being the relaxation time of the process considered. Fluctuations often show either distributions of relaxation times or memory effects (correlated phenomena), displayed by the oscillating behaviour of $R(\tau)$ or by discrete peaks in the power spectra.

2.1 Microelectrodes

The potential and current transients induced by bubble growth at microelectrodes (illustrated schematically by Fig. 5.7) were examined, and comparison made with photographic observations of bubble departure rate. Fig. 5.8 illustrates a typical autocorrelation function, and Fig. 5.9 the corresponding power spectral density function (which includes large amplitude harmonics due to the non-linearity of electrode processes) for single bubble growth at a 100 μm diameter platinum electrode. The modal potential was obtained from the normalised amplitude probability density function (Fig. 5.10).

The frequency of bubble evolution, given by the period of the autocorrelation function and the peak(s) of the power spectral density function, was consistent with that determined by photographic observation. This showed that useful information

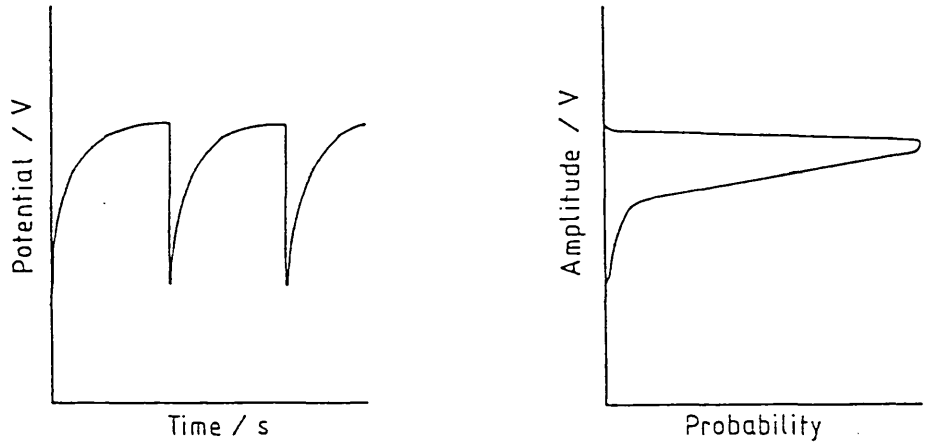


Fig. 5.7 Schematic illustration of the potential transients, and corresponding amplitude density function, observed during bubble growth.

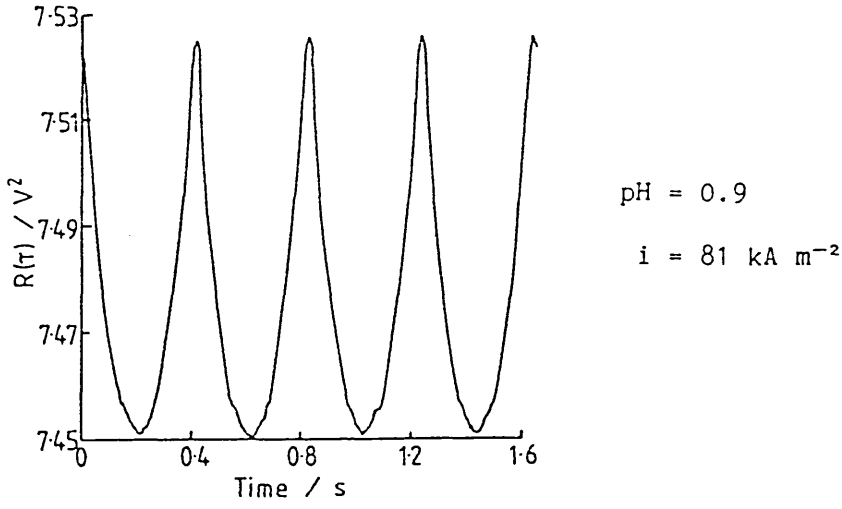


Fig. 5.8 Autocorrelation function at a 100 μm diameter electrode during the evolution of 260 μm diameter hydrogen bubbles.

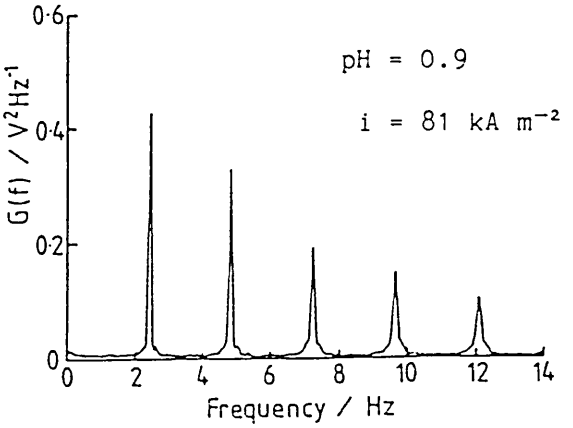


Fig. 5.9 Power spectral density function at a 100 μm diameter electrode during the evolution of 260 μm diameter hydrogen bubbles.

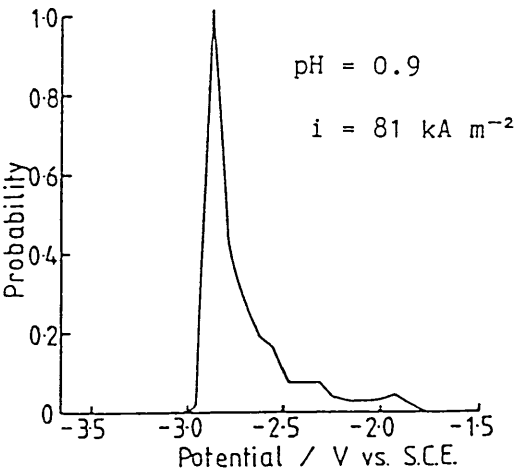


Fig. 5.10 Normalised amplitude probability density function at a 100 μm diameter electrode during the evolution of 260 μm diameter hydrogen bubbles.

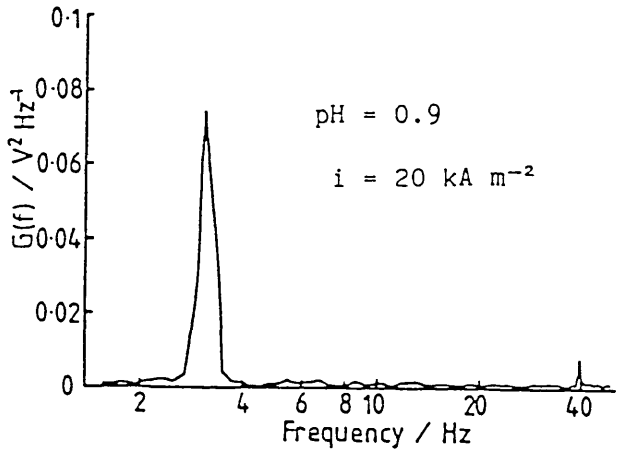


Fig. 5.11 Power spectral density function of multiple bubble growth at a 100 μm diameter electrode.

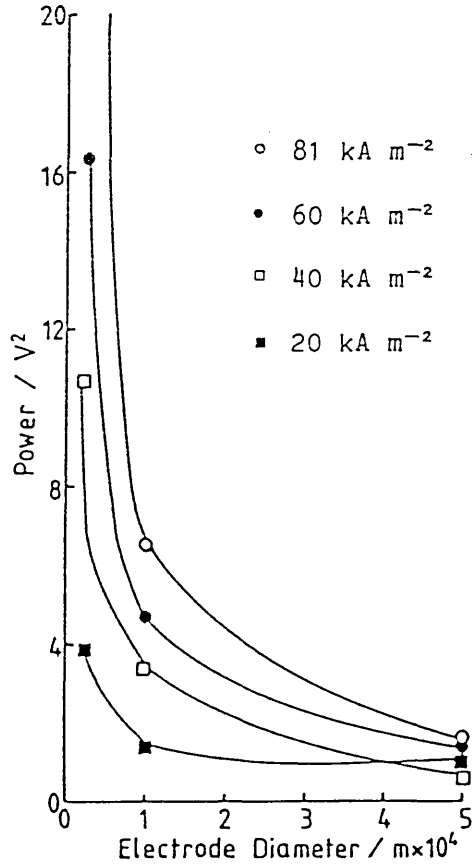


Fig. 5.12 The influence of electrode diameter on the power of the power spectral density function obtained during hydrogen evolution at microelectrodes.

about the kinetics of bubble growth could be obtained by the analysis of "noise", and hence the technique was extended to multiple bubble growth. Little information could be obtained directly from the autocorrelation function but multiple peaks, corresponding to the dominant frequencies of bubble growth, were observed in the power spectral density function (Fig. 5.11), allowing the range of bubble growth times to be determined.

The power of the power spectral density function, obtained by integration of the spectra, increased with increasing current density and decreasing electrode diameter. This is illustrated by Fig. 5.12, obtained during the evolution of 160-240 μm diameter hydrogen bubbles. The increase in power with reduced electrode diameter is further evidence that the ratio of bubble to electrode diameter determines the apparent electrode potential, i.e. whilst bubble diameter varied little (±20 %) the large changes in electrode diameter (20:4:1) resulted in enhanced shielding of the electrode at small electrode sizes, and hence increased potential.

Power increased with current density, reflecting the increase in the scale of the potential/current fluctuations with current density.

2.2 Macroelectrodes

The potential distribution between two plane parallel, gas evolving electrodes was measured using Luggin probes. Measurements of the amplitude probability density function, power spectral density function and auto correlation functions

were used to define the signal.

The modal potential, given by the amplitude probability density function, increased with lateral displacement from the electrode (Fig. 5.13). The linear increase follows that expected in the absence of bubbles and shows that, since bubble population density determines the net electrolyte conductivity (chap.1, section 3.4.1), the change in bubble distribution across the inter-electrode gap was negligible. The frequency of the potential perturbation, given by the power spectral density function, varied little with lateral displacement, keeping to the range 1-8 Hz. The power of the spectra increased with lateral displacement due to the accompanying increase in potential.

Vertical displacement had a significant effect on the modal potential (Fig. 5.14). The potential drop reached a maximum at the mid point of the electrode, with minima at the top and bottom. This is in direct contrast to the results of Sillen et al (95) who found that the potential drop between mesh electrodes in a pumped cell reached a minimum at the electrode centre. The bubble population density increased with height up the electrode, and it was the corresponding decrease in the effective solution conductivity (see chap.1, sections 3.4.1 and 3.4.2) with vertical displacement, coupled to a decrease in current, that led to a maximum iR loss towards the centre of the electrode, i.e.

(i) at the electrode base $i \rightarrow i(max)$ & $R \rightarrow R(min)$, thus $iR \rightarrow iR(min)$

(ii) " " " top $i \rightarrow i(min)$ & $R \rightarrow R(max)$, " $iR \rightarrow iR(min)$

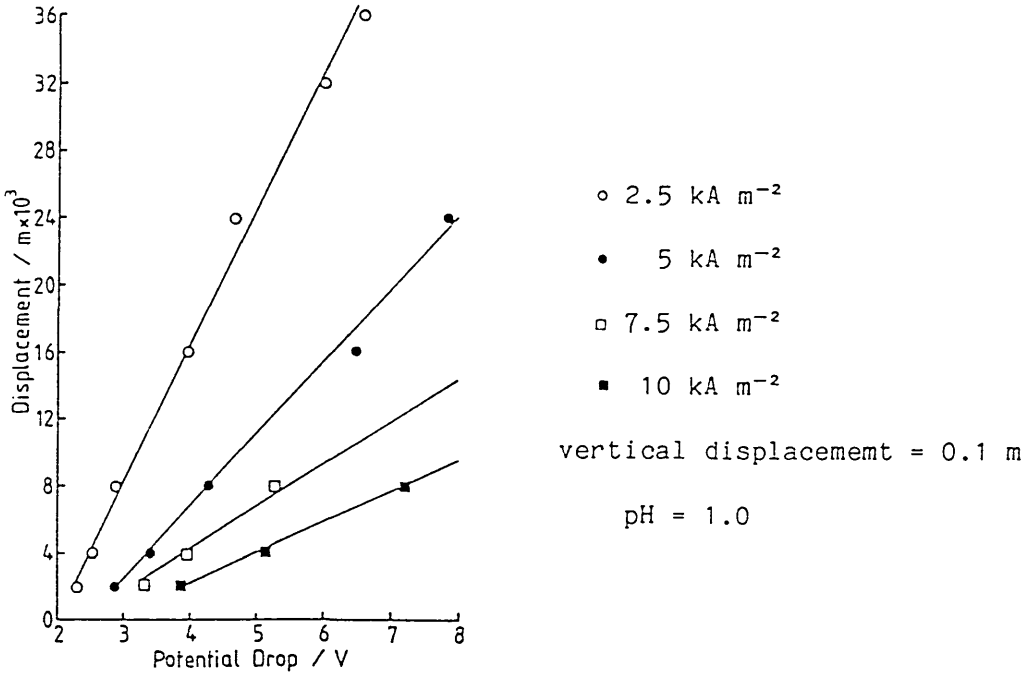


Fig. 5.13 Influence of the lateral displacement of a Luggin probe on the probe/cathode potential drop during gas evolution in a macro cell.

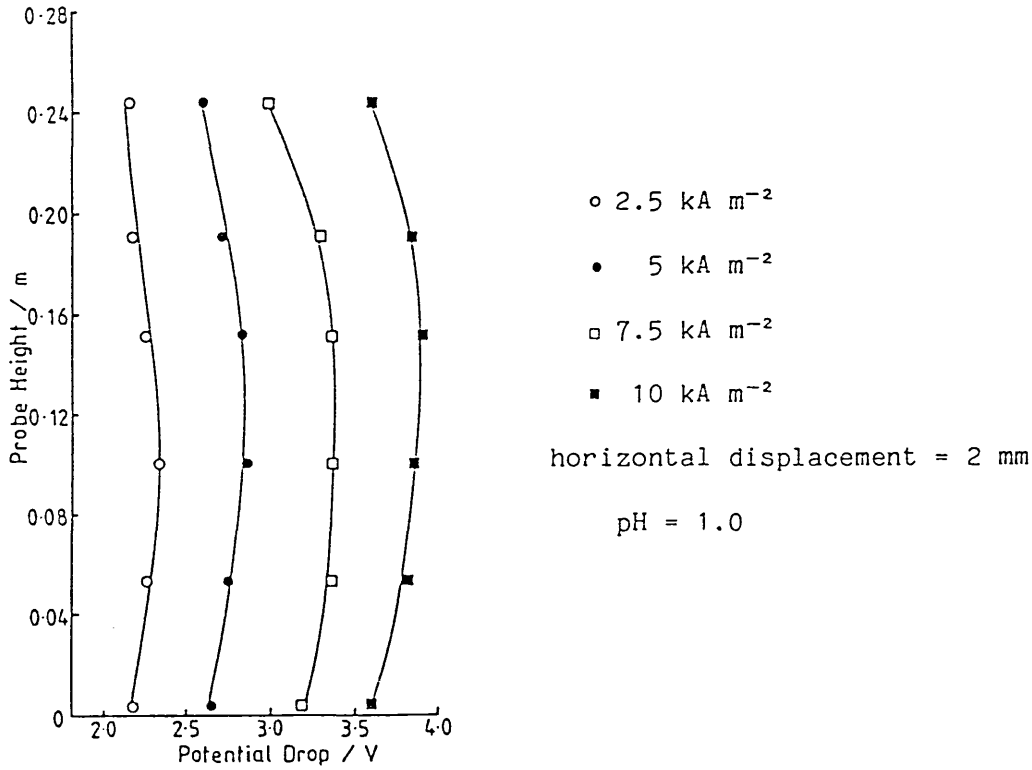


Fig. 5.14 Influence of the vertical displacement of a Luggin probe on the probe/cathode potential drop during gas evolution in a macro cell.

with a maximum ohmic potential loss between these extremes.

Fig. 5.14 also shows that the potential drop was greater at the bottom of the electrode than at the top, the ohmic loss becoming more evident with increasing current density. This can be attributed to iR losses within the electrode itself, which become particularly significant at high current densities (302).

Observations of bubble behaviour showed that the gas/electrolyte dispersion exhibited turbulent motion at the top and bottom of the cell, and this was further indicated by an increase in the frequency of the potential perturbations in these areas (i.e. from 1-8 to 2-40 Hz).

The use of two Luggin probes, placed the same distance away from the cathode and at a known vertical separation, allowed bubble rise rates to be calculated from the dominant frequencies of the cross power spectral density function. This technique gave rise rates of 0.1 to 0.8 m s^{-1}, which correspond to bubble diameters of 400 to 800 μm from Stokes law (chap.1, equation (3.2.1-4)). This size range is not as wide as that photographically observed (50-800 μm), though the low frequency peaks corresponding to small bubble sizes were difficult to determine in the cross spectra.

3 Summary

Analysis of the potential and current transients induced by bubble growth indicates the presence of a thin electrolyte film between the bubble and electrode. The magnitude of the potential/current perturbation increased with the ratio of

bubble to electrode diameter, leading to an increased electrode potential and ohmic potential loss. The addition of surfactant decreased such effects by lowering the bubble departure diameter. Statistical analysis of the potential and current transients allowed the frequency of bubble evolution to be determined during both single and multiple bubble growth.

The potential distribution between two macroelectrodes was mapped as a function of horizontal and vertical displacement. A minimum potential drop was found at the top and bottom of the cell, being due to the balance of current versus solution conductivity.

CONCLUSIONS

Essentially surfactant-free electrolytes were produced, characterised by bubble rise rate measurements. Three modes of bubble growth were identified; at short times inertia control dominated, followed by diffusion control until the bubble diameter exceeded that of the electrode, when gas became 'directly injected' into the bubble.

Bubble departure diameter was dependent on solution pH and applied potential; small hydrogen bubbles were evolved at high pH and large ones at low pH. The converse was observed for oxygen and chlorine evolution. Addition of ionic surfactants reduced bubble departure diameter, masking the influence of pH at high bulk concentrations.

Bubble electrophoretic mobilities showed a pH dependency, indicating preferential OH^- ion adsorption, and exhibited a point of zero charge at pH 2-3 (i.e. bubbles were positively charged at pH < 2, and negatively charged at pH > 3). In addition, their dependency on bubble diameter and electric field strength implied that both hydrodynamic and field induced polarisation of charge occured at mobile bubble surfaces.

The pH dependence of bubble departure diameter was interpreted in terms of an electrostatic interaction between

bubble and electrode double layers; the charge on the latter was dependent on applied potential, electrolyte pH, and concentration of ionic surfactant.

The fundamental frequency of the fluctuations in current and potential, arising from bubble growth, correlated with photographic information of the bubble departure frequency.

FUTURE WORK

Full interpretation of the bubble electrophoretic mobility curves obtained in this work cannot be made without knowing the distribution of charge around the surface of a bubble rising through an electric field applied normal to the direction of rise. Therefore, an extension of the work reported in Appendix 1 is necessary to couple together the effect of rise rate and electric field strength on the electrophoretic mobility. In addition, electrophoretic mobility measurements on very small bubbles, or in a gravity free environment, would be instructive in decoupling the influence of bubble rise rate and electric field strength on the surface charge distribution.

Solution of the Laplace equation for the geometry of a spherical bubble tangent to a planar disk microelectrode would allow the dissolved gas and potential/current distribution to be obtained. These are important if the local pH and supersaturation are to be calculated rigorously and, if determined for the non-steady state, would enable the bubble growth kinetics and the form of the power spectrum of the potential/current fluctuations to be predicted.

This work has shown that the analysis of bubble generated "noise" can reveal useful information about bubble departure

frequency and rise rate. Therefore, the technique should be extended to other gas evolving systems to allow such information to be extracted.

REFERENCES

1 T.Murakawa. J.Electrochem.Soc.Jpn. 25 (1957), E61

2 B.E.Conway, J.O'M.Bockris, E.Yeager, S.U.M.Khan, R.E.White. "Comprehensive Treatise of Electrochemistry." Vol.7. Plenum, New York (1984)

3 J.O'M.Bockris, A.K.N.Reddy. "Modern Electrochemistry." Vol.2 Plenum, New York (1973)

4 A.C.C.Tseung, P.R.Vassie. Electrochim.Acta. 4 (1976), 315

5 A.C.C.Tseung, S.Jasem. Electrochim.Acta. 22 (1977), 31

6 A.C.C.Tseung. Electrolytic Bubbles. SCI Conf. London, Sept. (1984)

7 I.R.Burrows, J.H.Entwisle, J.A.Harrison. J.Electroanal.Chem. 77 (1977), 21

8 I.R.Burrows, J.H.Entwisle, J.A.Harrison. Electrochim.Acta. 23 (1978), 493

9 D.A.Denton, J.A.Harrison, R.I.Knowles. Electrochim.Acta. 24 (1979), 521

10 D.A.Denton, J.A.Harrison, R.I.Knowles. Electrochim.Acta. 25 (1980), 1147

11 D.A.Denton, J.A.Harrison, R.I.Knowles. Electrochim.Acta. 26 (1981), 1197

12 J.A.Harrison, D.L.Caldwell, R.E.White. Electrochim.Acta. 28 (1983), 1561

13 J.A.Harrison. Electrolytic Bubbles. SCI Conf. London, Sept. (1984)

14 J.P.Glas, J.W.Westwater. Int.J.Heat Mass Transfer. 7 (1964), 1427

15 D.E.Westerheide, J.W.Westwater. A.I.Ch.E.J. 7 (1961), 351

16 L.E.Scriven. Chem.Eng.Sci. 1 (1959), 1

17 W.M.Buehl, J.W.Westwater. A.I.Ch.E.J. 12 (1966), 571

18 Lord Rayleigh. Phil.Mag. 94 (1917)

19 G.Houghton, L.A.Waldman. Chem.Eng.Sci. 20 (1965), 625

20 C.W.Sillen. Comm.Eur.Comm. EUR 6085 (1978)

21 C.W.Sillen, E.Barendrecht, L.J.J.Janssen, S.J.D.van Stralen. Int.J.Hydrogen Energy. 7 (1982), 577

22 H.F.A.Verhaart, R.M.De Jonge, S.J.D.van Stralen. Int.J.Heat Mass Transfer. 23 (1980), 293

23 L.J.J.Janssen. "Boiling Phenomena." Vol.1 Chap.13, Ed. S.J.D.van Stralen, R.Cole. McGraw-Hill, New York (1979)

24 A.N.Frumkin, O.A.Petrii, B.B.Damaskin. "Comprehensive Treatise of Electrochemistry." Vol.1, Ed. J.O'M.Bockris, B.E.Conway, E.Yeager. Plenum, New York (1980)

25 A.J.Bard. "Encyclopedia of Electrochemistry of the Elements." Vol.6, Marcel Dekker, New York (1976)

26 J.O'M.Bockris, M.A.Genshaw, M.Fullenwider. Electrochim.Acta. 15 (1970), 47

27 M.C.Witherspoon, R.C.Johnston, F.A.Lewis. Electrochim.Acta. 20 (1975), 519

28 P.K.Subramaryan. "Comprehensive Treatise of Electrochemistry." Vol.4, Ed. J.O'M.Bockris, B.E.Conway,

E.Yeager, R.E.White. Plenum, New York (1981)

29 F.A.Lewis, R.C.Johnston, M.C.Witherspoon, A.Obermann. Surface Tech. 18 (1983), 147

30 D.Gilroy. J.Electroanal.Chem. 71 (1976), 257

31 D.Gilroy. J.Electroanal.Chem. 83 (1977), 329

32 D.J.Schiffrin. "Electrochemistry." Vol.8, Ed. D.Pletcher. Roy.Soc.Chem., London (1983)

33 H.Angerstein-Kozlowska, B.E.Conway, W.B.A.Sharp. J.Electroanal.Chem.Electrochem. 43 (1973), 9

34 S.Gottesfeld, B.E.Conway. J.Chem.Soc.Faraday Trans. 6 (1973), 1090

35 B.V.Tilak, B.E.Conway, H.Angerstein-Kozlowska. J.Electroanal.Chem.Electrochem. 48 (1973), 1

36 J.P.Hoare. Electrochim.Acta. 27 (1982), 1751

37 G.Belanger, A.K.Vijh. "Oxide and Oxide Films." Vol.5, Ed.A.K.Vijh. Marcel Dekker, New York (1977)

38 E.Gileadi, S.D.Argade, J.O'M.Bockris. J.Phys.Chem. 70 (1966), 2044

39 A.N.Frumkin, O.Petrii, R.Marvet. J.Electroanal.Chem. 12 (1966), 504

40 A.N.Frumkin, O.Petrii, A.Kossaya, V.Entina, V.Topolov. J.Electroanal.Chem. 16 (1968), 175

41 A.N.Frumkin, N.A.Balaskova, V.E.Kazarinov. J.Electrochem.Soc. 113 (1966), 1011

42 A.N.Frumkin, O.A.Petrii, B.V.Damaskin. Elektrokhim. 6 (1970), 617

43 A.N.Frumkin. J.Electrochem.Soc. 107 (1960), 461

44 A.N.Frumkin. Electrochim.Acta. 15 (1970), 391

45 N.Ibl, R.Kind, E.Adam. An.Quim. 71 (1975), 1008

46 L.J.J.Janssen, S.J.D.van Stralen. Electrochim.Acta. 26 (1981), 1011

47 N.Ibl, J.Venczel. Metalloberflache. 24 (1970), 365

48 I.Rousar, V.Cezner. Electrochim.Acta. 20 (1975), 289

49 M.D.Birkett, A.T.Kuhn. Electrochim.Acta. 22 (1977), 1427

50 S.Mohanta, T.Z.Fahidy. J.Appl.Electrochem. 7 (1977), 235

51 L.J.J.Janssen. Electrochim.Acta. 23 (1978),81

52 M.Fouad, G.H.Sedamed. Electrochim.Acta. 17 (1972), 655

53 N.Ibl. Electrochim.Acta. 24 (1979), 1105

54 H.Vogt. Electrochim.Acta. 23 (1978), 203

55 N.Ibl. Chem.Ing.Tech. 43 (1971), 202

56 I.Rousar, J.Kacin, E.Lippert, F.Smirous, V.Cezner. Electrochim.Acta. 20 (1975), 295

57 K.Stephan, H.Vogt. Electrochim.Acta. 24 (1979), 11

58 L.J.J.Janssen, E.Barendrecht. Electrolytic Bubbles. SCI Conf. London, Sept. (1984)

59 G.Barthole, F.Giron, G.Valentin, A.Laurent, J.C.Carpenter, A.Storck. Electrolytic Bubbles. SCI Conf. London, Sept. (1984)

60 C.I.Elsner, S.L.Marchiano. J.Appl.Electrochem. 12 (1982), 735

61 L.J.J.Janssen, S.J.D.van Stralen, E.Barendrecht. Adv.Hygrogen Energy. 3 (1982), 309

62 T.Alkire, P.Yu. J.Electrochem.Soc. 126 (1979), 2118

63 A.T.Kuhn, H.B.Hamzah. Chem.Ing.Tech. 52 (1980), 762

64 A.T.Kuhn, H.B.Hamzah. J.Appl.Electrochem. 10 (1980), 635

65 P.Delahey. "Double Layer and Electrode Kinetics." Witney, Interscience, New York (1975)

66 F.N.Ngoya. Electrochim.Acta. 28 (1983), 1865

67 L.J.J.Janssen, J.G.Hoogland. Electrochim.Acta. 18 (1973), 543

68 B.N.Kabanov. "Electrochemistry of Metals and Adsorption." Nauka, Moscow (1966)

69 S.Shibata. Bull.Chem.Soc.Jpn. 33 (1960), 1635

70 S.Shibata. Bull.Chem.Soc.Jpn. 36 (1963), 53

71 S.Shibata. Denki.Kagaku. 44 (1976), 709

72 S.Shibata. Electrochim.Acta. 23 (1978), 619

73 C.K.Bon, C.W.Tobias. J.Electrochem.Soc. 115 (1968), 61C

74 H.Vogt. Fortschr.Verf. 20 (1982), 269

75 H.Vogt. Chem.Ing.Tech. 52 (1980), 418

76 H.Vogt. Electrochim.Acta. 25 (1980), 527

77 H.Vogt. Electrochim.Acta. 29 (1984), 167, 175

78 H.Reiss. Adv.Colloid Interface Sci. 7 (1977), 1

79 M.Blander. Adv.Colloid Interface Sci. 10 (1979), 1

80 R.Cole. Adv.Heat Transfer. 10 (1974), 85

81 R.Cole. "Boiling Phenomena." Vol.1 Chap.13, Ed. S.J.D.van Stralen, R.Cole. McGraw-Hill, New York (1979)

82 R.V.Dapkus, P.J.Sides. Electrolytic Bubbles. SCI Conf. London, Sept. (1984)

83 M.Blander, J.L.Katz. A.I.Ch.E.J. 21 (1975), 833

84 T.W.Forest, C.A.Ward. J.Chem.Phys. 66 (1977), 2322

85 T.W.Forest, C.A.Ward. J.Chem.Phys. 67 (1978), 2221

86 E.N.Harvey, D.K.Barnes, W.D.McElroy, A.H.Whiteley, D.C.Pease, K.W.Cooper. J.Cell.Comp.Phys. 24 (1944), 1

87 K.J.Mysels, A.T.Florence. "Clean Surfaces." Ed. G.Goldfinger Marcel Dekker, New York (1970)

88 A.Tognoni, B.Mazza, R.Piontelli, P.Pedeferri. Electrochim.Metall. 2 (1967), 257, 297, 377, 385

89 M.R.Urban. Ph.D Thesis, Imperial College, London (1978)

90 D.Landolt, R.Acosta, R.H.Muller, C.W.Tobias. J.Electrochem.Soc. 117 (1970), 839

91 R.M.De Jonge, E.Barendrecht, L.J.J.Janssen, S.J.D.van Stralen. Proc.3rd World Hydrogen Energy Conf.Tokyo (1980)

92 F.Hine, T.Sugimoto. Electrochem.Soc.Meeting. Seattle (1978)

93 Yu.G.Chirkov, A.G.Pshenichnikov. Elektrokhimya. 20 (1984), 279

94 L.J.J.Janssen, J.G.Hoogland. Electrochim.Acta. 15 (1970), 1013

95 C.W.Sillen, E.Barendrecht, L.J.J.Janssen, S.J.D.van Stralen. "Hydrogen as an Energy Vector." Ed. A.S.Strub, G.Imarisio. Reidel (1980)

96 J.Venczel. Electrochim.Acta. 15 (1970), 1909

97 C.W.Sillen, S.J.D.van Stralen. Conf.Altern.Energy Sources. Miami (1979)

98 Y.Y.Hsu. J.Heat Transfer. 84 (1962), 207

99 H.M.Wedershoven, R.M.De Jonge, C.W.Sillen, S.J.D.van Stralen. Int.J.Heat Mass Transfer. 25 (1982), 1239

100 A.A.Mamakov, V.A.Glembotskiy, U.N.Sorokhina. Electrochem.Ind.Proc.Biol. 6 (1973), 59

101 Z.Galus, J.O.Schenk, R.N.Adams. J.Electroanal.Chem 135 (1981), 1

102 R.Chris, S.Asakuru, K.Nobe. J.Electrochem.Soc. 119 (1972), 698

103 D.W.Dees, C.W.Tobias. 33rd ISE Conf. Lyon (1982)

104 H.Reller, E.Kirowa-Eisner, E.Gileadi. J.Electroanal.Chem. 138 (1982), 65

105 Z.G.Soos, P.J.Lingone. J.Phys.Chem. 68 (1964), 3821

106 J.B.Flanagan, L.Marcoux. J.Phys.Chem. 77 (1973), 1051

107 C.W.Sillen, E.Barendrecht, L.J.J.Janssen, S.J.D.van Stralen. Proc.3rd World Hydrogen Energy Conf. Tokyo (1980)

108 T.Z.Fahidy, M.S.Abdo. Electrochim.Acta. 27 (1982), 1521

109 A.T.Kuhn, H.Hamzah. J.Chem.Tech.Biotech. 30 (1980), 423

110 A.T.Kuhn, J.Bin Yusof, P.Hogan. J.Appl.Electrochem. 9 (1979), 765

111 A.Coehn, H.Neumann. Z.Phys. 20 (1923), 54

112 A.Coehn. Z.Electrochem. 29 (1923), 306

113 B.Kabanov, A.N.Frumkin. Z.Phys.Chem. 165 (1933), 433: 166 (1934), 316

114 G.Trivedi, J.E.Funk. Univ.Kentucky Tech.Report UKY 28-70-ME8 (1970)

115 L.J.J.Janssen, C.W.Sillen, E.Barendrecht, S.J.D.van Stralen. Electrochim.Acta. 29 (1984), 633

116 A.T.Kuhn, C.Y.Chan. J.Appl.Electrochem. 13 (1983), 189

117 M.J.Blandamer, F.Franks, K.H.Haywood, A.C.Tory. Nature. 216 (1967), 783

118 B.E.Bongenaar-Schlenter, L.J.M.Konings, C.J.Smeyers,

J.H.G.Verbunt, E.Barendrecht, L.J.J.Janssen, W.M.Sluyter, S.J.D.van Stralen. Comm.Eur.Comm. EUR 8651 (1983), 206

119 J.E.Funk, J.F.Thorpe. J.Electrochem.Soc. 116 (1969), 48

120 J.Clavier, N.Van Hong. J.Electroanal.Chem. 41 (1973), 193

121 M.E.Schrader. J.Phys.Chem. 74 (1970), 2313

122 R.E.Johnson. J.Phys.Chem. 63 (1959),1655

123 I.Morcos. J.Electroanal.Chem. 62 (1975), 313

124 G.Valette. J.Electroanal.Chem. 139 (1982), 285

125 M.C.Schrader. J.Coll. Interface Sci. 100 (1984), 372

126 J.R.Gardner, R.Woods. J.Electroanal.Chem. 81 (1977), 285

127 W.Fritz. Pysik.Z. 36 (1935), 379

128 N.Ibl, J.Venczel. Oberflache-Surface. 13 (1972), 1

129 J.Thonstad, C.W.Tobias. Electrolytic Bubbles. SCI Conf. London, Sept. (1984)

130 Y.M.Yang, J.R.Maa. J.Coll.Interface Sci. 98 (1984), 120

131 S.J.D.van Stralen. "Boiling Phenomena." Vol.1 Chap.7, Ed. S.J.D.van Stralen, R.Cole. McGraw-Hill, New York (1979)

132 A.Bhattacharya, J.H.Lienhard. Iranian J.Sci.Tech. 1 (1971), 113

133 A.Bhattacharya, J.H.Lienhard. Trans.A.S.M.E. 12 (1972), 804

134 A.Bhattacharya. Univ.Kentucky Tech.Report UKY 35-71-ME10 (1971)

135 H.Y.Cheh, C.W.Tobias. Int.J.Heat Mass Transfer. 11 (1968), 709

136 H.C.Unal. Int.J.Heat Mass Transfer. 19 (1976), 643

137 A.H.Abdelmessih, F.C.Cooper, S.Nongia. Int.J.Heat Mass Transfer. 15 (1972), 115

138 C.Y.Han, P.Griffith. Int.J.Heat Mass Transfer. 8 (1965), 887

139 R.Siegel. Adv.Heat Transfer. Vol.4, Academic Press, New York (1967)

140 P.H.Strenge, A.Orell, J.W.Westwater. A.I.Ch.E.J. 7 (1961), 578

141 B.B.Mikic, W.M.Rohsenow, P.Griffith. Int.J.Heat Mass Transfer. 13 (1970), 657

142 M.Saddy, G.J.Jameson. Int.J.Heat Mass Transfer. 14 (1971), 1771

143 M.S.Plesset, S.A.Zwick. J.Appl.Phys. 25 (1954), 493

144 H.K.Forster, N.Zuber. J.Appl.Phys. 25 (1954), 474

145 S.J.D.van Stralen, R.Cole. "Boiling Phenomena." Vol.1,2 McGraw-Hill, New York (1979)

146 S.J.D.van Stralen, W.Zijl. 6th Int.Heat Transfer Conf. Toronto (1978)

147 F.Geoola, A.R.H.Cornish. Int.J.Heat Mass Transfer. 25 (1982), 1677

148 R.Darby, S.Haque. Chem.Eng.Sci. 28 (1973), 1129

149 A.K.Chesters. "Boiling Phenomena." Vol.2 Chap.26, Ed. S.J.D.van Stralen, R.Cole. McGraw-Hill, New York (1979)

150 A.J.Bard, L.R.Faulkner. "Electrochemical Methods: fundamentals and applications." Wiley, New York (1980)

151 A.T.Kuhn, M.Stevenson. Electrochim.Acta. 27 (1982), 329

152 P.Gallone, L.Guiffre, G.Modica, S.Maffi. 33rd ISE Conf. Lyon (1982)

153 L.J.J.Janssen, E.Barendrecht. Electrochim.Acta. 28 (1983), 341

154 P.J.Sides, C.W.Tobias. J.Electrochem.Soc. 127 (1980), 288

155 J.Dukovic, C.W.Tobias. Electrolytic Bubbles. SCI Conf. London, Sept. (1984)

156 P.J.Sides, C.W.Tobias. Electrolytic Bubbles. SCI Conf. London, Sept. (1984)

157 S.D.Wilson, A.Hulme. Proc.Roy.Soc.London. A387, (1983), 133

158 H.Vogt. J.Appl.Electrochem. 13 (1983), 87

159 P.J.Sides. Ph.D Thesis. Berkeley, California (1981)

160 T.Murakawa, S.Nagura. J.Electrochem.Soc.Jpn. 23 (1955), 223

161 F.Hine, S.Yoshizawa, S.Okada. J.Electrochem.Soc.Jpn. 24 (1956), 370

162 K.Takata, H.Morishata. Electrochem. 32 (1964), 378

163 F.Hine, K.Murakami. J.Electrochem.Soc. 128 (1981), 64

164 E.Barendrecht, L.J.J.Janssen, R.M.De Jonge. ECS Meeting, Boston (1979)

165 C.W.Sillen, S.J.D.van Stralen. Altern.Energy Sources. 3 (1983), 357

166 R.M.De Jonge, E.Barendrecht, L.J.J.Janssen, S.J.D.van Stralen. Int.J.Hydrogen Energy. 7 (1982), 883

167 Z.Nagy. J.Appl.Electrochem. 6 (1976), 171

168 H.Vogt. Electrochim.Acta. 26 (1981), 1311

169 F.Hine, M.Yasuda, R.Nakamura, T.Nada. J.Electrochem.Soc. 122 (1975), 1185

170 F.Hine, K.Murakami. J.Electrochem.Soc. 127 (1980), 292

171 S.J.D.van Stralen, W.M.Sluijter. Electrolytic Bubbles. SCI Conf. London, Sept. (1984)

172 S.Fortin, M.Gerhardt, A.J.Gensing. Light Met. (1984), 721

173 R.J.Hunter. "Zeta Potential in Colloid Science." Academic Press, New York (1981)

174 R.W.Huddleston, A.L.Smith. "Foams." SCI Conf. Brunel University (1975). Ed. A.J.Akers, Academic Press, London (1976)

175 H.A.McTaggart. Phil.Mag. 44 (1914), 297

176 H.A.McTaggart. Phil.Mag. 105 (1922), 386

177 T.Alty. Proc.Roy.Soc. 106 (1924), 315

178 T.Alty. Proc.Roy.Soc. 112 (1926), 235

179 N.Bach, A.Gilman. Acta.Physic. 9 (1938), 1, 27

180 H.P.Dibbs, L.L.Sirois, R.Bredin. Can.Metall.Quart. 13 (1974), 35

181 V.D.Samygin, S.V.Derjaguin, S.S.Dukhin. Koll.Zh. 26 (1964), 424

182 S.Usui, H.Sasaki. J.Coll.Interface Sci. 65 (1978), 36

183 S.Usui, H.Sasaki, H.Matsukawa. J.Coll.Interface Sci. 81 (1981), 80

184 T.Sotskova, Yu.F.Bozhenov, L.Kul'skii. Koll.Zh. 44 (1982), 989

185 G.L.Collins. Ph.D Thesis. Imperial College, London (1975)

186 G.L.Collins, G.J.Jameson. Chem.Eng.Sci. 32 (1977), 239

187 G.L.Collins, M.Matarjemi, G.J.Jameson. J.Coll.Interface Sci. 63 (1978), 69

188 Y.Fukui, S.Yuu. A.I.Ch.E.J. 28 (1982), 866

189 K.Kubota, S.Hayaski, M.Inaoka. J.Coll.Interface Sci. 95 (1983), 362

190 H.Von Helmholtz. Ann.Physik. 7 (1879), 337

191 M.Von Smoluchowski. Bull.Acad.Sci.Crocovic. (1903), 182

192 E.Huckel. Physik.Z. 25 (1924), 204

193 D.C.Henry. Proc.Roy.Soc. A133 (1931), 106

194 F.Booth. Nature. 161 (1948), 83

195 F.Booth. Proc.Roy.Soc. A203 (1950), 514

196 J.G.Overbeek. Koll.Chem.Beih. 54 (1943), 287

197 J.G.Overbeek. Adv.Colloid.Sci. 3 (1950), 97

198 P.H.Wiersma, A.L.Loeb, J.G.Overbeek. J.Coll.Interface Sci. 22 (1966), 78

199 R.N.O'Brien, L.R.White. J.Chem.Soc.Faraday Trans. 74 (1978), 1607

200 F.Booth. J.Chem.Phys. 19 (1951), 1331

201 D.N.Biswas, M.Sengupta. J.Ind.Chem.Soc. 44 (1967), 1042

202 M.Sengupta. Ind.J.Chem. 6 (1968), 501

203 V.G.Levich. "Phsicochemical Hydrodynamics." Prentice Hall (1962)

204 S.Levine, R.N.O'Brien. J.Coll.Interface Sci. 43 (1973), 616

205 D.C.Henry. Trans.Faraday Soc. 44 (1948), 1021

206 F.Booth. Trans.Faraday Soc. 44 (1948), 955

207 F.Fukui, S.Yuu. Chem.Eng.Sci. 35 (1980), 1097

208 S.V.Lopatenko,. Khim.Tekhnol.Vody. 5 (1983), 41

209 K.Kubota, S.Hayaski, A.Yasue. Kagaku.Kogaku.Ron. 8 (1982), No.3310

210 C.Cichos. Neue Bergbautechnik. 1 (1971), 941

211 C.Cichos. Neue Bergbautechnik. 2 (1972), 928

212 J.A.McShea, I.C.Callaghan. Colloid Polym.Sci. 261 (1983), 757

213 B.M.Matov. Elektrokhim. 9 (1973), 1495

214 B.M.Matov, E.P.Okun. Vost.Iz.Det.Mashin Ga.i Polimer.Pok.Kishinev. (1982), 78

215 G.N.Nazarova, L.N.Dorokhina, L.V.Kostina. Fiz.Khim Met.Pov.Eff.Prot.Pererab Miner.Syr'ya (1973), 44. Chem.Abs. 83 170117z

216 G.N.Nazarova, L.N.Dorokhina. Ref.Zh.Khim. (1979), Abstr. 7131530. Chem.Abs. 93 33973

217 V.Ya.Poberezhnyi, L.A.Kul'skii. Elektron.Obrab.Mater. 6 (1981), 48

218 S.S.Dukhin, B.V.Derjaguin, V.A.Lisichenko. Russ.J.Phys.Chem. 33 (1959), 389

219 S.S.Dukhin, B.V.Derjaguin, V.A.Lisichenko. Russ.J.Phys.Chem. 34 (1960), 248

220 S.S.Dukhin, B.V.Derjaguin. Russ.J.Phys.Chem. 35 (1961), 715

221 S.S.Dukhin. "Research in Surface Forces." Vol.2,3. Ed. B.V.Derjaguin. Consultants Bureau, New York (1966), (1971)

222 B.V.Derjaguin, S.S.Dukhin. Surface.Colloid Sci. 7 (1974), 273

223 J.F.Harper. Adv.Fluid Mech. 12 (1972), 59

224 W.Rybczynski. Bull.Intern.Acad.Sci.Cracovia. A (1911), 40

225 J.Hadamard. Comp.Rend. 154 (1911), 1735

226 D.W.Moore. J.Fluid Mech. 16 (1963), 161

227 R.M.Davies, G.I.Taylor. Proc.Roy.Soc. 200 (1950), 375

228 R.M.Griffith. Chem.Eng.Sci. 17 (1962), 1057

229 A.Detwiler. "Symposium on Surface Contamination." Vol.2. Ed. K.L.Mittal, Plenum, New York (1979)

230 R.E.Davies, A.Acrivos. Chem.Eng.Sci. 21 (1966), 681

231 N.N.Rulev, E.S.Leschov. Koll.Zh. 42 (1980), 521

232 E.Chifu, I.Stan, Z.Finta, E.Gavrila. J.Coll.Interface Sci. 93 (1983), 140

233 R.M.Pashley. Ph.D Thesis. London University. (1978)

234 J.F.Anfruns, J.A.Kitchener. Trans.I.M.M. C86 (1977), 9

235 M.Linton, K.L.Sutherland. Proc.2nd.Int.Congr.Surf.Act. 1 (1957), 494

236 P.H.Calderbank, A.C.Lochiel. Chem.Eng.Sci. 19 (1964), 471, 485

237 D.R.Raymond, S.A.Zieminski. A.I.Ch.E.J. 17 (1971), 57

238 J.Bridgewater, G.S.McNab. Chem.Eng.Sci. 27 (1972), 837

239 F.H.Deindoerfer, A.E.Humphrey. I.E.C. 53 (1971), 755

240 S.K.Friedlander. A.I.Ch.E.J. 7 (1961), 317

241 T.Takadi, S.Maeda. Chem.Eng.Sci.Tokyo. 25 (1961), 254

242 P.H.Calderbank, M.B.Moo-Young. Chem.Eng.Sci. 16 (1962), 39

243 B.T.Chao. Phys.Fluids. 5 (1962), 69

244 E.Ruckenstein. Chem.Eng.Sci. 19 (1964), 131

245 J.A.Redfield, G.Houghton. Chem.Eng.Sci. 20 (1965), 131

246 A.I.Johnson, F.Besik, A.E.Hamielec. Can.J.Chem.Eng. 47 (1969), 559

247 A.Weiner, S.W.Churchill. Conf.Physicochemical Hydrodynamics, Oxford (1977), Vol.11. Ed. D.B.Spalding, Advance, London (1977)

248 M.Motarjemi, G.J.Jameson. Chem.Eng.Sci. 33 (1978), 1415

249 D.Azbel. "Two-Phase Flows in Chemical Engineering." Cambridge University Press (1981)

250 P.H.Calderbank. Chem.Eng. CE220 (1968)

251 R.E.De La Rue, C.W.Tobias. J.Electrochem.Soc. 106 (1959), 827

252 J.C.Maxwell. "A Treatise on Electricity and Magnetism." Vol.1. Clarendon (1892)

253 D.A.G.Bruggeman. Ann.Phsik. 24 (1935), 659

254 Lord Rayleigh. Phil.Mag. 34 (1892), 481

255 I.Runge. Z.Tech.Physik. 6 (1925), 61

256 R.E.Meredith, C.W.Tobias. Adv.Electrochem.Electrochem.Eng. 2 (1962), 15

257 C.Elsner, F.Coeuret. Electrolytic Bubbles. SCI Conf. London, Sept. (1984)

258 G.Kreysa, M.Kuhn. Electrolytic Bubbles. SCI Conf. London, Sept. (1984)

259 H.Vogt. Electrolytic Bubbles. SCI Conf. London, Sept. (1984)

260 F.Hine, M.Yasuda, Y.Ogata, K.Hara. J.Electrochem.Soc. 1 (1984), 83

261 L.J.J.Janssen, B.E.Bongenaar-Schlenter, S.J.D.van Stralen, E.Barendrecht. Electrolytic Bubbles. SCI Conf. London, Sept. (1984)

262 L.J.J.Janssen, J.J.M.Geraets, E.Barendrecht, S.J.D.van Stralen. Electrochim.Acta. 27 (1982), 1207

263 C.W.Tobias. J.Electrochem.Soc. 106 (1959), 833

264 K.Hertwig, J.Nicht, R.Thiele. Chem.Techn. 30 (1978), 560

265 I.Rousar, A.Regner, V.Cezner. Coll.Czech.Chem.Comm. 31 (1966), 4193

266 I.Rousar. J.Electrochem.Soc. 116 (1969), 676

267 I.Rousar, V.Cezner, J.Nejepsara, M.M.Jacksic, M.Spasojevic, B.Z.Nikolic. J.Appl.Electrochem. 7 (1977), 427

268 L.Sigrist, O.Dossenbach, N.Ibl. Int.J.Heat Mass Transfer. 22 (1979), 1393

269 E.J.Ferech, C.W.Tobias. Electrochim.Acta. 2 (1960), 311

270 D.Jennings, A.T.Kuhn, J.B.Stepanek, R.Whitehead. Electrochim.Acta. 20 (1975), 903

271 H.B.Bull. J.Am.Chem.Soc. 67 (1945), 4

272 N.L.Jarvis, M.A.Scheimann. J.Phys.Chem. 72 (1968), 74

273 J.C.Scott. J.Fluid Mech. 69 (1975), 339

274 G.Goldfinger. "Clean Surfaces." Marcel Dekker, New York (1970)

275 J.C.Scott. "Symposium on Surface Contamination." Ed. K.L.Mittal, Plenum, New York (1978)

276 B.D.McNicol, R.Miles, R.T.Short. Electrochim.Acta. 28 (1983), 1285

277 B.E.Conway, H.Angerstein-Kozlowska, W.B.A.Sharp. Anal.Chem. 45 (1973), 1331

278 R.V.Bucur, L.Stoicovici. J.Electroanal.Chem. 25 (1970), 342

279 D.J.Ives, G.J.Janz. "Reference Electrodes, Theory and Practice." Academic Press, New York (1961)

280 W.J.McG.Tegart. "The Electrolytic and Chemical Polishing of Metals." Pergamon, London (1956)

281 "Handbook of Chemistry and Physics." 53rd Edition. Chemical Rubber Company (1972)

282 G.R.Wiese, R.O.James, T.W.Healy. Disc.Faraday Soc. 52 (1971), 302

283 B.McGhee. PhD Thesis. Manchester University (1966)

284 A.L.Howard. "Physical Properties of Inorganic Compounds." Edward Arnold, London (1975)

285 R.D.Armstrong, M.F.Bell, A.A.Metcalfe. Electrochem. 6 (1978), 98

286 M.Pourbaix. "Atlas of Electrochemical Equilibria in Aqueous Solution." N.A.C.E., Houston (1974)

287 R.D.Armstrong, K.Edmunson. Electrochim.Acta. 18 (1973), 937

288 J.Rogers. Trans.I.M.M. 66 (1957), 439

289 S.K.Doss. Trans.I.M.M. 85 (1976), C195

290 L.N.Milne Thompson. "Theoretical Hydrodynamics." Macmillan, London (1955)

291 R.Buscall, R.H.Ottewill. "Colloid Science." Vol.2, Ed. D.H.Everett, Chem.Soc. (1975)

292 R.Hogg, T.W.Healy, D.W.Fuerstenau. Trans.Faraday Soc. 62 (1966), 1638

293 H.J.Schulze, C.Cichos. Z.Phys.Chem. 251 (1972), 252

294 A.D.Read, J.A.Kitchener. J.Coll.Interface Sci. 30 (1969), 391

295 T.D.Blake, J.A.Kitchener. J.Chem.Soc.Faraday Trans. 68 (1972), 1435

296 D.B.Hough, R.H.Ottewill. Progress Coll.Polym.Sci. 68 (1983), 101

297 J.Leja. "Surface Chemistry of Froth Flotation." Chap.4, Plenum, New York (1982)

298 A.Hamelin, T.Vitanov, E.Sevastyanov, A.Popov. J.Electroanal.Chem. 145 (1983), 225

299 G.K.Batchelor. "An Introduction to Fluid Dynamics." Cambridge University Press, London (1967)

300 C.R.Wylie. "Differential Equations." McGraw-Hill, New York (1979)

301 J.S.Bendat, A.G.Piersol. "Random Data: analysis and measurement procedures." Wiley, New York (1971)

302 P.M.Robertson. Electrochim.Acta. 22 (1977), 411

303 K.J.Vetter. "Electrochemical Kinetics. Theoretical and Experimental Aspects." Academic Press, New York (1967)

NOMENCLATURE

a	radius
B	surface coverage of electrode by bubbles
$[c]$	electrolyte concentration
c_i	concentration of ion i
C	capacitance
C_D	drag coefficient
C_o	initial dissolved gas concentration
C_s	dissolved gas concentration at saturation
C_∞	dissolved gas concentration at supersaturation
d	diameter
D	diffusion coefficient
e	elementary charge
E	electric field strength
f	frequency
F	Faraday's constant
F_e	electrostatic force
g	acceleration due to gravity
i	current density
I	current
j	complex plane operator
Ja	Jakob number, $\Delta C_o/\rho'$
k	Boltzmann constant

$\bar{k}$	mass transfer coefficient
K	conductivity
m_i	perturbation in the density of ion i
n	number of bubbles per unit area
n_i	number of ions of type i per unit volume
N_A	Avagadros constant
P	pressure
q	charge required to form one molecule
Q	differential charge density
r	bubble radius
R	resistance
$\hat{R}$	Universal gas constant
Re	Reynolds number, $vd\rho/\eta$
S	electrode area
Sc	Schmidt number, $\eta/\rho D$
Sh	Sherwood number, $\bar{k}d/D$
t	time
T	temperature
u	electrophoretic velocity
u_e	electrophoretic mobility
v	terminal velocity
V	volume rate of gas evolution
$\bar{V}$	molar volume
w	weight
x	time constant
z_i	valency of ion i
Z	impedance

β	growth coefficient
γ	surface tension
Γ	surface concentration of adsorbed species
∂	thin film thickness
δ	diffuse layer thickness
ϵ	dielectric constant
Σ	current efficiency
ζ	zeta potential
η	viscosity
θ	contact angle
κ	inverse Debye length
μ	electrochemical potential
ν	kinematic viscosity
ξ	gas voidage
Π	dimensionless bubble radius
ρ	density
σ	surface charge density
τ	reciprocal of the induction time for bubble nucleation
ϕ	potential perturbation
ψ	equilibrium potential
Ψ	Stoke's axisymmetric stream function
ω	dimensionless temperature
ℓ	thickness of supersaturated layer

Subscripts

G	gas
I	imaginary component
L	liquid
$_0$	original value
R	real component
s	surface
S	solid
$_1$	perturbed value

Supersripts

'	gas phase.

APPENDIX 1

THE ELECTROPHORESIS OF A BUBBLE

BY

N.BRANDON & S.LEVINE[1]

1 Application of the Levich Theory to Bubble Electrophoresis

2 Investigation of the Validity of the Lippmann Equation

3 The Influence of an Electric Field on the Electrophoretic Mobility of a Bubble

4 The Distribution of Charge on the Surface of a Rising Bubble

[1] Division of Chemistry
National Research Council
Canada

1 Application of the Levich Method to Bubble Electrophoresis

In this treatment a detailed study of the electric double layer at the gas/liquid interface is avoided by adapting Levich's theory (203) of the electrophoresis of charged mercury drops. Levich introduced a thin-shell model for the double layer, and his treatment is simpler than the classical theories of electrophoresis developed by Henry (193,205), Booth (194,195,200,206) and Overbeek (196,197), since it works in terms of quantities averaged over the double layer. The Levich approach is restricted to small surface potentials (< 25 mV) and large bubbles (such that the double layer thickness is very small compared to the bubble radius).

The model used both here and by Levich separates the aqueous medium surrounding the bubble into a thin shell of thickness δ containing the double layer charge, and an electrically neutral bulk electrolyte. Fig. A1 illustrates this.

Outside the thin shell ($r > a+\delta$) the electrical potential is governed by the Laplace equation:

$$\nabla^2\phi=0 \qquad (1-1)$$

with the boundary conditions of:

$$\phi \to 0 \text{ as } r \to \infty \qquad (1-2)$$

and a conservation of charge condition:

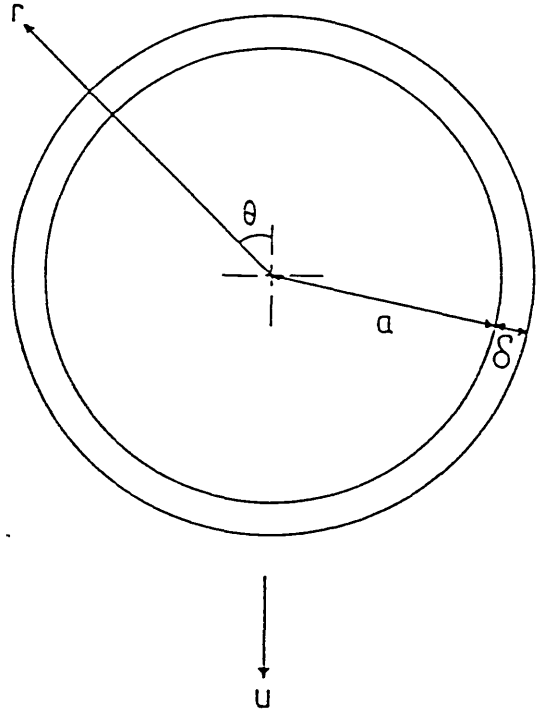


Fig. A1 Schematic illustration of the "thin shell" model of the double layer.

$$div_s(\Sigma \mathbf{v}_t) = i_r \qquad \text{at } r=a \qquad (1\text{-}3)$$

where div_s represents a surface divergence of charge, Σ the mobile charge per unit area in the double layer, i_r the inward radial component of current density at $r=a+\delta$, and $\mathbf{v}_t$ the tangential component of the fluid velocity vector at $r=a$. Since $\delta \ll a$, i_r can be equated to the current density at $r=a$.

Assuming the electrolyte to be incompressible, the Navier-Stokes hydrodynamic equations of motion for the fluid velocity $\mathbf{v}$ are (299):

$$\eta \nabla^2 \mathbf{v} - \rho \mathbf{v}.\text{grad}\mathbf{v} = \text{grad}(P) + \rho g \mathbf{k} \qquad (1\text{-}4)$$

$$\text{div}\mathbf{v} = 0 \qquad (1\text{-}5)$$

where $\mathbf{k}$ is the unit vector, and P the hydrodynamic pressure.

For small Reynolds numbers ($Re < 1$) equation (1-4) simplifies to:

$$\eta \nabla^2 \mathbf{v} = \text{grad}(P) \qquad (1\text{-}6)$$

and the boundary conditions on $\mathbf{v}$ are:

$$\mathbf{v} \to 0 \quad \text{as} \quad r \to \infty \qquad (1\text{-}7)$$

$$div_s(\Sigma \mathbf{v}_t) = K \partial\phi/\partial r \quad \text{at} \quad r=a \qquad (1\text{-}8)$$

If u is the velocity of the bubble then the introduction of

spherical polar co-ordinates (r,θ) with origin at the bubble centre, transforms equation (1-5) to the form:

$$\partial v_r/\partial r+1/r.\partial v_\theta/\partial\theta+2v_r/r+v_\theta\cot\theta/r=0 \qquad (1\text{-}9)$$

with the boundary conditions for the velocity distribution being:

$$v_r=-u.\cos\theta,\ v_\theta=u.\sin\theta \quad \text{as} \quad r\to\infty \qquad (1\text{-}10)$$

Solutions to equation (1-9) take the form:

$$v_r=f(r).\cos\theta \qquad (1\text{-}11)$$

$$v_\theta=g(r).\sin\theta \qquad (1\text{-}12)$$

$$P=\eta\dot{h}(r).\cos\theta \qquad (1\text{-}13)$$

though it should be noted that equations (1-11) to (1-13) constitute only the first terms in the expansion of the Legendre polynomials $P_n\cos\theta$. Substitution of (1-11) to (1-13) into (1-9) and (1-10) gives:

$$v_r=(b_2/r+b_1/r^3-u)\cos\theta \qquad (1\text{-}14)$$

$$v_\theta=(b_1/2r^3-b_2/2r+u)\sin\theta \qquad (1\text{-}15)$$

$$P=(\eta b_2/r^2)\cos\theta+P_h \qquad (1\text{-}16)$$

where P_h is the hydrodynamic pressure far away from the bubble, and b_1 and b_2 are constants.

b_1, b_2 and u can be determined from the following boundary conditions at the bubble interface (r=a):

(i) The radial velocity of the fluid at the bubble interface is zero relative to the bubble centre:

$$v_r=0 \qquad (1\text{-}17)$$

(ii) Continuity of the normal component of the stress tensor must be maintained:

$$-P'=-P_h-(\eta b_2/r^2)\cos\theta+\rho g r.\cos\theta+2\eta.\partial v_r/\partial r-2\gamma/a \qquad (1\text{-}18)$$

where P' is the constant pressure inside the bubble.

(iii) Continuity of the tangential component of the stress tensor must be maintained (tangential stress can be taken as zero inside the bubble and therefore zero in the liquid at the interface):

$$1/a.\partial\gamma/\partial\theta+\eta(\partial v_\theta/\partial r-v_\theta/r)=0 \qquad (1\text{-}19)$$

If charge is moved around the bubble (through the influence of an applied electric field or bubble rise) surface tension (γ) will be dependent on the angle (θ) relative to the fluid. This can be expressed in the form:

$$\gamma(\theta)=\gamma_0+\gamma_1\cos\theta+\gamma_2 P_2(\cos\theta)^2+... \qquad (1\text{-}20)$$

where γ_1 represents the perturbation in the equilibrium surface tension ($\gamma_0=\gamma(\pi/2)$).

Levich (203) used the Lippmann equation:

$$\sigma=-\partial\gamma/\partial(\Delta\phi) \qquad (1\text{-}21)$$

to relate interfacial tension to the surface charge density (σ), where $\Delta\phi$ represents the potential drop across the thin "double layer" shell. However, two problems arise with the application of the Lippmann equation to the gas/liquid interface:

(i) The equation strictly applies only to a metal/liquid interface.

(ii) The equation is derived on thermodynamic grounds and hence assumes equilibrium, whereas the movement of charge around the bubble disturbs equilibrium.

2 Investigation of the Validity of the Lippmann Equation

To investigate the application of the Lippmann equation to the gas/liquid interface consider first the Gibbs adsorption isotherm (173):

$$d\gamma=-\Gamma_i d\mu_i-\Gamma_+ d\mu_+-\Gamma_- d\mu_- \qquad (2\text{-}1)$$

where Γ_i and μ_i are respectively the surface excess per unit area and the chemical potential of adsorbed univalent ions (OH^- for negatively charged bubbles), and Γ_+, μ_+ and Γ_-, μ_- are the corresponding quantities for the cations and anions of an

indifferent 1:1 supporting electrolyte. It is assumed that all quantities in equation (2-1) depend on θ.

If local thermodynamic equilibrium is assumed across the thin shell (the thickness of which is extremely small compared to the bubble radius) so that the chemical potentials μ_+ and μ_- are independent of distance (r) from the bubble centre, then:

$$d\gamma(\theta)/d\theta=-\Gamma_i d\mu_i(\theta)/d\theta-\Gamma_+(\theta)d\mu_+(\theta)/d\theta$$
$$-\Gamma_-(\theta)d\mu_-(\theta)/d\theta \qquad (2\text{-}2)$$

At equilibrium the adsorbed ions are uniformly distributed on the bubble surface. Therefore, the following can be written:

$$\Gamma_i=\Gamma_i^{\circ}+\Gamma_i'(\theta) \qquad (2\text{-}3)$$

where, assuming no additional ionic adsorption results from bubble motion:

$$\int_0^{\pi} \Gamma_i'(\theta)\sin\theta.d\theta=0 \qquad (2\text{-}4)$$

The volume densities of the cations and anions in the 1:1 electrolyte are given by:

$$\nu_+(r,\theta)=n_+(r)+m_+(r,\theta) \qquad (2\text{-}5)$$
$$\nu_-(r,\theta)=n_-(r)+m_-(r,\theta) \qquad (2\text{-}6)$$

where $n_+(r)$ and $n_-(r)$ are the equilibrium ion densities, and

$m_+(r,\theta)$, $m_-(r,\theta)$ are the departures in density due to the movement of charge around the bubble. The Boltzmann equations (173) give:

$$n_+(r)=n.\exp(-e\psi(r)/kT) \qquad (2\text{-}7)$$

$$n_-(r)=n.\exp(e\psi(r)/kT) \qquad (2\text{-}8)$$

where $\psi(r)$ is the equilibrium potential and n the volume density of either ionic species far away from the bubble. The chemical potential of the cation in the electrolyte is assumed to be:

$$\mu_+(\theta)=\mu_+^{\circ}+kT.\ln\nu_+(r,\theta)+e(\psi(r)+\phi(r,\theta)) \qquad (2\text{-}9)$$

where $\phi(r,\theta)$ is the perturbation in the equilibrium potential resulting from the movement of surface charge. Since the thickness of the "double layer" shell is small compared to the bubble radius, chemical potential should vary only slightly with position across the shell. Taking $r_o=a+\delta$ and $r=r_o$ gives:

$$d\mu_+(\theta)/d\theta=kT/\nu_+(r_o,\theta).dm_+(r_o,\theta)/d\theta+e.d\phi(r_o,\theta)/d\theta \qquad (2\text{-}10)$$

$$d\mu_-(\theta)/d\theta=kT/\nu_-(r_o,\theta).dm_-(r_o,\theta)/d\theta-e.d\phi(r_o,\theta)/d\theta \qquad (2\text{-}11)$$

Assuming the chemical potential of an adsorbed ion to be:

$$\mu_i(\theta)=\mu_i^{\circ}+kT.\ln\Gamma_i-e(\psi(a)+\phi(a,\theta)) \qquad (2\text{-}12)$$

equation (2-3) yields:

$$d\mu_i(\theta)/d\theta=kT/\Gamma_i.d\Gamma_i'(\theta)/d\theta-e.d\phi(a,\theta)/d\theta \qquad (2\text{-}13)$$

Therefore, substituting (2-10), (2-11) and (2-13) into equation (2-2) gives:

$$\begin{aligned} d\gamma(\theta)/d\theta=&-kT.d\Gamma_i'(\theta)+e.\Gamma_i.d\phi(a,\theta)/d\theta \\ &-\Gamma_+(\theta)\left[kT/\nu_+(r_o,\theta).dm_+(r_o,\theta)/d\theta+e.d\phi(r_o,\theta)/d\theta\right] \\ &-\Gamma_-(\theta)\left[kT/\nu_-(r_o,\theta).dm_-(r_o,\theta)/d\theta-e.d\phi(r_o,\theta)/d\theta\right] \end{aligned} \qquad (2\text{-}14)$$

The total surface excess of cations in the electrolyte is:

$$\Gamma_+^t=2\pi\int_o^\pi \sin\theta.d\theta\int_a^\infty r^2dr(\nu_+(r,\theta)-n) \qquad (2\text{-}15)$$

where the dividing surface is placed at r=a. Since $\Gamma_+(\theta)$ gives:

$$\Gamma_+^t=2\pi a^2\int_o^\pi \sin\theta\Gamma_+(\theta).d\theta \qquad (2\text{-}16)$$

it follows that:

$$\begin{aligned} \Gamma_+(\theta)&=1/a^2.\int_a^\infty r^2dr(\nu(r,\theta)-n) \\ &=n/a^2.\int_a^\infty(\exp(-e\psi(r)/kT)-1)r^2dr \\ &\quad+1/a^2\int_a^\infty m_+(r,\theta)r^2dr \end{aligned} \qquad (2\text{-}17)$$

The first integral on the right hand side of (2-17) is independent of θ and will be denoted by Γ_+^o. Hence:

$$\Gamma_+(\theta)=\Gamma_+^o+1/a^2\int_a^\infty m_+(r,\theta)r^2dr$$

$$=\Gamma_+^{\circ}+\Gamma_+'(\theta) \qquad (2\text{-}18)$$

and similarly:

$$\Gamma_-(\theta)=\Gamma_-^{\circ}+\Gamma_-'(\theta) \qquad (2\text{-}19)$$

At equilibrium the condition of electrical neutrality over the whole double layer yields the relation:

$$\Gamma_+^{\circ}-\Gamma_-^{\circ}=\Gamma_i^{\circ} \qquad (2\text{-}20)$$

Therefore, assuming electrical neutrality to similarly hold in each infinitesimal sector of the double layer ($\theta \rightarrow \theta+d\theta$), yields:

$$\Gamma_+(\theta)-\Gamma_-(\theta)=\Gamma_i(\theta) \qquad (2\text{-}21)$$

The potential across the thin "double layer" shell is given by:

$$\Delta\phi(\theta)=\psi(a)+\phi(a,\theta)-\phi(r_o,\theta) \qquad (2\text{-}22)$$

noting that $\psi(r_o)$ is negligible. The use of (2-20) and (2-21), and of the expression for the charge density ($\sigma(\theta)$) on the bubble surface:

$$\sigma(\theta)=-e\Gamma_i(\theta) \qquad (2\text{-}23)$$

allows equation (2-17) to be written as:

$$d\Upsilon(\theta)/d\theta=-\sigma(\theta).d\Delta\phi(\theta)/d\theta$$
$$-kT\left[d\Gamma_i'(\theta)/d\theta+\Gamma_+(\theta)/\nu_+(r_o,\theta).dm_+(r_o,\theta)/d\theta\right.$$
$$\left.+\Gamma_-(\theta)/\nu_-(r_o,\theta).dm_-(r_o,\theta)/d\theta\right] \qquad (2\text{-}24)$$

It should be noted that if only the first term on the right hand side of (2-24) is retained the equation becomes equivalent to the Lippmann equation used by Levich (see equation (1-21)). Neglecting terms of order m_+^2 and m_-^2 gives the following for the second and third terms in the square brackets of (2-24):

$$1/n.\left[\Gamma_+^{\circ}.dm_+(r_o,\theta)/d\theta+\Gamma_-^{\circ}.dm_-(r_o,\theta)/d\theta\right] \qquad (2\text{-}25)$$

where, for small values of $\psi(r)$, equation (2-17) gives:

$$\Gamma_+^{\circ}=-\Gamma_-^{\circ}=-ne/kTa^2.\int_a^{\infty} r^2\psi(r).dr \qquad (2\text{-}26)$$

Therefore, equation (2-25) can be written as:

$$\Gamma_+^{\circ}/n.d/d\theta\left[m_+(r_o,\theta)-m_-(r_o,\theta)\right] \qquad (2\text{-}27)$$

If:

$$M(r,\theta)=m_+(r,\theta)-m_-(r,\theta) \qquad (2\text{-}28)$$

then Poissons equation (173) for the departure of potential from

equilibrium in the double layer at small potentials takes the form:

$$\nabla^2\phi(r,\theta)=-4\pi eM(r,\theta)/D \qquad (2\text{-}29)$$

where D is the dielectric constant of the double layer. Since $\phi(r,\theta)$ satisfies Laplace's equation (1-1) for $r > r_o$, it follows that $M(r_o,\theta)=0$. Therefore, equation (2-27) is also equal to zero. The remaining term in the square brackets of (2-24) is given by:

$$d\Gamma_i'(\theta)d\theta=d/d\theta\left[\Gamma_+'(\theta)-\Gamma_-'(\theta)\right]$$
$$=1/a^2.\partial/\partial\theta\int_a^{r_o} M(r,\theta)r^2dr \qquad (2\text{-}30)$$

Assuming $M(r,\theta)=M(r)\cos\theta \qquad (2\text{-}31)$

$$\phi(r,\theta)=y(r)\cos\theta \qquad (2\text{-}32)$$

and representing the surface charge density as:

$$\sigma(\theta)=\sigma_o+\sigma_1\cos\theta=-\Sigma_o-\Sigma_1\cos\theta=-\Sigma(\theta) \qquad (2\text{-}33)$$

where σ_1 represents the perturbation in surface charge from the equilibrium value σ_o, allows integration of (2-24) to give:

$$\Upsilon(\theta)-\Upsilon(\pi/2)=-\sigma_o(y(a)-y(r_o))\cos\theta$$
$$-1/2.\sigma_1(y(a)-y(r_o))\cos^2\theta$$
$$-kT/a^2.\cos\theta\int_a^{r_o} M(r)r^2dr$$
$$=\Upsilon_1\cos\theta+\text{higher order terms} \qquad (2\text{-}34)$$

Equation (2-34) represents the integrated form of the generalized Lippmann equation, and expresses γ_1, the perturbation in surface tension due to the non-uniform distribution of surface charge, in terms of y(r) and M(r).

3 The Influence of an Electric Field on the Electrophoretic Mobility of a Bubble

Here the electrophoretic mobility induced by an electric field on an otherwise stationary bubble will be considered. Substitution of equation (1-17) into (1-14) gives:

$$b_2/a+b_1/a^3-u=0 \qquad (3-1)$$

Additionally the coefficients of (1-18) and (1-19) must be zero for the given boundary conditions to be fulfilled. Hence:

$$-\eta b_2/a_2+2\eta(-b_2/a^2-3b_1/a^4)-2\gamma_1/a=0 \qquad (3-2)$$

$$-\gamma_1/a+\eta(-2b_1/a^4+b_2/a^2-u/a)=0 \qquad (3-3)$$

Solving (3-1), (3-2) and (3-3) yields:

$$b_2=0 \qquad b_1=ua^3 \qquad u=-\gamma_1/3\eta \qquad (3-4)$$

Therefore γ_1, given by the generalized Lippmann equation, must be obtained in order to determine the electrophoretic velocity (u).

Expressing the law of conservation of charge (equation (1-8)) in spherical polar coordinates gives:

$$1/a\sin\theta.\partial/\partial\theta(\Sigma(\theta)\sin\theta v_\theta)=K.\partial\phi(r,\theta)/\partial r \quad \text{at} \quad r=a \qquad (3\text{-}5)$$

This condition equates the radial component of the current density associated with the indifferent electrolyte at the outer edge of the thin shell, to the surface divergence of the tangential current density. It should be noted that because $\delta << a$, equation (3-5) is taken at r=a, whereas it strictly holds at $r=r_o$.

The Laplace equation gives:

$$\nabla^2\phi(r,\theta)=0 \qquad r \geq r_o \qquad (3\text{-}6)$$

the solution of which, retaining only terms in θ since only the angle dependence of ϕ is being considered here, is given by:

$$\phi(r,\theta)=(A/r^2-Er)\cos\theta \qquad r \geq r_o \qquad (3\text{-}7)$$

which relates the potential perturbation to the applied field strength (E). Substituting (3-4) into (1-15) gives:

$$v_\theta=-0.5Y_1/\eta\sin\theta \quad \text{at} \quad r=a \qquad (3\text{-}8)$$

Therefore, from (2-33) and (3-5):

$$-3\sigma_o u/a=\sigma_o Y_1/\eta a=-K(2A/a^3+E) \qquad (3\text{-}9)$$

which relates u, γ_1 and E in terms of the constant A. Therefore it is necessary to determine A.

The assumption of local thermodynamic equilibria (see section 2) implies that $\mu_+(\theta)$ and $\mu_-(\theta)$ are independent of distance (r) across the thin shell ($a < r < r_o$). It follows from (2-9) that for a cation within the double layer:

$$\mu_+^o+kT.\ln\nu_+(r,\theta)+e(\psi(r)+\phi(r,\theta))=\mu_+^o+kT.\ln\nu_+(r_o,\theta) +e(\psi(r_o)+\phi(r_o,\theta)) \quad (3\text{-}10)$$

A similar relation holds for an anion and which, if subtracted from (3-10) and equations (2-5) and (2-8) substituted, yields:

$$M(r,\theta)=e/kT.(\phi(r,\theta)-\phi(r_o,\theta)) \quad (3\text{-}11)$$

retaining only linear powers of ψ.

The inverse Debye length is defined by (173):

$$\kappa^2=8\pi ne^2/DkT \quad (3\text{-}12)$$

and substituting this into (3-11) gives:

$$M(r,\theta)=D\kappa^2/8\pi ne.(\phi(r,\theta)-\phi(r_o,\theta)) \quad (3\text{-}13)$$

Combining (3-13) with (2-29) and (3-7) yields:

$$\nabla^2\phi(r,\theta)-\kappa^2\phi(r,\theta)=-\kappa^2\phi(r_o,\theta)$$

$$=-\kappa^2(A/r_0^2-Er_0)\cos\theta \qquad (3\text{-}14)$$

Therefore, the introduction of equation (2-32) yields an ordinary differential equation for y(r):

$$d^2y(r)/dr^2+2/r.dy(r)/dr-(\kappa^2r^2+2)/r^2.y(r)$$
$$=-\kappa^2(A/r_0^2-Er_0) \qquad (3\text{-}15)$$

To solve for y(r) the potential in three regions must be considered.

(i) $0 < r < a$

(ii) $a < r < r_0$

(iii) $r > r_0$

For the first and third stages the potential satisfies the Laplace equation. The solution inside the bubble takes the form:

$$\psi(r,\theta)=\psi(a)+\phi(r,\theta)=\psi(a)+\psi_1 r.\cos\theta \qquad (3\text{-}16)$$

where ψ_1 is a constant. Therefore, it follows that $y(r)=\psi_1 r$.

The potential $\phi(r,\theta)$ in the thin shell ($a < r < r_0$) is given by (2-32), where y(r) satisfies equation (3-15). Using the method of variation of parameters (300) the general solution of (3-15) can be written as:

$$y(r)=F'(\kappa r+1)/(\kappa r)^2.\exp(-\kappa(r-a))+G'(\kappa r-1)/(\kappa r)^2.\exp(\kappa(r-a))$$
$$-\kappa^2(A/r_0^2-Er_0)\int_a^r h(r,z)dz \qquad (3\text{-}17)$$

where F' and G' are constants of integration, and:

$$h(r,z)=z/2\kappa r.\left[(\kappa z+1)(\kappa r-1)/\kappa^2 zr.\exp(-\kappa(z-r))\right.$$
$$\left.-(\kappa z-1)(\kappa r+1)/\kappa^2 zr.\exp(\kappa(z-r))\right] \quad (3\text{-}18)$$

Terms involving $\exp(-\kappa r)$ must be retained even though small because (3-17) holds only in a finite range of r.

Solving (3-18), and adsorbing functions of the same form as the first two terms of (3-17) into F' and G', yields:

$$y(r)=F'(\kappa r+1)/(\kappa r)^2.\exp(-\kappa(r-a))+G'(\kappa r-1)/(\kappa r)^2.\exp(\kappa(r-a))$$
$$+(A/r_0^2-Er_0)(1-2/(\kappa r)^2) \quad a \leq r \leq r_0 \quad (3\text{-}19)$$

Outside the thin "double layer" shell ($r \geq r_0$), $\phi(r,\theta)$ is given by equation (2-32) with:

$$y(r)=A/r^2-Er \qquad r \geq r_0 \quad (3\text{-}20)$$

The constants F', G', A and ψ_1 can be determined from the boundary conditions:

(i) At $r=r_0$, y(r) and its derivatives must be continuous.

(ii) At r=a, y(r) is continuous and equation (3-21) applies:

$$4\pi\sigma_1=\psi_1-D(dy/dr) \qquad r=a \quad (3\text{-}21)$$

The above condition represents the conventional electrostatic relationship between surface charge density and discontinuity in the

normal component of the dielectric displacement (203). On eliminating A the continuity conditions at $r=r_0$ yield:

$$G'=-F'\exp(-2\kappa(r_0-a))-3E/\kappa.\exp(-\kappa(r_0-a)) \qquad (3\text{-}22)$$

and hence:

$$A=r_0^2F'\exp(-\kappa(r_0-a))+E((3/2.r_0^2/\kappa)-r_0^3/2) \qquad (3\text{-}23)$$

After substitution of (3-22) to eliminate G', the requirement of continuity of y(r) at r=a gives:

$$\begin{aligned}\psi_1 a=F'/(\kappa a)^2.&[\kappa a+1-((\kappa a)^2-2)\exp(-\kappa(r_0-a))-(\kappa a-1)\exp(-2\kappa(r_0-a))]\\&+E/(\kappa a)^2.[((\kappa a)^2-2).(3/2\kappa.(1-\kappa r_0))\\&-3(\kappa a-1)/\kappa.\exp(-\kappa(r-a)]\end{aligned} \qquad (3\text{-}24)$$

Substituting (3-24) for ψ_1, and (3-22) for G', the boundary condition (3-21) yields:

$$\begin{aligned}4\pi\sigma_1=F'/a(\kappa a)^2.&[D((\kappa a)^2+2\kappa a+2)+(\kappa a+1)-(4D+(\kappa a)^2-2)\exp(-\kappa(r_0-a))\\&+\{D((\kappa a)^2-2\kappa a+2)+(1-\kappa a)\}\exp(-2\kappa(r_0-a))]\\&+E/a(\kappa a)^2.[3/2\kappa.((\kappa a)^2-2)(1-\kappa r_0)+6D(r_0-1/\kappa)\\&+\{3D/\kappa.((\kappa a)^2-2\kappa a+2)-3/\kappa.(\kappa a-1)\}\exp(-\kappa(r_0-a))]\end{aligned} \qquad (3\text{-}25)$$

Since r_0 represents the outer boundary of the double layer, $\exp(-\kappa(r_0-a)) \ll 1$. Therefore, for $\kappa a \gg 1$ (where $r_0/a \approx 1$ and $(\kappa a)^2 \gg D$), equations (3-24) and (3-25) closely approximate to:

$$\psi_1 a = F'/\kappa a - 3/2.Er_0 \qquad (3\text{-}26)$$

$$4\pi\sigma_1 = F'D/a - 3/2.E \qquad (3\text{-}27)$$

Eliminating F' gives:

$$4\pi\sigma_1 = D\kappa a(3E/2+\psi_1) \qquad (3\text{-}28)$$

and thus:

$$y(a) = \psi_1 a = 4\pi\sigma_1/D\kappa - 3/2.Ea \qquad (3\text{-}29)$$

Substitution of (3-22) and (3-23) into (3-19) yields (since $\kappa r_0 >> 1$):

$$\begin{aligned} y(r_0) &= F'\exp(-\kappa(r_0-a)) + 3E/2\kappa.(1-\kappa r_0) \\ &= (y(a)+3/2.Ea)\kappa a.\exp(-\kappa(r_0-a)) - 3Ea/2 \\ &\approx -3Ea/2 \end{aligned} \qquad (3\text{-}30)$$

Taking $\exp(-\kappa(r_0-a))\kappa a << 1$ gives:

$$y(a) \approx y(r_0) = 4\pi\sigma_1/D\kappa \qquad (3\text{-}31)$$

and therefore the leading term in the integrated form of the generalized Lippmann equation (see (2-34)) becomes:

$$\gamma(\theta) = \gamma(\pi/2) - \sigma_0(y(a)-y(r_0))\cos\theta = \gamma_0 + \gamma_1\cos\theta \qquad (3\text{-}32)$$

where $\gamma_1=-4\pi\sigma_0\sigma_1/D\kappa$ (3-33)

Therefore, from equation (3-4), the electrophoretic velocity is given by:

$$u=4\pi\sigma_0\sigma_1/3D\kappa\eta \quad (3\text{-}34)$$

It should be noted that in the absence of charge deformation ($\sigma_1=0$) equation (3-34) is consistent with Booth's result of zero velocity (200). However, the contribution made to the electrophoretic velocity by the second and third terms of (2-34) must also be considered. The second term gives:

$$-1/2.\sigma_1(y(a)-y(r_0))\cos^2\theta=4\pi\sigma_1/6D\kappa.(1+2P_2\cos\theta) \quad (3\text{-}35)$$

Thus: $\gamma(\theta)=\gamma(\pi/2)-2/3.\pi\sigma_1/D\kappa+\gamma_1\cos\theta+\gamma_2P_2\cos\theta$ (3-36)

Therefore, taking second order terms of the Legendre polynomial to be negligible (see section 4) means that equation (3-36) makes no significant contribution to γ_1, and hence does not influence the electrophoretic velocity.

The third term of (2-34) yields:

$$-kT/a^2.\cos\theta\int_a^{r_0} M(r).r^2dr=-\left[D\kappa^2kT/4\pi ea^2.\cos\theta \int_a^{r_0}(y(r)-y(r_0)).r^2dr\right] \quad (3\text{-}37)$$

where, since $\kappa a \gg 1$ and $r_0/a\approx1$, equations (3-26), (3-27) and

(3-29) give:

$$\int_a^{r_o}(y(r)-y(r_o)).r^2dr=(\kappa a(\psi_1 a+3/2.Ea)-3Ea)/\kappa^3$$
$$\approx 4\pi\sigma_1 a/D\kappa^2 \qquad (3\text{-}38)$$

Therefore, the third term becomes:

$$kT\sigma_1/e.\cos\theta/\kappa a \qquad (3\text{-}39)$$

and the contribution to Υ_1 is $kT\sigma_1/e\kappa a$. However, this is much smaller than the contribution made by the first term to Υ_1 (equation (3-33)), so that equation (3-34) represents the dominant contribution to the electrophoretic velocity. To obtain an expression for the electrophoretic mobility it is necessary to relate σ_1 to the electric field strength. From equations (3-23), (3-26) and (3-27):

$$A=a^3\kappa(y(a)+3/2.Ea)\exp(-\kappa(r_o-a))+a^2E(3/2\kappa-a/2)$$
$$\approx a^2E(3/2\kappa-a/2) \quad \text{since } \kappa a.\exp(-\kappa(r_o-a)) << 1 \qquad (3\text{-}40)$$

Therefore, because:

$$2A/a^3+E=3E/\kappa a \qquad (3\text{-}41)$$

the substitution of (3-31) into (3-9) yields:

$$u=EK/\kappa\sigma_o \qquad (3\text{-}42)$$

The electrophoretic mobility is then defined by:

$$u_e = K/\kappa\sigma_o \qquad (3\text{-}43)$$

4 The Distribution of Charge on the Surface of a Rising Bubble

Here the movement of charge around the bubble surface induced by bubble rise (at velocity v) through a 1:1 supporting electrolyte, will be considered. The solution procedure follows that applied to the derivation of the effect of an electric field on the charge distribution around a stationary bubble. However, the solution will be expanded to incorporate second order terms arising from the expansion of Legendre polynomials (these were assumed negligible in section 3).

In the absence of an electric field the generalized solution to the Laplace equation (equation (1-1)), subject to the boundary conditions (1-2) and (1-10), is given by:

$$\phi(r,\theta) = A/r^2.\cos\theta + B/r^3.P_2\cos\theta = \phi' + \phi'' \qquad (4\text{-}1)$$

where B is a measure of the quadrupole moment of the double layer induced by bubble rise. The solution of the Navier-Stokes equation must be correspondingly expanded to the "next term", and it is convenient to do so in terms of the Stokes axisymmetric stream function (Ψ), given in spherical polar co-ordinates as (299):

$$v_r = -1/r^2\sin\theta.\partial\Psi/\partial\theta \qquad (4\text{-}2)$$

$$v_\theta = 1/r\sin\theta . \partial\Psi/\partial r \qquad (4\text{-}3)$$

Ψ satisfies:

$$D^2D^2\Psi = 0 \qquad (4\text{-}4)$$

where, with $\cos\theta$ denoted by μ:

$$D^2 = \partial^2/\partial r^2 + (1-\mu^2)/r^2 . \partial^2/\partial\mu^2 \qquad (4\text{-}5)$$

The general solution of (4-4) is given by:

$$\Psi/va^2 = (r^2/a^2 - \alpha_2 r/a + \beta_2 a/r)\chi_2(\mu) - \sum_{n=3}^{\infty}(\alpha_n(a^{n-3}/r^{n-3}) - \beta_n(a^{n-1}/r^{n-1})\chi_n(\mu) \qquad (4\text{-}6)$$

where $\chi_n(\mu)$ is defined in terms of the Legendre polynomial $P_{n-1}(\mu)$:

$$\chi_n(\mu) = (1-\mu^2)/n(n-1) . dP_{n-1}(\mu)/d\mu \qquad (4\text{-}7)$$

so that: $\chi_2(\mu) = 1/2 . \sin^2\theta \qquad (4\text{-}8)$

$$\chi_3(\mu) = 1/2 . \cos\theta\sin^2\theta \qquad (4\text{-}9)$$

Therefore, the first two terms in (4-6) give:

$$\Psi = va^2/2 . \sin^2\theta(r^2/a^2 - \alpha_2 r/a + \beta_2 a/r) + 1/2 . va^2\cos\theta\sin^2\theta(-\alpha_3 + \beta_3 a^2/r^2) \qquad (4\text{-}10)$$

and substituting (4-10) into (4-2) and (4-3) yields:

$$v_r=v_r'+v_r''=v.\cos\theta(\alpha_2 a/r-\beta_2 a^3/r^3-1)$$
$$-va^2/r^2.(-\alpha_3+\beta_3 a^2/r^2)P_2\cos\theta \quad (4\text{-}11)$$

$$v_\theta=v_\theta'+v_\theta''=v.\sin\theta(-\alpha_2 a/2r-\beta_2 a^3/2r^3+1)$$
$$-v\beta_3 a^4/r^4.\cos\theta\sin\theta \quad (4\text{-}12)$$

Consider now the boundary condition (1-17). The two terms in (4-11) are separately zero at r=a, and hence:

$$\alpha_2=\beta_2+1 \qquad \alpha_3=\beta_3 \quad (4\text{-}13)$$

Similarly the two terms proportional to $\sin\theta$ and $\sin\theta\cos\theta$ in the boundary condition (1-19) are separately zero. Therefore, from (1-20):

$$\gamma_1=\eta v(\alpha_2+2\beta_2-1) \qquad \gamma_2=5/3.\eta v\beta_3 \quad (4\text{-}14)$$

To incorporate the boundary condition that the normal stress at r=a must be continuous, the next pressure term must be determined. This corresponds to the second term in the expansion for Ψ (equation (4-10)), and can be obtained by the substitution of v_r'' and v_θ'' for v_r and v_θ in the spherical polar representation of equation (1-6) (see Batchelor (299)). This gives P", the second order contribution to the hydrodynamic pressure, to be of the form:

$$P''=2\eta v a^2\alpha_3/r^3.P_2\cos\theta \qquad (4\text{-}15)$$

and this is added to the left hand side of (1-18). Equating to zero the coefficients of $\cos\theta$ and $P_2\cos\theta$ in the expanded form of the boundary condition (1-18) yields:

$$2\gamma_1/a=\rho ga-3\eta v/a.(\alpha_2-2\beta_2) \qquad (4\text{-}16)$$

$$\gamma_2=\eta v(-3\alpha_3+2\beta_3) \qquad (4\text{-}17)$$

Therefore, from (4-13) and (4-17):

$$\gamma_2=-\eta v\beta_3 \qquad (4\text{-}18)$$

which can only be consistent with equation (4-14) if $\gamma_2=0$, and thus $\beta_3=\alpha_3=0$. Therefore, second order terms arising from the expansion of Legendre polynomials are negligible.

Eliminating α_2 and β_2 from the remaining equations gives the surface tension perturbation induced by bubble rise:

$$v=(\rho ga^2-\gamma_1)/3\eta \qquad (4\text{-}19)$$

It should be noted that in the absence of any such perturbation, equation (4-19) is consistent with the Rybczynski-Hadamard relation (224,225) for bubble rise rate at low Reynolds numbers.

To relate γ_1 to σ_1, representing the change in surface charge density due to bubble rise, the generalized Lippmann equation

can be used in exactly the same manner as described in section 3. Therefore, substitution of (3-33) into (4-19) yields:

$$\sigma_1=(3\eta v-\rho g a^2).(D\kappa/4\pi\sigma_0) \qquad (4\text{-}20)$$

which describes the influence of bubble rise rate on the perturbation of charge on the bubble surface.